Title
Principles of Tactile Stimulus Integration in the Rodent's Whisker Somatosensory Cortex

Author
Laboy-Juárez, Keven Joel

Publication Date
2018

Peer reviewed|Thesis/dissertation

Principles of Tactile Stimulus Integration in the Rodent's Whisker Somatosensory Cortex

By

Keven J. Laboy-Juárez

A dissertation submitted in partial satisfaction of the

requirements for the degree of

Doctor of Philosophy

in

Neuroscience

in the

Graduate Division

of the

University of California, Berkeley

Committee in charge:

Professor Daniel E Feldman, Chair

Professor Frederic Theunissen

Professor Jon McAuliffe

Professor Hillel Adesnik

Fall 2018

Abstract

Principles of Tactile Stimulus Integration in the Rodent Whisker Somatosensory Cortex

By

Keven J. Laboy-Juárez

Doctor of Philosophy in Neuroscience

University of California, Berkeley

Professor Daniel E. Feldman, Chair

Understanding how cortical circuits process sensory information and support perception is a fundamental problem in neuroscience. Rodents, being tactile experts, actively use their whiskers to sense complex tactile features like surface texture, object shape and location. In this dissertation I address how cortical neurons integrate sensory information from individual whiskers to support accurate and precise representations of complex tactile features.

Natural whisking during tactile exploration generates complex spatiotemporal sequences of whisker stimulation. Objects with different textures and shapes result in different patterns of whisker stimulation, sequentially stimulating different combinations of whiskers across time. I thus hypothesized that individual neurons in primary whisker somatosensory cortex (S1) are sensitive to specific features of tactile sequences. Chapter 2 describes the timescales at which S1 neurons integrated sensory input while rats discriminated between whisker impulse sequences that varied in single-impulse kinematics. While discrimination performance was consistent with integration at a relatively slow timescale (approximately 150ms), most S1 neurons integrated whisker input at a fast timescale (<20ms), generating a precise code for vibrotactile sequences in S1. Neurons with slower integration windows (>60ms) did not accurately represent the stimulus but were instead related to the rat's behavioral choice. These findings show that S1 neurons encode whisker input at a fast timescale and suggest that areas downstream of S1 temporally integrate this information to guide perceptual discrimination.

Given the precise representations of tactile sequences in S1, Chapter 3 explores the elementary computations underlying tactile stimulus integration by S1 neurons. Tactile sequences vary in spatial identity of stimulated whiskers and inter-whisker-deflection-intervals (Δt). Dense stimulation of local whisker pairs over a physiological range of Δt revealed a somatopically organized rate code for whisker combinations that was precise in space and coarser in time. Sublinear suppression for suboptimal combinations sharpened tuning relative to that expected from linear integration alone; analogous to the computation of motion direction selectivity in many visual circuits thus suggesting a common computation for spatiotemporal feature extraction. Taken together, this dissertation shows that S1 neurons integrate sensory input in space and time to generate robust tuning for spatiotemporal features of tactile scenes.

Table of Contents

Acknowledgments

I would like to thank my family, friends, peers, mentors and federal funding agencies because this dissertation would not have been possible without their continued support.

First, I must thank my mentors. My PhD advisor, Professor Dan Feldman, was and continues to be an incredible source of support. He taught me how to focus on relevant questions and avoid getting lost in unimportant details. He taught me how to communicate my science effectively and clearly. I will always appreciate that he never closed the doors to his office and was available to chat every single time I wanted advice or wanted to show him some new analysis. I can honestly say that I wouldn't be the scientist I am today without his mentorship. This is also true for my undergraduate mentors, Professor Carlos Jimenez-Rivera and Professor Barry Connors, who taught me how to do research before joining graduate school. All of my Berkeley friends, Vlad, Amy, Thom, Jon, Alex, James, Katie, Brian, Melanie, Sam and all others, many thanks for making my move to Berkeley from Puerto Rico easier. Especially to Amy who joined the Feldman lab the same year as me, gave me a lot of scientific advice and ended up becoming one of my best friends. I want to thank the Feldman lab as a whole, they're all amazing scientists and people, I couldn't have asked for a better group to do research with. I also have to thank Sei Ahn and Ching Fang for their amazing work as my undergraduate research assistants.

Importantly, I must thank my friends and family from Puerto Rico. To my parents (Luis and Marilyn), grandparents (Billy and Marina), uncles (Orly and Oscar), aunts (Lesbia and Nivia) and cousins (Keneth, Orlandito and Kiara) for your unquestionable and unending support. To my friends, especially Georgie, Malito, Carla, Luis, Mohammad, Diego, Alberto and Ricky for keeping in touch and supporting me even though we live more than 3000 miles apart.

My research career has also been supported by generous funding from the National Institute of Health (NIH) and National Science Foundation (NSF). These agencies have been supporting my career since my undergraduate studies in Puerto Rico. It's unquestionable that the NIH RISE, NSF GRFP and NIH F99/K00 awards played an essential role in helping me become the scientist I am today.

Finishing graduate school and publishing my research has been one of my biggest challenges. Graduate school was hard, not only because systems neuroscience is a challenging field, but because I had to leave Puerto Rico, the place I called home for 23 years of my life. This whole process taught me some important life lessons. First, a PhD in science taught me how easy it's to be wrong and that I must continually question my assumptions in science and life to become a better scientist and overall human being. Second, having to leave Puerto Rico taught me that you must be willing to sacrifice something to achieve something worthwhile. In this case I had to leave my home, family and friends to start becoming the scientist I want to be. Lastly, nothing can be achieved in isolation, my family and friends gave me the support I needed to finish my goals and my peers and amazing research environment in UC Berkeley gave me the tools and resources needed to get the best scientific training. I will be eternally grateful to all the people and institutions that supported me and hope that one day I will be able to return the favor.

Chapter 1

Introduction

A key aspect of sensation is the ability of individual neurons to integrate information across many specialized sensory receptors. Generally, however, how this process constructs tuning to complex sensory features remains poorly understood. In the rodent whisker somatosensory cortex (S1) whiskers form a discrete array of tactile sensors that are represented by functional columns called barrels[1]. Within each barrel, neurons have a whisker receptive field-measured via isolated deflections of individual whiskers-peaked at one 'best' whisker, with most cells tuned to the anatomically correct columnar whisker (CW)[2,3]. This topographical and functional organization makes S1 uniquely suited for studying how single neurons integrate localized sensory input across peripheral sensors like whiskers. Nevertheless, the computations underlying sensory integration and representations of complex multi-whisker stimuli remain poorly understood[4].

The topographical organization of S1 suggests a labeled-line coding scheme, where individual whiskers are represented in parallel by different barrels, generating a strong code for stimulus location in space. This single-whisker tuning model, however, has problems. Many S1 neurons respond weakly to single-whisker stimuli; even in awake, actively whisking rats, S1 neurons show temporally precise, low probability spiking that results in weak tuning[5]. Also, single-whisker stimuli rarely occur during natural whisker-based sensation[6–8]. Many S1 neurons, especially in non-granular layers, have broad receptive fields spanning multiple whiskers[9,10] and some even have their strongest response to surround whiskers (SWs) rather than the CW[11,12]. Although it's possible that these SW-tuned neurons are simply misplaced in the barrel map (i.e. located in the wrong barrel column), it's been a longstanding hypothesis that these neurons integrate sensory input to construct tuning for complex patterns of multi-whisker stimulation. Indeed, recent studies have shown that S1 neurons can be tuned to different multi-whisker features like global motion[13,14], correlation levels across whiskers[15] and specific spatiotemporal patterns of whisker stimulation generated via sparse noise[16]. Nevertheless, whether neurons with different whisker receptive fields systematically differ in their multi-whisker tuning remains to be assessed. Thus, currently, the whisker receptive field, the primary tool for characterizing sensory tuning in S1, has no known function in coding for ethologically relevant multi-whisker stimuli[4].

This problem is due to a relatively poor understanding of multi-whisker integration in single neurons which, in turn, arises from a highly nonlinear mapping between single-whisker and multi-whisker responses. Linear, sublinear and supralinear responses have all been recorded in

S1 and show a complex dependence on the identity of the whiskers being deflected[17–21], whisker kinematics[22], number of whiskers[21,23], inter-whisker-deflection-intervals[17–19] and level of sensory adaptation[16,17]. A particularly important type of inter-whisker nonlinearity is the second-order or pairwise interactions between sequential whisker deflections. Single neuron responses to periodic vibrotactile sequences involving two whiskers have been found to be almost entirely determined by the corresponding combination of second-order nonlinearities[20]. Pairwise nonlinearities also predict neuronal tuning to whisker features that involve the whole whisker array like global motion[13]. These studies, and the fact that any spatiotemporal pattern of whisker deflections is built from a set of elementary 2-whisker sequences imply that second-order computations powerfully shape S1 representations of tactile scenes. Despite this, the systematic structure of these elementary inter-whisker nonlinearities and whether/how they support spatiotemporal feature extraction remains poorly understood.

Nonlinearities are essential in the visual system, where spatially asymmetric sublinear suppression or supralinear facilitation yield tuning to the direction of moving objects[24–26]. It's possible that elementary cross-whisker interactions are organized in a similar way, supporting tuning to complex features of tactile scenes and suggesting generalized and evolutionary conserved neural computations for spatiotemporal feature extraction. Nevertheless the complexity and diversity of 2-whisker interactions has prevented this hypothesis from being formally tested.

Neurons in primary sensory cortex generate tuning to spatiotemporal features generally integrate across sensory space and time to generate tuning for local spatiotemporal features[27–29]. Thus, this dissertation explores the computations underlying tactile stimulus integration by S1 neurons in both space and time. Tactile sequences vary in spatial identity of stimulated whiskers (space) and inter-whisker-deflection-intervals (time). Accordingly, Chapter 2 describes how S1 neurons integrate tactile input from specific whiskers in time while rats discriminated between vibrotactile sequences of whisker stimulation. Chapter 3 explores the elementary computations underlying tactile stimulus integration through temporally dense stimulation of local whisker pairs over the physiologically relevant range of inter-whisker-deflection-intervals. Overall, this dissertation makes substantial advances on the computations involving spatiotemporal feature extraction and complex tactile feature representation in S1.

References

1. Woolsey, T. A. & Van der Loos, H. The structural organization of layer IV in the somatosensory region (S I) of mouse cerebral cortex. The description of a cortical field composed of discrete cytoarchitectonic units. *Brain Res.* (1970). doi:10.1016/0006-8993(70)90079-X

2. Armstrong-James, M., Fox, K. & Das-Gupta, A. Flow of excitation within rat barrel cortex on striking a single vibrissa. *J. Neurophysiol.* (1992). doi:10.1152/jn.1992.68.4.1345

3. Simons, D. J. Temporal and spatial integration in the rat SI vibrissa cortex. *J Neurophysiol*

(1985). doi:10.1152/jn.1985.54.3.615

4. Estebanez, L., Férézou, I., Ego-Stengel, V. & Shulz, D. E. Representation of tactile scenes in the rodent barrel cortex. *Neuroscience* (2018). doi:10.1016/j.neuroscience.2017.08.039

5. Jadhav, S. P., Wolfe, J. & Feldman, D. E. Sparse temporal coding of elementary tactile features during active whisker sensation. *Nat. Neurosci.* (2009). doi:10.1038/nn.2328

6. Sachdev, R. N. S., Sellien, H. & Ebner, F. Temporal organization of multi-whisker contact in rats. *Somatosens. Mot. Res.* (2001). doi:10.1080/135578501012006192

7. Grant, R. A., Mitchinson, B., Fox, C. W. & Prescott, T. J. Active Touch Sensing in the Rat: Anticipatory and Regulatory Control of Whisker Movements During Surface Exploration. *J. Neurophysiol.* (2008). doi:10.1152/jn.90783.2008

8. Hobbs, J. A., Towal, R. B. & Hartmann, M. J. Z. Spatiotemporal Patterns of Contact Across the Rat Vibrissal Array During Exploratory Behavior. *Front. Behav. Neurosci.* (2016). doi:10.3389/fnbeh.2015.00356

9. Moore, C. I. & Nelson, S. B. Spatio-Temporal Subthreshold Receptive Fields in the Vibrissa Representation of Rat Primary Somatosensory Cortex. *J. Neurophysiol. Chapin Chapin Lin Simons Carvell* (1992). doi:8930286

10. Zhu, J. J. & Connors, B. W. Intrinsic firing patterns and whisker-evoked synaptic responses of neurons in the rat barrel cortex. *J. Neurophysiol.* (1999). doi:10.1111/j.1469-7793.1999.00123.x

11. Sato, T. R., Gray, N. W., Mainen, Z. F. & Svoboda, K. The functional microarchitecture of the mouse barrel cortex. *PLoS Biol.* (2007). doi:10.1371/journal.pbio.0050189

12. Clancy, K. B., Schnepel, P., Rao, A. T. & Feldman, D. E. Structure of a Single Whisker Representation in Layer 2 of Mouse Somatosensory Cortex. *J. Neurosci.* (2015). doi:10.1523/JNEUROSCI.3887-14.2015

13. Jacob, V., Le Cam, J., Ego-Stengel, V. & Shulz, D. E. Emergent Properties of Tactile Scenes Selectively Activate Barrel Cortex Neurons. *Neuron* (2008). doi:10.1016/j.neuron.2008.10.017

14. Vilarchao, M. E., Estebanez, L., Shulz, D. E. & Férézou, I. Supra-barrel Distribution of Directional Tuning for Global Motion in the Mouse Somatosensory Cortex. *Cell Rep.* (2018). doi:10.1016/j.celrep.2018.03.006

15. Estebanez, L., Boustani, S. El, Destexhe, A. & Shulz, D. E. Correlated input reveals coexisting coding schemes in a sensory cortex. *Nat. Neurosci.* (2012). doi:10.1038/nn.3258

16. Ramirez, A. *et al.* Spatiotemporal receptive fields of barrel cortex revealed by reverse correlation of synaptic input. *Nat. Neurosci.* (2014). doi:10.1038/nn.3720

17. Ego-Stengel, V., Mello e Souza, T., Jacob, V. & Shulz, D. E. Spatiotemporal characteristics of neuronal sensory integration in the barrel cortex of the rat. *J. Neurophysiol.* (2005). doi:10.1152/jn.00912.2004

18. Shimegi, S., Ichikawa, T., Akasaki, T. & Sato, H. Temporal characteristics of response integration evoked by multiple whisker stimulations in the barrel cortex of rats. *J. Neurosci.* (1999).

19. Shimegi, S., Akasaki, T., Ichikawa, T. & Sato, H. Physiological and anatomical organization of multiwhisker response interactions in the barrel cortex of rats. *J. Neurosci.* (2000). doi:10.1523/JNEUROSCI.20-16-06241.2000

20. Boloori, A.-R. The Dynamics of Spatiotemporal Response Integration in the Somatosensory Cortex of the Vibrissa System. *J. Neurosci.* (2006). doi:10.1523/JNEUROSCI.4056-05.2006

21. Mirabella, G., Battiston, S. & Diamond, M. E. Integration of multiple-whisker inputs in rat somatosensory cortex. *Cereb. Cortex* (2001). doi:10.1093/cercor/11.2.164

22. Boloori, A.-R., Jenks, R. A., Desbordes, G. & Stanley, G. B. Encoding and Decoding Cortical Representations of Tactile Features in the Vibrissa System. *J. Neurosci.* (2010). doi:10.1523/JNEUROSCI.0807-10.2010

23. Ghazanfar, a a & Nicolelis, M. a. Nonlinear processing of tactile information in the thalamocortical loop. *J. Neurophysiol.* (1997). doi:10.1152/jn.1997.78.1.506

24. Barlow, H. B. & Levick, W. R. The mechanism of directionally selective units in rabbit's retina. *J. Physiol.* (1965). doi:10.1113/jphysiol.1965.sp007638

25. Hassenstein, B. & Reichardt, W. Systemtheoretische analyse der zeit, reihenfolgen, und vorzeichenauswertung bei der bewegungsperzepion des Rüsselkäfers Chlorophanus. *Naturforsch* (1956).

26. Mauss, A. S., Vlasits, A., Borst, A. & Feller, M. Visual Circuits for Direction Selectivity. *Annu. Rev. Neurosci.* (2017). doi:10.1146/annurev-neuro-072116-031335

27. Priebe, N. J. & Ferster, D. Mechanisms of Neuronal Computation in Mammalian Visual Cortex. *Neuron* (2012). doi:10.1016/j.neuron.2012.06.011

28. Sadagopan, S. & Wang, X. Nonlinear Spectrotemporal Interactions Underlying Selectivity for Complex Sounds in Auditory Cortex. *J. Neurosci.* (2009). doi:10.1523/JNEUROSCI.1286-09.2009

29. Stettler, D. D. & Axel, R. Representations of Odor in the Piriform Cortex. *Neuron* (2009). doi:10.1016/j.neuron.2009.09.005

Chapter 2

Short Time-Scale Sensory Coding in S1 during Discrimination of Whisker Vibrotactile Sequences

Leah M. McGuire☯, Gregory Telian☯, Keven J. Laboy-Juárez☯, Toshio Miyashita, Daniel J. Lee, Katherine A. Smith, Daniel E. Feldman

☯ These authors contributed equally to this work.

This chapter, in full, is a republication of the material as it appears in McGuire LM, Telian G, Laboy-Juárez KJ, Miyashita T, Lee DJ, Smith KA, et al. (2016) Short Time-Scale Sensory Coding in S1 during Discrimination of Whisker Vibrotactile Sequences. PLoS Biol 14(8): e1002549. doi:10.1371/journal. pbio.1002549

2.1 Summary

Rodent whisker input consists of dense microvibration sequences that are often temporally integrated for perceptual discrimination. Whether primary somatosensory cortex (S1) participates in temporal integration is unknown. We trained rats to discriminate whisker impulse sequences that varied in single-impulse kinematics (5–20 ms time scale) and mean speed (150 ms time scale). Rats appeared to use the integrated feature, mean speed, to guide discrimination in this task, consistent with similar prior studies. Despite this, 52% of S1 units, including 73% of units in L4 and L2/3, encoded sequences at fast time scales (≤20 ms, mostly 5–10 ms), accurately reflecting single impulse kinematics. 17% of units, mostly in L5, showed weaker impulse responses and a slow firing rate increase during sequences. However, these units did not effectively integrate whisker impulses, but instead combined weak impulse responses with a distinct, slow signal correlated to behavioral choice. A neural decoder could identify sequences from fast unit spike trains and behavioral choice from slow units. Thus, S1 encoded fast time scale whisker input without substantial temporal integration across whisker impulses.

2.2 Introduction

Natural sensory input comprises dense temporal series of discrete events, which animals often temporally integrate to guide perceptual decisions. The temporal integration process has been studied in primate somatosensation and vision[1,2], but less in rodents, in which modern tools could reveal the underlying circuit mechanisms. In the whisker tactile system, active whisking generates dense streams of stick-slip events on surfaces (5–10 ms duration, ~60 ms interval)[3,4] and contact events on object edges[5,6]. These temporal series constitute the whisker vibrotactile signal. While animals can perceive individual brief whisker impulses alone or within trains[7-11], behavioral discrimination of vibrotactile sequences is often based on a time-averaged composite feature, mean whisker speed, rather than the kinematics or precise pattern of individual deflections[12,13]. This suggests that the brain generates both short time-scale (individual impulse) and temporally integrated, long time-scale (mean speed or intensity) representations of whisker input. How these time scales are represented in the cortex is unknown.

We tested which time scale(s) of information are represented in S1 in awake behaving rats discriminating rapid whisker sequences. Under anesthesia, most S1 neurons spike phasically to whisker deflections, and responses adapt strongly during stimulus trains. This suggests that S1 does not temporally integrate across impulses (we use "integration" to mean temporal summation or averaging)[14-18]. Most S1 neurons also spike phasically to whisker deflection in basic detection tasks[7-10,19] or when rats must detect kinematically distinct impulses within ongoing stimulus trains[8]. However, these tasks do not require stimulus integration for behavioral performance[7-10]. Whether temporal integration occurs in S1 during tasks in which animals behaviorally integrate whisker information is unknown. A subset of S1 neurons exhibit sustained responses to stimulus sequences in awake mice[20], but whether these contribute to perceptual integration is unclear.

We trained rats to discriminate rapid sequences of three brief whisker impulses with an ~60 ms interpulse interval. This interval matches the median interval between stick-slip events during texture palpation[21]. S1 is required for passive vibrotactile discrimination[13,22,23]. Stimuli differed in both rapid temporal structure (kinematics and order of individual impulses) and time-integrated information (mean speed of the entire sequence). Rats could use either for discrimination. Behavioral choice correlated with mean speed, suggesting that rats temporally integrated whisker impulse sequences, as shown explicitly in similar prior studies in which both rapid kinematic and slow intensity cues were available[12,13]. In tetrode recordings during behavior, most S1 units accurately encoded single-impulse kinematics on a rapid (≤20 ms) time scale with modest adaptation. A minority of units responded weakly to individual impulses but

exhibited slowly increasing or decreasing spiking during the stimulus period. However, these units did not effectively integrate across impulses and instead combined transient impulse responses with a distinct, slow signal correlated to behavioral choice. Thus, S1 appears to represent only short time-scale information about whisker impulse trains during vibrotactile discrimination. This suggests that temporal integration may occur downstream of S1.

2.3 Results

Behavioral Discrimination of FFF, FMS, SMF, and SSS Sequences

We developed a novel whisker vibrotactile discrimination task in which rats initiated trials by entering a nose poke with their right whiskers resting on a wall panel coupled to a hidden piezoelectric actuator (Fig 1). The panel delivered a rapid sequence of three up-down impulses. Each impulse was 16–26 ms long and had Fast (F), Medium (M), or Slow (S) rise/fall velocity. Sequences had FFF, FMS, SMF, or SSS pulse order (34 ms interval from end of a pulse to beginning of next pulse; 120–148 ms sequence duration). Sequences were constructed so that mean speed was greatest for FFF, lowest for SSS, and equal and intermediate for FMS and SMF sequences (Fig 1; Table 1; S1 Fig). One sequence was delivered per trial, beginning 75–100 ms after nose poke entry. Rats had to maintain nose poke for 250 ms to ensure delivery of the entire sequence and then discriminate by selecting a right or left drink port for water reward. FFF and FMS sequences were rewarded right, and SMF and SSS were rewarded left. Training was conducted under infrared light, and sound cues from the piezo were masked. In a subset of trials (43 trials, 4 rats), we verified with high-speed video that whiskers remained on the panel throughout the stimulus period and that rats did not whisk while in the nose poke, as shown previously[22]. Head movement averaged 0.8 mm in right-left position and 1.0 mm in rostrocaudal position during the stimulus period. Rats initially trained on FFF versus SSS discrimination and then FMS and SMF stimuli were added (see Materials and Methods).

These sequences differed in both rapid stimulus features, like identity of individual impulses, and slow features, like mean speed of the entire sequence. We designed the task so that fully correct discrimination is only possible if rats attend to fine time-scale information, like precise internal structure of the train (FFF or FMS indicates choose right, SMF or SSS indicates choose left), or identity of the first impulse (F indicates choose right, S indicates choose left). In contrast, if behavior is guided by mean speed (or duration) of the entire sequence, then rats should respond to FFF and SSS correctly but make mistakes in which they treat SMF and FMS identically and intermediate to FFF or SSS. Using a similar task design in which both rapid and slow, integrated cues were available, two prior studies found that rats choose to guide vibrotactile discrimination by the integrated variable, mean speed or intensity[12,13].

After 14.2 ± 4.4 (standard deviation [s.d.]) (range: 8–22) d of training on FFF-FMS-SMF-SSS discrimination, all eight rats successfully discriminated FFF from SSS stimuli, but failed to respond appropriately to FMS and SMF stimuli, instead treating them as equivalent and intermediate between FFF and SSS (Fig 2A and 2B). Seven out of eight rats failed to differentiate at all between FMS from SMF stimuli (proportion test, Bonferroni-adjusted *p*-value >0.00625). One rat (62SC) showed modest but significant discrimination, with more right-side choices to FMS than SMF stimuli ($p = 0.0039$). Behavior was stable, on average, across the training period (S2 Fig). Thus, seven out of eight rats showed behavior consistent with guiding decisions by time-integrated whisker information. To examine this further, we plotted the mean behavioral performance of each rat versus the mean speed of panel movement across the entire sequence (150 ms). Behavioral performance was computed as (fraction of right drink port choices for each stimulus) – (mean fraction of right drink port choices for all stimuli), to account for right-left choice bias by some rats (Fig 2B). Right drink port choice was strongly related to mean sequence speed for all rats (Fig 2C).

To confirm that rats guided behavior by panel movement, we ran a "fixed panel" control in six rats, immediately after the final normal training session. The panel was fixed in place, while the piezo behind it moved normally. Panel fixation strongly impaired behavioral discrimination in all but one rat (example rat, Fig 2A; population data using d-prime analysis, Fig 2D; population data using a simpler non-parametric analysis, S2B Fig). Some residual discrimination did persist and may have been mediated by inadequately masked piezo sound cues. Further analysis showed that three rats treated the average fixed-panel stimulus similarly to SSS stimuli; one rat responded by choosing right or left randomly; and one rat stopped completing trials in the fixed-panel condition (S2C Fig). Thus, different rats had different strategies for handling the unfamiliar fixed panel trials.

These results suggests that, as in prior studies[12,13], rats used slow, integrated information (mean speed or intensity) to guide discrimination, rather than rapid information (first or last impulse identity or impulse order). This may reflect either a predisposition for intensity cues, or task factors such as our use of strong intensity cues in initial training or the nose poke time requirement, which may have promoted an integration-based strategy. Rats are known to sense fast kinematic cues during ongoing sequences[7-11], and they can utilize these cues for discrimination in some cases[8]. We did not apply additional stimuli to further dissociate slow from rapid information (as was done in[12,13]), and thus we cannot independently rule out the possibility that rats guided behavior from a hidden fast cue (e.g., second impulse identity) that correlated with mean speed.

Discrimination of FSFS versus SFFS Sequences

To test whether failure to discriminate FMS versus SMF reflected insufficient training on these sequences or the presence of easier FFF and SSS stimuli on 50% of trials, we trained two rats on a modified task. This used a very simple task structure with only two stimuli: an FSFS sequence (rewarded at the right drink port) and an SFFS sequence (rewarded at the left drink port). F and S impulses had 216 and 120 mm/s peak velocity and 1.2 and 0.7 mm amplitude, respectively. Both trains had 34 ms interpulse interval and 188 ms total duration (Fig 3A). We constructed two sets of stimuli: a "same-intensity" version in which FSFS and SFFS trains had nearly identical mean speed (25.7 and 26.4 mm/s, calculated across the full sequence), and a "different-intensity" version in which FSFS and SFFS stimuli were scaled in amplitude so that mean speed was 27.8 and 8.7 mm/s, respectively.

Two rats (58B and 60W) were initially trained to discriminate the different-intensity sequences (>65% correct over 3 d). Then, we replaced these stimuli with the same-intensity FSFS and SFFS sequences, so that discrimination could only occur by detecting differences in fine temporal structure, not mean speed. Performance dropped to chance and did not improve over 5 d of training (Fig 3B). We then alternated weekly training on different- and same-intensity sequences. Both rats consistently discriminated FSFS from SFFS when they had different mean speed (58B: 70 ± 1.5% correct, 60W: 69.2 ± 1.6%), but not when they had the same mean speed, even after >20 cumulative days of training (58B: 52 ± 0.8% correct; 60W: 53 ± 0.8% correct). This was evident in the d-prime measure of discrimination between FSFS and SFSF stimuli, which was 1.02 for different-intensity stimuli and 0.12 for same-intensity stimuli (Fig 3C). Thus, behavior correlated with the presence of a slow, integrated cue.

S1 Recordings during Behavioral Discrimination

To study S1 coding of whisker sequences during vibrotactile discrimination, we recorded S1 spiking during the FFF-FMS-SMF-SSS behavioral task using chronic multi-tetrode microdrives. Four tetrodes (~350 um lateral spacing) were driven as a group, enabling simultaneous recording of many neurons in several whisker-related columns (Fig 4A). Tetrodes were initially implanted into mid-L2/3 and advanced by ~140 µm every one to two recording sessions, sampling neurons from L3 to L6 over 12–22 d of recording. Spike sorting yielded 3.8 (range: 0–11) well-separated single units per recording session (Fig 4B). Additional units showed clear separation from noise but failed the interspike interval criterion for single units and were classified as multi-units. We obtained 306 single units and 167 multi-unit clusters (total: 473 units) across 80 recording sessions in five rats (18FB, 18Ri, 18Ro, 62BS, 107St), spanning across L3 to L6 (Fig 4C). Fast-spike (FS) and regular-spike (RS) units were well separated by spike width. Recordings were localized to C1-4, D2-4, and E3 columns based on receptive field mapping under light isoflurane anesthesia and recovery of marking lesions. These whiskers

were visually confirmed to contact the panel, as in a prior study using this behavioral apparatus[22].

Mean firing rate during a 25-ms prestimulus baseline period in the nose poke was 6–10 Hz across layers for RS units, 8–32 Hz for FS units, and higher for multi-unit clusters (Table S1). Lowest firing rates were observed in L2/3, L4, and L6. Firing rate distributions were positively skewed (S3A Fig). Firing rates for RS units were higher than in prior studies using cell-attached or whole-cell recording in rodents whisking mostly in air[6,24,25]. This likely reflects recording bias for more active units and the fact that whiskers contacted the stimulus panel through the entire nose poke duration, including the baseline period.

We first identified units whose average firing rate was significantly temporally modulated with any dynamics during the nose poke period ($p < 0.05$, temporal modulation permutation test, see Materials and Methods). Three hundred five out of 473 units (63.5%) showed significant temporal modulation. Temporally modulated units were distributed uniformly across whisker columns and layers (Fig 4C) and had higher baseline firing rates than non-modulated units (S3B Fig). Subsequent analysis focused only on these temporally modulated (i.e., task-involved) units. Single- and multi-units showed similar response properties and were combined for analysis unless indicated.

The average population response, compiled across all temporally responsive units in each layer, was dominated by a brief, phasic increase in firing rate following each panel impulse (Fig 4D). This was greatest in L2/3, L4, and L5b, and weakest in L5a and L6. The mean impulse-evoked firing rate modulation (in Hz above pre-impulse baseline) was 14.2 ± 2.3 in L2/3, 15.2 ± 1.9 in L4, 6.3 ± 1.2 in L5a, 14.4 ± 2.3 in L5b, and 7.0 ± 1.5 in L6 (n = 28–82 units per layer). Among units with significant impulse responses, peak response latency was shortest in L4, L5a, and L5b (9.8, 10.3, and 12.0 ms) and longest in L2/3 and L6 (13.8 and 16.1 ms). Superimposed on these phasic responses to individual impulses was a gradual decrease in average firing rate during the nose poke period, observed in all layers except L5a (Fig 4D).

Individual units most commonly showed phasic responses to individual impulses (examples, Fig 5A and 5B). However, some units instead showed cumulatively increasing firing rate during the stimulus period (Fig 5C and 5D) or decreasing firing rate (not shown). These were intermixed in the same columns and recording sites.

Regression Analysis to Identify Fast- and Slow-Time Scale Units

To quantify the time scales of stimulus representation in S1, we performed a multiple regression analysis for each temporally modulated unit (n = 305), whose goal was to identify

the time window of stimulus integration that best predicted the neuron's firing rate (Fig 6). The dependent variable was firing rate, in 5 ms bins, calculated over all trials for each stimulus sequence. The regressors were integrated speed of panel movement over a variety of temporal integration windows (5, 10, 15, … 180 ms, for a total of 36 regressions). Firing rate in each 5 ms bin was predicted from the integrated panel speed in the preceding bin. Two hundred four units showed a significant regression for at least one stimulus integration window ($\alpha = 0.05/36 = 0.0014$, using Bonferroni correction for the multiple regressions). For each unit, we defined the best fit integration window as the stimulus integration window with the highest R^2 value.

Most units had a short best fit integration window (5–20 ms), indicating that firing rate was best predicted by stimulus speed on a short time scale (examples, Fig 6A and 6B). However, some units exhibited slowly increasing or decreasing firing that was correlated with integrated speed over long timescales, most often the whole stimulus period (example, Fig 6C). Individual cells had high R^2 values for either short or long integration windows but rarely both (Fig 6D). Most units showed a positive regression slope for the best integration window, indicating that firing rate increased with integrated stimulus speed, while ~20% showed a negative slope (Fig 6D and 6E). Empirically, units with 5–20 ms best integration windows (Fast units; *n* = 158) had positive slopes. Units with 25–55 ms integration windows were rarer (Medium units; *n* = 52) and had largely negative slopes. Units with slow (55–180 ms) integration windows had either positive regression slope (Slow Positive units; *n* = 51) or negative regression slope (Slow Negative units; *n* = 44).

Fast units were 73% of temporally modulated units in L2/3 and L4, 50% in L5, and 23% in L6. Overall, 52% of temporally modulated units were Fast units. Both Fast and Medium units were most prevalent in L2/3, L4, and L5b. In contrast, both Slow Positive and Slow Negative units were located primarily in L5 and L6 (Fig 6F and 6G). Overall, slow units were 13% of temporally responsive units in L2/3 and L4, 31% in L5 and 56% in L6. Fast, Medium, Slow Positive, and Slow Negative categories each contained both single- and multi-units and both RS and FS units.

Fast and Medium Time Scale Units

Fast time scale units showed temporally precise coding of individual panel impulses and sequences (Fig 7A–7C). Population PSTHs for the fastest units (5 ms best integration window) showed responses to F impulses (16 ms duration) that lasted just ~20 ms and responses to S impulses that tracked impulse onset and offset separately. Units with 10 ms and 15–20 ms best integration windows had somewhat slower responses, as expected, but still tracked individual impulses. Adaptation within each train was quantified as mean firing rate to pulse N/pulse 1 and was modest in FFF trains (2/1: 0.80 ± 0.11, 3/1: 0.70 ± 0.14, $p < 0.05$ by *t* test, *n* = 61 single

RS units with significant response to F impulses) and statistically absent in SSS trains (2/1: 1.09 ± 0.26, 3/1: 0.86 ± 0.35, all mean ± SEM) (Figs 7A and S4). This is less adaptation than reported for non-whisking, non-task-engaged rats[16,26] and is similar to passive whisker detection[10].

To determine whether Fast units accurately discriminate impulse velocity, we calculated the average response to all individual F, M, or S impulses (compiled across all sequences). The firing rate of Fast units (*n* = 158) in a brief window after each impulse was greater for F versus S impulses, and intermediate for M impulses (Fig 7C, left). Mean firing rate measured over the entire duration of a sequence (0–150 ms after sequence onset) varied closely with mean speed of the sequence, being highest for FFF, lowest for SSS, and intermediate and equal for FMS and SMF (Fig 7C, right). Thus, population average firing rate of Fast units over the entire sequence closely matched the mean behavioral performance of the animals (Fig 2C).

In addition to coding pulse velocity, Fast unit coding was also influenced by pulse order because of adaptation. Fast RS single units (*n* = 61) showed greater adaptation during FFF than SSS sequences. Consistent with this, the middle M pulse in FMS sequences appeared weaker than in SMF sequences, though this did not achieve statistical significance (*p* = 0.08, paired *t* test, *n* = 61 units) (S4A Fig). Thus, Fast units represent impulse velocity, but with some history dependence due to adaptation, and no sign of positive temporal integration across impulses.

In contrast, medium time scale units responded to impulses with a modest decrease in firing rate, rather than an increase, consistent with the negative regression slope for most of these cells (Figs 6E and 7D). In firing rate analysis, these cells were inhibited by F, M, and S impulses and did not distinguish either individual impulse identity or whole sequence identity (Fig 7D and 7E). Thus, medium time scale units do not represent stimulus information useful for this discrimination task.

Slow Positive and Slow Negative Units

Slow positive units (*n* = 51) also showed a time-locked increase in firing rate after panel impulses, on average, but mostly to the second and third impulses in the sequence. Responses were small and sustained (unlike the large, transient responses by Fast units) and were evident for F and M impulses but not S impulses (Fig 8A). However, mean firing was not different for FFF, FMS, SMF, or SSS trains, suggesting that these neurons do not appreciably integrate impulse information for sequence discrimination (Fig 8A). Slow negative units did not respond to impulses at all, and firing rate steadily declined over time, not locked to panel impulses (Fig 8B).

Unexpectedly, firing of Slow Positive units correlated with the animal's behavioral choice on each trial. Fig 8C shows population PSTHs for Slow Positive units in L5a and L5b, divided into trials in which the rat chose the right- or left-side drink port. Slow Positive units fired more on trials when the rat chose right (contralateral to the S1 recording). This was true for both FFF and FMS stimuli, for which right was the correct response, and SMF and SSS stimuli, for which right was the incorrect response. We quantified right-choice bias as the firing rate difference on right versus left trials, measured 5–50 ms after the start of the final impulse. Right-choice bias was significant for Slow Positive units in L5a and L5b, but not other layers (Fig 8D). Firing rate began to diverge on right versus left choice trials after the second impulse and was consistently significant by 125 ms, which is during the third impulse ($p < 0.05$, sliding paired *t* test) (Fig 8E). This preceded the earliest withdrawals (150 ms) and mean withdrawal time (190 ms). Choice-related activity was absent in fast time scale units in L4 (Fig 8E).

Thus, L5 Slow Positive units exhibited weak impulse-evoked spiking and strong choice-related spiking (Fig 8). We tested for stimulus integration in these units by comparing firing rate during each impulse of FFF, FMS, SMF, and SSS sequences on right- and left-choice trials separately, which removes choice as a factor (S5 Fig). Evoked firing was minimal for pulses 1 and 2 and was not correlated with pulse velocity. Pulse 3 firing rate was higher but was essentially identical for FFF, FMS, SMF, and SSS sequences and did not correlate with mean speed of the entire sequence or of the last two impulses. Thus, these units did not effectively summate stimulus information across impulses.

We asked whether choice-related firing could reflect a feed-forward sensory reafferent signal generated by decision-related movements in the nose poke. Reafference from fast whisker deflections is unlikely, because L4 Fast units did not exhibit choice-related firing (Fig 8). However, a distinct slow reafferent signal is possible. We tested for choice-related postural movements by analyzing high-speed videos in 43 trials (22 left choice, 21 right choice) from four rats. In each trial, we tracked head position, head angle, and whisker tip position with ~100 μm precision at 8.4-ms intervals from 0 to 150 ms after stimulus onset. Head angle and whisker tip trajectories were invariant between right- and left-choice trials. Head position differed modestly between right- and left-choice trials beginning at 100 ms, with a 0.6 mm difference at 125 ms (S6 Fig). Thus, slow head movements are a potential reafferent driver of choice-related firing in L5.

RS and FS Single Units

Fast, Medium, Slow Positive, and Slow Negative response classes all included RS, FS, and multi-unit clusters, although few FS cells were found in the Slow classes (S7 Fig). Among Fast units, all

three unit types had similar sequence-related PSTHs. Among L5 Slow Positive units, both RS units and multi-unit clusters had similar choice-related firing, and no FS units existed in this category (S7 Fig). Thus, all response classes involved RS units.

Neural Decoding of Stimulus Identity and Behavioral Choice

S1 neurons spike sparsely, with individual whisker deflections eliciting mostly zero spikes, occasionally one spike, and, very infrequently, two spikes on a single trial[21,27,28]. We also observed this highly variable, sparse single-trial spiking behavior (Fig 5). To test whether S1 accurately encodes whisker sequences on single trials, we constructed a neural population decoder that predicted stimulus identity from single-trial spike trains. In the model, each recorded neuron was represented by a separate, independent one-vs-all (OVA) classifier that predicted the probability of each sequence (FFF, FMS, SMF, or SSS) given one spike train, chosen randomly from that neuron's recorded spike trains in vivo, and binned in discrete time bins. Each OVA classifier was trained by logistic regression from a randomly chosen subset of spike trains for that unit. The output of each classifier was the probability of each stimulus type versus all others, based on the presented spike train. To create a population prediction, stimulus probabilities were summed across units, and the sequence with highest summed probability was taken as the population stimulus prediction (Fig 9A). This model assumes independence between neurons and allows stimulus prediction by both firing rate and temporal information within spike trains.

We first constructed a decoder from all Fast and Medium units, using 10 ms time bins. This model predicted sequence identity, using one single-trial spike train per model unit, with 83% overall accuracy (range: 74% for FMS to 88% for FFF spike trains). Chance performance is 25% (Fig 9B). The individual neurons with best stimulus prediction were those with 5–10 ms best integration windows (Fig 9C). Remarkably, this model identified SMF and FMS sequences with 78% accuracy, even though rats could not. A second decoder constructed of all Slow units, also using 10 ms bins, predicted sequence identity at near chance levels (32% correct, not significantly different from chance, $p = 0.47$) (Fig 9B). Decoding from mean firing rate in a single 150-ms bin substantially reduced Fast/Medium decoder accuracy (43% correct) and did not improve Slow decoder accuracy (Fig 9D).

To test whether the Fast/Medium model recognized sequences by mean firing rate or temporal spike pattern, we rate-normalized the spike train data (preserving temporal information across the 10-ms bins) or time-scrambled spike trains within trials (preserving firing rate information). Fast/Medium decoders trained on rate-normalized data performed well (80% correct), but time-scrambling spikes abolished performance (Fig 9E). Thus, the

Fast/Medium decoder primarily identified stimuli by temporal spike patterns, which varied between FFF, FMS, SMF, and SSS sequences (Fig 7). Thus, sequence identity was primarily encoded in short time-scale spiking information, carried by Fast units.

We constructed a similar decoder to predict behavioral choice. This was trained on spike data from all four sequences and was tested for prediction of right versus left drink port choice separately for FFF, FMS, SMF, and SSS trials. A choice decoder based on Fast/Medium units was unable to predict drink port choice, either using 10 ms bins (not shown), mean firing rate in a single 150-ms bin, or mean firing rate in the last 100 ms prior to nose poke withdrawal (Fig 9F). A choice decoder based on Slow units successfully predicted drink port choice using a single 150-ms bin, or mean firing rate in the last 100 ms before nose poke withdrawal (65% correct for both models) (Fig 9F). Post-hoc analysis showed that units with best choice prediction were Slow Positive units located primarily in L5b (Fig 9G). Thus, spiking of Slow Positive units was sufficient to decode behavioral choice but not sequence identity.

2.4 Discussion

Behavioral Integration of Stimulus Sequences

Cortical sensory systems temporally integrate sensory signals for many types of perceptual decision-making[2]. Where and how integration is performed is unclear. In fingertip vibrotactile discrimination by primates, S1 neurons spike to each rapid skin deflection, and this information is temporally integrated downstream of S1 to guide behavioral discrimination[1,29]. In the rodent whisker system, passive vibrotactile discrimination is often based on slow, time-integrated input[12,13], although rats are also capable of discrimination based on rapid kinematics[8]. Integration is also implicated in discrimination of surface texture (roughness), in which surface whisking generates temporally dense sequences of stick-slip whisker micromotions, whose mean statistics, including mean whisker speed, correlate with roughness[3,4,21,30-33]. S1 neurons spike phasically to stick/slip events and other features such as dynamic changes in whisker bend[3,21,34], and behavioral judgments of surface roughness correlate with mean firing rate and rate of synchronous spiking across S1 neurons[21,35,36]. Thus, roughness discrimination likely involves temporal integration of stick/slip events and S1 spike trains. Integration is useful because it reduces the complexity of the vibrotactile signal to a single scalar quantity of stimulus intensity. Intensity-based discrimination is common across modalities and is a defining feature of texture discrimination in people and non-human primates[37]. Integration is also evident in whisker-based object localization, in which S1 spikes are time-locked to object contact, but mice judge object location by behaviorally integrating spike counts over ~50 ms, rather than using precise timing[19].

In our task, rats were able to distinguish FFF versus SSS sequences that differed in mean speed, but not FMS versus SMF sequences that had the same mean speed, and choice behavior was strongly related to mean speed across the sequence (Fig 2). Similar performance was observed in the SFSF versus FSSF task (Fig 3). Task performance was relatively low (d-prime for FFF versus SSS: 0.5–1.5), as in a prior study[13], indicating the difficulty of these tasks. The results suggest that rats utilized slow, time-integrated information for task performance, even though simple, short time-scale cues (e.g., identity of the first impulse) would have led to more rewards. This hypothesis is consistent with two prior vibrotactile discrimination studies using a similar design, in which rapid kinematics and slow intensity cues were manipulated separately to prove that rats guided discrimination by slow, time-integrated cues[12,13]. We did not test this causally in our study, so we cannot rule out that rats may have solved our task using a hidden short time scale cue.

Integration is not required for simpler detection tasks[7,9,10] or detection-of-change tasks[8], and rodents can perceive single brief whisker impulses within ongoing deflection trains[7-11,38]. This suggests that rats generate neural codes for both rapid and integrated features that guide different aspects of sensory-guided behavior. Rats may differentially use these codes depending on task demands and training strategies. In our task, initial training involved strong intensity cues, which may have promoted adoption of an integration-based strategy. An intensity-like feature of vibrotactile stimuli is encoded in primate dorsolateral prefrontal cortex during a working memory task[39], but no explicit intensity representation is known yet in the rodent whisker system.

Stimulus Encoding in S1 Occurs at Fast (5–20 ms) Time Scales

We tested for stimulus integration in S1 during task performance but found that S1 encoded whisker sequences almost exclusively at very rapid time scales. Forty-four percent and 52% of temporally responsive units showed very fast (5–10 ms) and fast (5–20 ms) stimulus integration, respectively (Fig 6E). These units spiked to individual whisker impulses, with firing rate encoding impulse velocity, and mean firing rate correlated with mean whisker speed across the sequence (Fig 7A–7C). Seventeen percent of units showed firing rate modulations on medium (25–55 ms) time scales, but these were inhibited by whisker impulses and did not discriminate different impulses or sequences (Fig 7D and 7E). Sequence identity could be decoded accurately from Fast units but not Medium units, and stimulus information was abolished by scrambling spike times across 10-ms bins. Thus, Fast units encode sequence identity by representing the velocity and timing of individual impulses. Fast units accurately distinguished FMS from SMF sequences, even though rats could not (Fig 9B). Thus, accurate short time-scale representation of vibrotactile sequences exists in S1 but does not appear to be

used efficiently to guide behavior in our task. This is identical to primate S1, in which precise spike timing discriminates vibrotactile flutter more accurately than the animal[40].

Fast units had phasic whisker responses similar to classic anesthetized studies[14,41] and S1 units recorded during detection tasks[7,8,11]. Responses were weak in L5a and L6 (Fig 4), which may reflect involvement of this layer in active whisking, which was absent in our task[42]. Adaptation was minimal: ~25% for FFF trains and absent for SSS trains (Fig 7A–7C). This level of adaptation is less than occurs under anesthesia[15,18] or in quiescent, non-task engaged rats[16,26] and is similar to that during active exploration[16,26] or in a whisker detection task[10]. While adaptation generates history dependence and thus carries information about prior impulses[43,44], Fast units showed no evidence of positive integration across impulses.

Slow Units Do Not Integrate Stimuli but Reflect Behavioral Choice

Seventeen percent of units, primarily in deep layers, were Slow Positive units with small, sustained responses to individual whisker impulses and progressively increasing firing rate during the stimulus period. However, these units did not accurately encode or integrate whisker impulses. Responses were generally absent to the first impulse of sequences, and firing rate did not differ between FFF, FMS, SMF, and SSS sequences or correlate with mean speed (Figs 8A and S5). Thus, Slow Positive units do not appear to carry integrated stimulus information for sequence discrimination. Slow Negative units had slowly decreasing firing rate and no stimulus-related firing modulation at all (Fig 8). Consistent with these observations, sequence identity could not be decoded from Slow unit spike trains (Fig 9B). Slow whisker-evoked spiking occurs in some L2/3 units in mice [20] but was not evident in our dataset in rats.

Instead, firing of Slow Positive units in L5 was strongly related to drink port choice. Choice-related spiking[45] occurs in many cortical areas, including primary visual cortex[46], S1 of primates and rodents[11,47-49], and even subcortically[49,50]. In rodent S1, many L2/3 neurons exhibit choice-related spiking in near-threshold detection tasks[11,49]. Choice-related firing emerged significantly after the second impulse of the sequence and was consistent during the third impulse, 65 ms before the average nose poke withdrawal (Fig 8E). A neural decoder built from Slow unit spike trains predicted behavioral choice from mean firing rate in the stimulus period and in the 100 ms prior to nose poke withdrawal (Fig 9). Choice-related firing was absent in L4 Fast units, suggesting it did not represent reafference from fast whisker sensory signals (Fig 8E). Choice-related spiking could reflect reafference from slow head movements prior to nose poke withdrawal, potentially mediated by POm afferents to L5[51] or an internal decision or motor preparatory signal. Its onset after the second impulse could reflect an early behavioral decision based on first and second impulse stimulus information or an early stimulus-independent “guess” that biased subsequent stimulus-dependent drink port choice. Thus, Slow Positive units do not appear to integrate across whisker impulses but combine weak impulse responses with a distinct, slow signal related to behavioral choice.

Where in the Brain Does Temporal Integration Occur?

We found that during vibrotactile discrimination, most S1 neurons represent the velocity and timing of individual whisker impulses at rapid, 5–20 ms time scales. While there was some history dependence of whisker responses due to modest adaptation, we did not observe evidence of positive integration across whisker impulses in S1 firing rates. Thus, temporal integration for discrimination is likely to occur downstream of S1, in higher sensory or premotor regions. These may include S2, prefrontal cortex, and premotor cortex, as in primate vibrotactile discrimination[1]. We cannot rule out that S1 could learn to temporally integrate under conditions in which rats were more reliant on slow cues for behavioral discrimination. For whisker texture perception, our finding of short time scale coding in S1 suggests that S1 primarily encodes low-level kinematics of individual stick/slips and bends[6,21], which are integrated downstream to represent texture or other surface features.

2.5 Conclusion

We recorded neural activity in primary somatosensory cortex as rats discriminated rapid vibrotactile sequences and found that neurons in the primary somatosensory cortex encoded whisker sensory information at very fast time scales (<20 ms), without evidence for substantial temporal integration. A subset of neurons encoded relatively little stimulus information but strongly encoded the rat's behavioral choice on each trial. Thus, primary sensory cortex represents immediate sensory input, suggesting that temporal integration occurs in downstream brain areas.

2.6 Methods

Female Long-Evans rats were >3 mo of age. All procedures were approved by the UC Berkeley Animal Care and Use Committee (protocol R309-0516BC) and comply with NIH guidelines.

FFF-SMF-FMS-SSS Discrimination Task

The computer-automated chamber contained a nose poke, flanked by a wall-mounted whisker stimulus panel (2 x 2 cm) that was carried on a hidden piezoelectric actuator (Piezo Systems PSI-5H4E). Whiskers were trimmed to 15 mm in length. The right-side C, D, and E row whisker tips rested against the panel while the rat was in the nose poke (Fig 1A). Nearby right and left drink

ports contained infrared-LED beam sensors to detect nose entry and delivered calibrated water rewards. Trials were monitored by infrared video.

Each trial was self-initiated by entry into the nose poke. After a variable delay (75–100 ms), a sequence of three rapid whisker deflections was delivered via the panel. The rat was required to remain in the nose poke for 250 ms to ensure full sequence delivery. The rat then withdrew from the nose poke and was rewarded (0.05–0.1 mL water) for choosing the drink port that was associated with the presented stimulus. Incorrect drink port choice or premature nose poke withdrawal triggered a time-out tone (4–6 s) and no reward. In a subset of sessions, high-speed video (119 Hz) was recorded.

Whisker sequences

Each whisker deflection sequence consisted of three up-down ramp-return deflections (pulses). Each pulse had either slow (S), medium (M), or fast (F) rise-fall velocity. These pulses differed in rise-fall time and therefore had different pulse durations but similar amplitude (Fig 1B and 1C; Table 1). Sequences had either FFF, FMS, SMF, or SSS pulse order, with 34 ms between the end of one pulse and the beginning of the next, yielding 50–62 ms interval between pulse onsets. Total train duration (from beginning of the first pulse to end of the last pulse) was 120–146 ms. Mean speed, calculated over the entire train, was highest for FFF, intermediate and equal for FMS and SMF, and lowest for SSS sequences (Fig 1D; Table 1; S1 Fig). One sequence was presented per trial, with random order across trials. Training was in the dark, and acoustic cues were obscured using masking noise composed of white noise densely intermixed with sampled piezo sounds. To further mask any unintended auditory cues, an additional "dummy" piezo was hidden behind the stimulus panel and actuated on each trial in a manner uncorrelated with panel movement.

Table 1. Knematiics of FFF-FMS-SMF-SSS whisker sequences

Impulse	Rise/Fall Time (ms)	Peak Velocity (mm/s)	Duration* (ms)	Peak Amplitude (mm)
Fast (F)	8	220	16	1.03
Medium (M)	11	170	22	1.15
Slow (S)	14	110	28	1.14

Sequence	Interpulse Interval (ms)	Peak Velocity (mm/s)	Duration* (ms)	Peak amplitude (mm)
FFF	34	120	65.7	Right
FMS	34	132	54.4	Right
SMF	34	132	54.7	Left
SSS	34	148	44.6	Left

* Duration measured as time from initial deflection to return to baseline position.

Training stages and reward contingency

First, rats were trained to nose poke for >150 ms and to drink from the drink ports. Next, rats were presented in the nose poke with exaggerated amplitude and velocity versions of FFF and SSS stimuli and were trained to choose the right drink port for FFF stimuli and the left drink port for SSS. When each rat achieved >60% correct, stimulus amplitude was stepped closer to the final amplitude, and the nose poke time requirement was incrementally increased. This was iterated until the final stimulus amplitude and 250 ms nose poke time requirement were reached. Rats then performed FFF versus SSS discrimination using final-amplitude stimuli for 1–4 wk. At this point, the chronic recording drive was implanted, rats rested for 1 week of recovery, and then training was re-initiated until performance regained pre-surgical levels, usually about a week. Finally, FMS and SMF stimuli were added (rewarded right and left, respectively). All behavioral and neural data reported in the study were collected during this final stage.

FSFS-SFFS Discrimination Task

In this task, each whisker sequence consisted of four pulses. Two pulses were low-amplitude, slow pulses (S) that were 0.7 mm amplitude, 120 mm/sec peak velocity, 12.5 ms rise and fall time, and 25 ms total duration. Two were higher-amplitude, fast pulses (F) that were 1.2 mm amplitude, 216 mm/sec peak velocity, 9 ms rise and fall time, and 18 ms total duration. Trains of F-S-F-S or F-S-S-F pulses were presented (34 ms inter-pulse interval, total train duration 188 ms). In the “same-intensity” stimulus set, both FSFS and SFFS trains had identical pulse amplitude and, therefore, mean speed (mean speed 25.7 mm/sec for FSFS, and 26.4 mm/sec for SFFS). In the “different intensity” stimulus set, FSFS stimulus amplitude (and velocity) was increased to achieve a mean speed of 27.8 mm/sec, and SFFS stimulus amplitude (and velocity) was decreased to achieve a mean speed of 8.7 mm/sec. Training was performed in identical steps as above, using the “different-intensity” stimuli at the second training stage. No recordings were performed.

Neural Recordings

Recordings were made with an array of four tetrodes carried in a custom 3D-printed chronic microdrive. Tetrodes (12.5 µm nichrome wire, gold plated to 0.2–0.3 MΩ impedance) were spaced 0.35 mm apart in a square configuration and moved together as a single bundle along a radial penetration. The tetrode drive was mounted in a surgical procedure under initial ketamine-xylazine anesthesia (90 mg/kg and 10 mg/kg), maintained by transition to 0.5%–3% isoflurane. A 4-mm craniotomy was opened over S1 (5.5 mm lateral, 2.5 mm caudal to bregma), the dura was removed, and the microdrive was positioned over the durotomy. The tetrodes were lowered into L2 of S1 and the microdrive was mounted with dental cement,

sealing the craniotomy. Reference and ground electrodes were mounted in the skull. Postoperative analgesia was provided with Buprenorphine (0.05 mg/kg every 8 h) for 1–2 d post-surgery. Animals recovered 5–10 d prior to behavioral and recording sessions.

Recordings were made during one to two behavioral sessions per day for each rat. Tetrode signals were amplified and filtered (Plexon, 100x gain, 0.3–8 kHz bandpass filter) and digitized at 32 kHz, using methods as in[21]. Neural data was acquired continuously. Tetrodes were advanced a half-turn (140 µm) every one to two recording sessions, at least 30 min before recording started. A new set of units was sampled in every session. If new units appeared spontaneously overnight, the tetrode was not advanced. Recording ended when the tetrode entered the white matter, as judged by absence of spiking activity when advancing the drive. Twelve to 22 d of recording were performed per animal.

Recordings were made in C1–4, D2–4, and E3 whisker columns, as determined by hand mapping under isoflurane anesthesia prior to the recording sessions. An electrolytic lesion was made at the final recording location to determine recording depth. Lesions were recovered in cytochrome oxidase-stained histological sections (100 µm thick) cut in the "across-row" plane, 45^{o} coronal to the midsagittal plane[52,53]. This allowed the whisker row identity (A–E) of the recorded column and laminar identity of recording sites to be confirmed. Laminar boundaries were determined by aligning lesions with layer-specific CO staining boundaries, and were as follows: L2/3: 200–650 µm, L4: 650–975 µm; L5A: 975–1285 µm; L5B: 1285–1575 µm; L6: 1575–2200 µm.

Single units were isolated offline using Wave_clus in Matlab[54]. After an initial automated clustering step, manual evaluation of all clusters was performed and manual changes to the clustering were carried out as needed. Single units were required to meet an interspike interval criterion (<0.5% of intervals less than 1.5 ms) and a signal-to-noise (STN) criterion for spike height (STN>2, with STN defined as the difference from trough to peak in the mean waveform divided by the average standard deviation across all samples in the waveform). Fast-spiking and regular-spiking units were classified by spike width, which was bimodally distributed. Fast spiking units had width <0.375 ms trough-peak delay.

Neural Data Analysis

Neural data were analyzed for five rats, including one rat for whom the fixed-panel control task showed substantial task performance in the absence of panel movement (filled circles in Fig 2D). This rat's data were included because panel-evoked responses, stimulus decoding, and choice decoding did not differ from other rats (not shown).

Temporal response modulation: We identified units whose firing rate was significantly temporally modulated during the stimulus presentation period (0–180 ms after NP entry) using a permutation test [55]. Measured firing rate was compared in 10-ms bins with randomly time-

permuted spikes (10,000 permutations). Units with significant difference from permuted data ($p < 0.05$) were considered temporally modulated and were included in further analysis.

Stimulus-evoked responses: PSTHs were calculated with 1 ms time bins, aligned to onset of the first impulse. Unit PSTHs were smoothed (10 ms boxcar) for display only (Fig 4). Stimulus-evoked firing modulation quantifies the peak evoked response in a 40-ms window post-stimulus. It was calculated as the difference between mean baseline firing rate (0–10 ms prior to pulse onset) and maximum or minimum firing rate anywhere in a 40 ms window after stimulus onset (with 10 ms smoothing). Peak response latency was defined as the time of this maximum response. Mean impulse-evoked firing rate was quantified in a 5–35 ms window after impulse onset. Impulse-responsive units were defined as those neurons whose mean impulse-evoked firing rate was significantly greater than baseline firing rate (0–10 ms before impulse onset) by *t* test.

Stimulus regression: We performed a multiple regression to determine the optimal stimulus integration window for each unit. The neural responses from 0 to 180 ms relative to stimulus onset were binned into 5 ms windows and used as the dependent variable in this regression. The independent variables (regressors) were the integrated speed of the panel over a series of fixed integration windows, from 5 to 180 ms in 5-ms steps. Each speed bin (e.g., from -20 to 0 ms in the 20 ms integration window regression) was used to predict firing rate in the subsequent 5-ms bin (from 0 to 5 ms in this example). For cells that had significant regressions in at least one stimulus integration window ($p < 0.05/36 = 0.0014$, Bonferroni correction for 36 integration windows tested), the best fit integration window was taken as the stimulus integration window with the highest R^2 value. Regression was performed in Matlab. Integration window is not independent from latency in this analysis; however, inspection of PSTHs shows that units identified by the regression as having progressively longer best integration windows exhibited progressively slower whisker-evoked responses, not just longer latencies (Figs 7A, 7B, 8A, and 8B).

Neural Decoders

A neural decoder was constructed to predict stimulus identity (FFF, FMS, SMF, SSS) from single-trial spike trains of the recorded units. Each unit was represented by a one-versus-all (OVA) classifier that was trained by logistic regression to report the probability of each stimulus given a single-trial spike train (0–150 ms after stimulus onset, binned using either 10 ms bins or a single fixed time bin), selected randomly from recorded spike trains for that unit. Each classifier comprised four logistic functions, one for each stimulus. Logistic functions were fit using logistic regression and k-fold cross-validation and were specified by coefficients (one for each time bin, plus a bias term) that relate spike rate in each time bin to the probability of stimulus *s* being delivered. Model fitting was performed using a randomly chosen subset of the recorded trials (70%), and decoder performance was assessed on the remaining trials. The output of

each unit classifier was normalized so that each unit had the same weight in population decoding. The population stimulus prediction s_p was calculated by summing the probabilities of each stimulus over all units and selecting the stimulus with the maximal summed probability. Model fitting and population decoding were repeated 300 times, and average performance is reported. This framework is equivalent to determining s_p as the stimulus that maximizes the conditional probability of the four stimuli given the neural population response, assuming that all single units are independent and the prior distribution of s is uniform. Rate-normalized and time-scrambled spike trains were generated by dividing each spike train by its -Euclidean norm and shuffling spike times within trials, respectively.

A separate behavioral choice decoder was constructed similarly and was used for predicting right or left drink port choice on a given trial. Since this is a binary decision, a single logistic function was fit for each unit. The model was fit using spike train and behavioral choice data from all four stimuli. Decoder performance was assessed separately for FFF, FMS, SMF, or SSS stimulus trials in order to dissociate stimulus identity from the rat's behavioral choice. The population choice prediction c_p was selected as the choice with maximal summed probability across all units, given single-trial spike trains from trials with the chosen stimulus type. Model fitting and decoding procedures were the same as above. All decoding analysis was performed using Python and the scikit-learn machine learning toolbox [56].

2.7 References

1. Romo R, Salinas E. Flutter discrimination: neural codes, perception, memory and decision making. Nat Rev Neurosci. 2003;4: 203–218. doi:10.1038/nrn1058

2. Gold JI, Shadlen MN. The neural basis of decision making. Annu Rev Neurosci. 2007;30: 535–574. doi:10.1146/annurev.neuro.29.051605.113038

3. Arabzadeh E, Zorzin E, Diamond ME. Neuronal encoding of texture in the whisker sensory pathway. PLoS Biol. 2005;3: e17. doi:10.1371/journal.pbio.0030017

4. Wolfe J, Hill DN, Pahlavan S, Drew PJ, Kleinfeld D, Feldman DE. Texture coding in the rat whisker system: slip-stick versus differential resonance. PLoS Biol. 2008;6: e215. doi:10.1371/journal.pbio.0060215

5. O'Connor DH, Clack NG, Huber D, Komiyama T, Myers EW, Svoboda K. Vibrissa-based object localization in head-fixed mice. The Journal of Neuroscience. 2010;30: 1947–1967. doi:10.1523/JNEUROSCI.3762-09.2010

6. Andrew Hires S, Gutnisky DA, Yu J, O'Connor DH, Svoboda K. Low-noise encoding of active touch by layer 4 in the somatosensory cortex. Elife. 2015;4.

doi:10.7554/eLife.06619

7. Stüttgen MC, Schwarz C. Psychophysical and neurometric detection performance under stimulus uncertainty. Nature Neuroscience. 2008;11: 1091–1099. doi:10.1038/nn.2162

8. Waiblinger C, Brugger D, Schwarz C. Vibrotactile discrimination in the rat whisker system is based on neuronal coding of instantaneous kinematic cues. Cereb Cortex. 2015;25: 1093–1106. doi:10.1093/cercor/bht305

9. Ollerenshaw DR, Bari BA, Millard DC, Orr LE, Wang Q, Stanley GB. Detection of tactile inputs in the rat vibrissa pathway. J Neurophysiol. 2012;108: 479–490. doi:10.1152/jn.00004.2012

10. Stüttgen MC, Schwarz C. Integration of vibrotactile signals for whisker-related perception in rats is governed by short time constants: comparison of neurometric and psychometric detection performance. The Journal of Neuroscience. 2010;30: 2060–2069. doi:10.1523/JNEUROSCI.3943-09.2010

11. Sachidhanandam S, Sreenivasan V, Kyriakatos A, Kremer Y, Petersen CCH. Membrane potential correlates of sensory perception in mouse barrel cortex. Nature Neuroscience. 2013;16: 1671–1677. doi:10.1038/nn.3532

12. Gerdjikov TV, Bergner CG, Stüttgen MC, Waiblinger C, Schwarz C. Discrimination of vibrotactile stimuli in the rat whisker system: behavior and neurometrics. Neuron. 2010;65: 530–540. doi:10.1016/j.neuron.2010.02.007

13. Adibi M, Diamond ME, Arabzadeh E. Behavioral study of whisker-mediated vibration sensation in rats. Proc Natl Acad Sci USA. 2012;109: 971–976. doi:10.1073/pnas.1116726109

14. Simons DJ. Response properties of vibrissa units in rat SI somatosensory neocortex. J Neurophysiol. 1978;41: 798–820.

15. Khatri V, Hartings JA, Simons DJ. Adaptation in thalamic barreloid and cortical barrel neurons to periodic whisker deflections varying in frequency and velocity. J Neurophysiol. 2004;92: 3244–3254. doi:10.1152/jn.00257.2004

16. Castro-Alamancos MA. Absence of rapid sensory adaptation in neocortex during information processing states. Neuron. 2004;41: 455–464.

17. Chung S, Li X, Nelson SB. Short-term depression at thalamocortical synapses contributes to rapid adaptation of cortical sensory responses in vivo. Neuron. 2002;34: 437–446.

18. Hirata A, Castro-Alamancos MA. Effects of cortical activation on sensory responses in barrel cortex. J Neurophysiol. 2011;105: 1495–1505. doi:10.1152/jn.01085.2010

19. O'Connor DH, Hires SA, Guo ZV, Li N, Yu J, Sun Q-Q, et al. Neural coding during active somatosensation revealed using illusory touch. Nature Neuroscience. 2013;16: 958–965. doi:10.1038/nn.3419

20. Yamashita T, Pala A, Pedrido L, Kremer Y, Welker E, Petersen CCH. Membrane potential dynamics of neocortical projection neurons driving target-specific signals. Neuron. 2013;80: 1477–1490. doi:10.1016/j.neuron.2013.10.059

21. Jadhav SP, Wolfe J, Feldman DE. Sparse temporal coding of elementary tactile features during active whisker sensation. Nature Neuroscience. 2009;12: 792–800. doi:10.1038/nn.2328

22. Miyashita T, Feldman DE. Behavioral Detection of Passive Whisker Stimuli Requires Somatosensory Cortex. Cereb Cortex. 2012. doi:10.1093/cercor/bhs155

23. Adibi M, Arabzadeh E. A comparison of neuronal and behavioral detection and discrimination performances in rat whisker system. J Neurophysiol. 2011;105: 356–365. doi:10.1152/jn.00794.2010

24. de Kock CPJ, Sakmann B. High frequency action potential bursts (>or= 100 Hz) in L2/3 and L5B thick tufted neurons in anaesthetized and awake rat primary somatosensory cortex. J Physiol (Lond). 2008;586: 3353–3364. doi:10.1113/jphysiol.2008.155580

25. Crochet S, Poulet JFA, Kremer Y, Petersen CCH. Synaptic mechanisms underlying sparse coding of active touch. Neuron. 2011;69: 1160–1175. doi:10.1016/j.neuron.2011.02.022

26. Fanselow EE, Nicolelis MA. Behavioral modulation of tactile responses in the rat somatosensory system. The Journal of Neuroscience. 1999;19: 7603–7616.

27. Barth AL, Poulet JFA. Experimental evidence for sparse firing in the neocortex. Trends Neurosci. 2012;35: 345–355. doi:10.1016/j.tins.2012.03.008

28. de Kock CPJ, Bruno RM, Spors H, Sakmann B. Layer- and cell-type-specific suprathreshold stimulus representation in rat primary somatosensory cortex. J Physiol (Lond). 2007;581: 139–154. doi:10.1113/jphysiol.2006.124321

29. Luna R, Hernandez A, Brody CD, Romo R. Neural codes for perceptual discrimination in primary somatosensory cortex. Nature Neuroscience. 2005;8: 1210–1219. doi:10.1038/nn1513

30. Diamond ME. Texture sensation through the fingertips and the whiskers. Curr Opin Neurobiol. 2010;20: 319–327. doi:10.1016/j.conb.2010.03.004

31. Jadhav SP, Feldman DE. Texture coding in the whisker system. Curr Opin Neurobiol. 2010;20: 313–318. doi:10.1016/j.conb.2010.02.014

32. Ritt JT, Andermann ML, Moore CI. Embodied information processing: vibrissa mechanics and texture features shape micromotions in actively sensing rats. Neuron. 2008;57: 599–613. doi:10.1016/j.neuron.2007.12.024

33. Zuo Y, Perkon I, Diamond ME. Whisking and whisker kinematics during a texture classification task. Philos Trans R Soc Lond, B, Biol Sci. 2011;366: 3058–3069. doi:10.1098/rstb.2011.0161

34. Pammer L, O'Connor DH, Hires SA, Clack NG, Huber D, Myers EW, et al. The mechanical variables underlying object localization along the axis of the whisker. The Journal of Neuroscience. 2013;33: 6726–6741. doi:10.1523/JNEUROSCI.4316-12.2013

35. Heimendahl von M, Itskov PM, Arabzadeh E, Diamond ME. Neuronal activity in rat barrel cortex underlying texture discrimination. PLoS Biol. 2007;5: e305. doi:10.1371/journal.pbio.0050305

36. Zuo Y, Safaai H, Notaro G, Mazzoni A, Panzeri S, Diamond ME. Complementary contributions of spike timing and spike rate to perceptual decisions in rat S1 and S2 cortex. Curr Biol. 2015;25: 357–363. doi:10.1016/j.cub.2014.11.065

37. Johnson KO, Hsiao SS, Yoshioka T. Neural coding and the basic law of psychophysics. Neuroscientist. 2002;8: 111–121.

38. Waiblinger C, Brugger D, Whitmire CJ, Stanley GB, Schwarz C. Support for the slip hypothesis from whisker-related tactile perception of rats in a noisy environment. Front Integr Neurosci. 2015;9: 53. doi:10.3389/fnint.2015.00053

39. Romo R, Brody CD, Hernandez A, Lemus L. Neuronal correlates of parametric working memory in the prefrontal cortex. Nature. 1999;399: 470–473. doi:10.1038/20939

40. Hernandez A, Zainos A, Romo R. Neuronal correlates of sensory discrimination in the somatosensory cortex. Proc Natl Acad Sci USA. 2000;97: 6191–6196.

41. Armstrong-James M, Fox K. Spatiotemporal convergence and divergence in the rat S1 “barrel” cortex. J Comp Neurol. 1987;263: 265–281. doi:10.1002/cne.902630209

42. Oberlaender M, Boudewijns ZSRM, Kleele T, Mansvelder HD, Sakmann B, de Kock CPJ. Three-dimensional axon morphologies of individual layer 5 neurons indicate cell type-specific intracortical pathways for whisker motion and touch. Proc Natl Acad Sci USA. 2011;108: 4188–4193. doi:10.1073/pnas.1100647108

43. Pitas A, Albarracin AL, Molano-Mazon M, Maravall M. Variable Temporal Integration of Stimulus Patterns in the Mouse Barrel Cortex. Cereb Cortex. 2016. doi:10.1093/cercor/bhw006

44. Webber RM, Stanley GB. Nonlinear encoding of tactile patterns in the barrel cortex. J

Neurophysiol. 2004;91: 2010–2022.

45. Britten KH, Newsome WT, Shadlen MN, Celebrini S, Movshon JA. A relationship between behavioral choice and the visual responses of neurons in macaque MT. Vis Neurosci. 1996;13: 87–100.

46. Nienborg H, Cohen MR, Cumming BG. Decision-related activity in sensory neurons: correlations among neurons and with behavior. Annu Rev Neurosci. 2012;35: 463–483. doi:10.1146/annurev-neuro-062111-150403

47. Romo R, Hernandez A, Zainos A, Lemus L, Brody CD. Neuronal correlates of decision-making in secondary somatosensory cortex. Nature Neuroscience. 2002;5: 1217–1225.

48. de Lafuente V, Romo R. Neural correlate of subjective sensory experience gradually builds up across cortical areas. Proc Natl Acad Sci USA. 2006;103: 14266–14271. doi:10.1073/pnas.0605826103

49. Yang H, Kwon SE, Severson KS, O'Connor DH. Origins of choice-related activity in mouse somatosensory cortex. Nature Neuroscience. 2016;19: 127–134. doi:10.1038/nn.4183

50. Liu S, Gu Y, DeAngelis GC, Angelaki DE. Choice-related activity and correlated noise in subcortical vestibular neurons. Nature Neuroscience. 2013;16: 89–97. doi:10.1038/nn.3267

51. Bureau I, Saint Paul von F, Svoboda K. Interdigitated paralemniscal and lemniscal pathways in the mouse barrel cortex. PLoS Biol. 2006;4: e382. doi:10.1371/journal.pbio.0040382

52. Finnerty GT, Roberts LS, Connors BW. Sensory experience modifies the short-term dynamics of neocortical synapses. Nature. 1999;400: 367–371. doi:10.1038/22553

53. Allen CB, Celikel T, Feldman DE. Long-term depression induced by sensory deprivation during cortical map plasticity in vivo. Nature Neuroscience. 2003;6: 291–299. doi:10.1038/nn1012

54. Quiroga RQ, Nadasdy Z, Ben-Shaul Y. Unsupervised spike detection and sorting with wavelets and superparamagnetic clustering. Neural Comput. 2004;16: 1661–1687. doi:10.1162/089976604774201631

55. Good P. Permutation Tests. 2nd ed. Heidelberg: Springer; 2000.

56. Pedregosa F, Varoquaux G, Gramfort A, Michel V, Thirion B, Grisel O, et al. Scikit-learn: Machine Learning in Python. Journal of Machine Learning Research. 2011;12: 2825–2803.

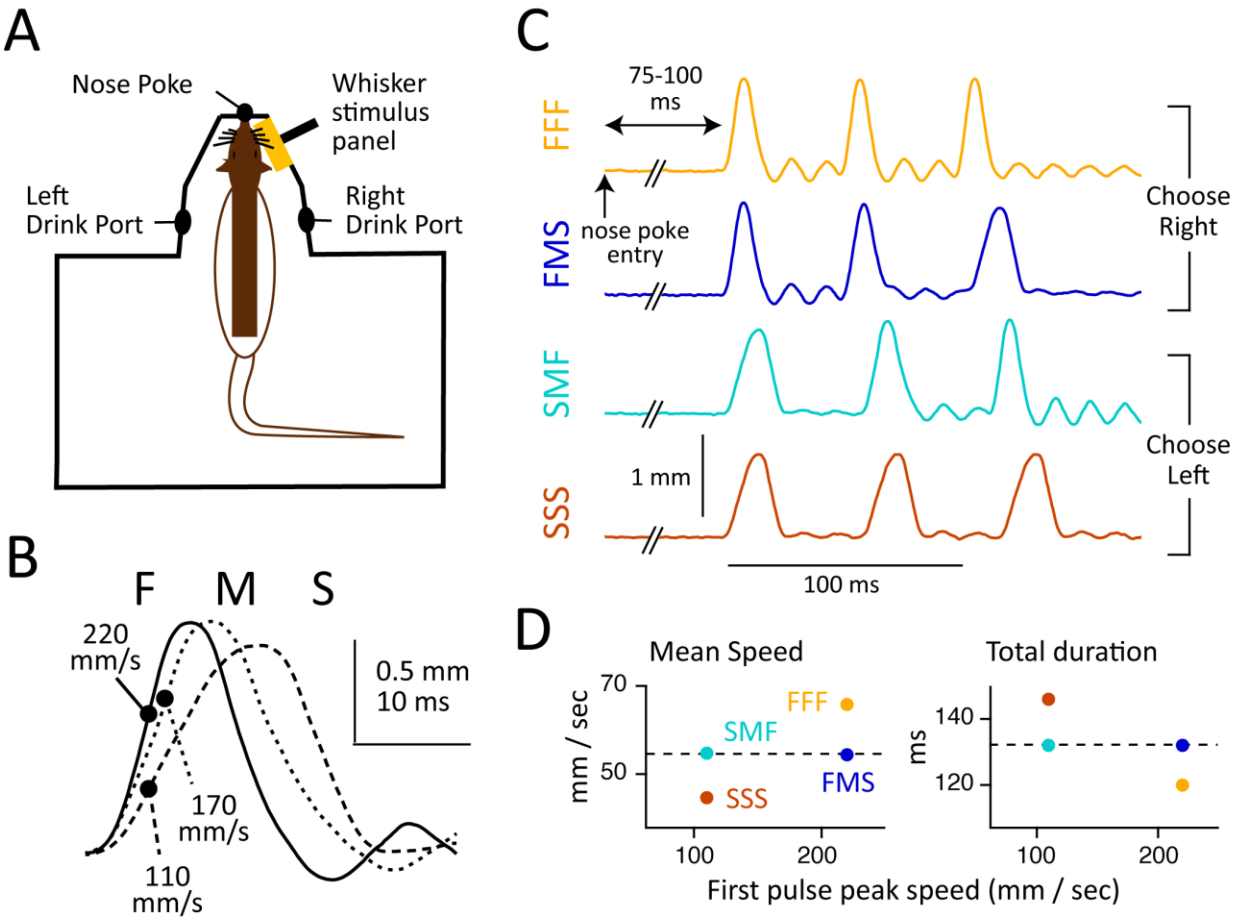

Fig 1. Whisker stimuli and behavioral apparatus. (A) Schematic of training apparatus, showing the rat's right whiskers resting on the moveable stimulus panel. (B) Panel kinematics for fast, medium, and slow impulses. Circles indicate maximum velocity. (C) Panel kinematics for FFF, FMS, SMF, and SSS sequences. Data for this panel are in S1 Data. (D) Mean speed, total duration, and first pulse peak velocity for the four sequences. SMF and FMS sequences had similar mean speed and duration (dashed lines).

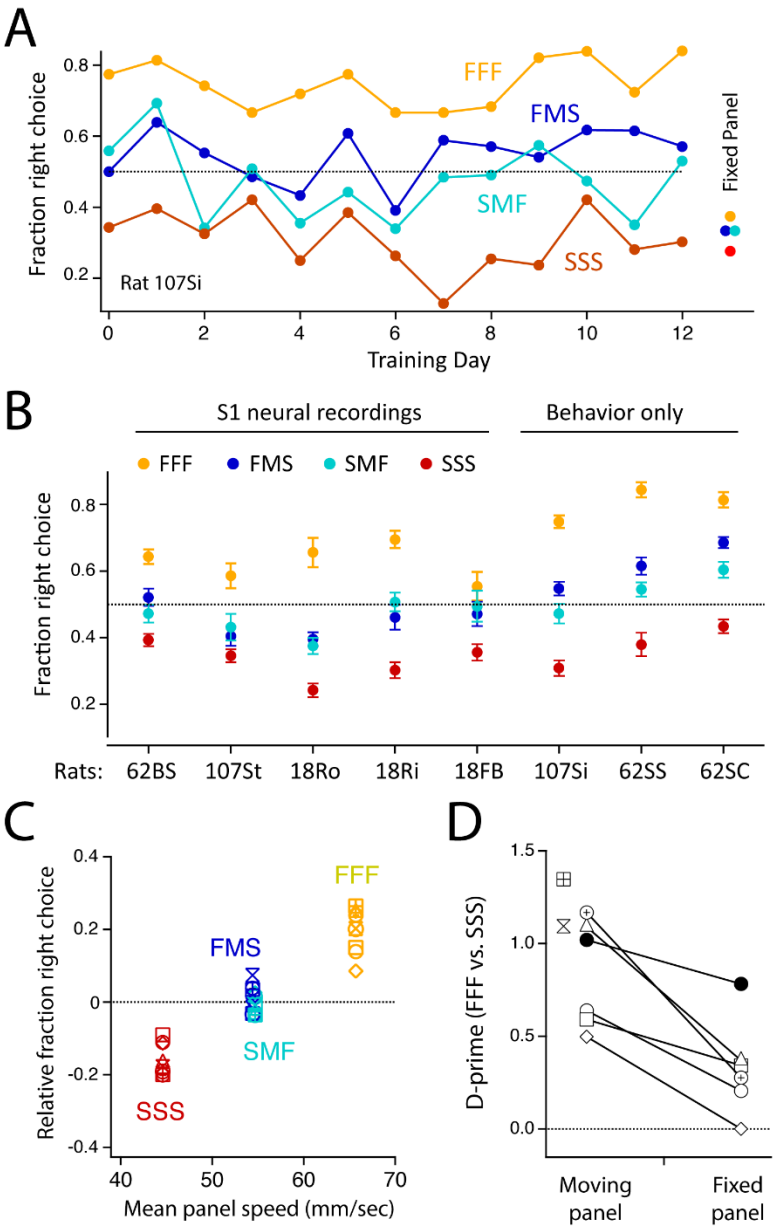

Fig 2. Behavioral performance on FFF-FMS-SMF-SSS discrimination task. (A) Discrimination performance for one example rat, across 13 d of training (44–50 trials for each stimulus per day). FMS and SMF stimuli were first introduced on Day 0. The rat reliably discriminated FFF from SSS stimuli but treated FMS and SMF stimuli identically and at chance. The rat responded similarly to all stimuli when the panel was fixed, and thus was not discriminating based on piezo auditory cues. (B) Mean performance (± SEM) for all rats across all behavior sessions. (C) Relative right drink port choice as a function of mean panel speed over the entire 150-ms sequence. Each symbol is a different rat (n = 8). (D) D-prime analysis of FFF versus SSS discrimination in fixed-panel control experiments versus normal sessions. Solitary points show rats not tested on the fixed-panel control. Data for this figure are in S1 Data.

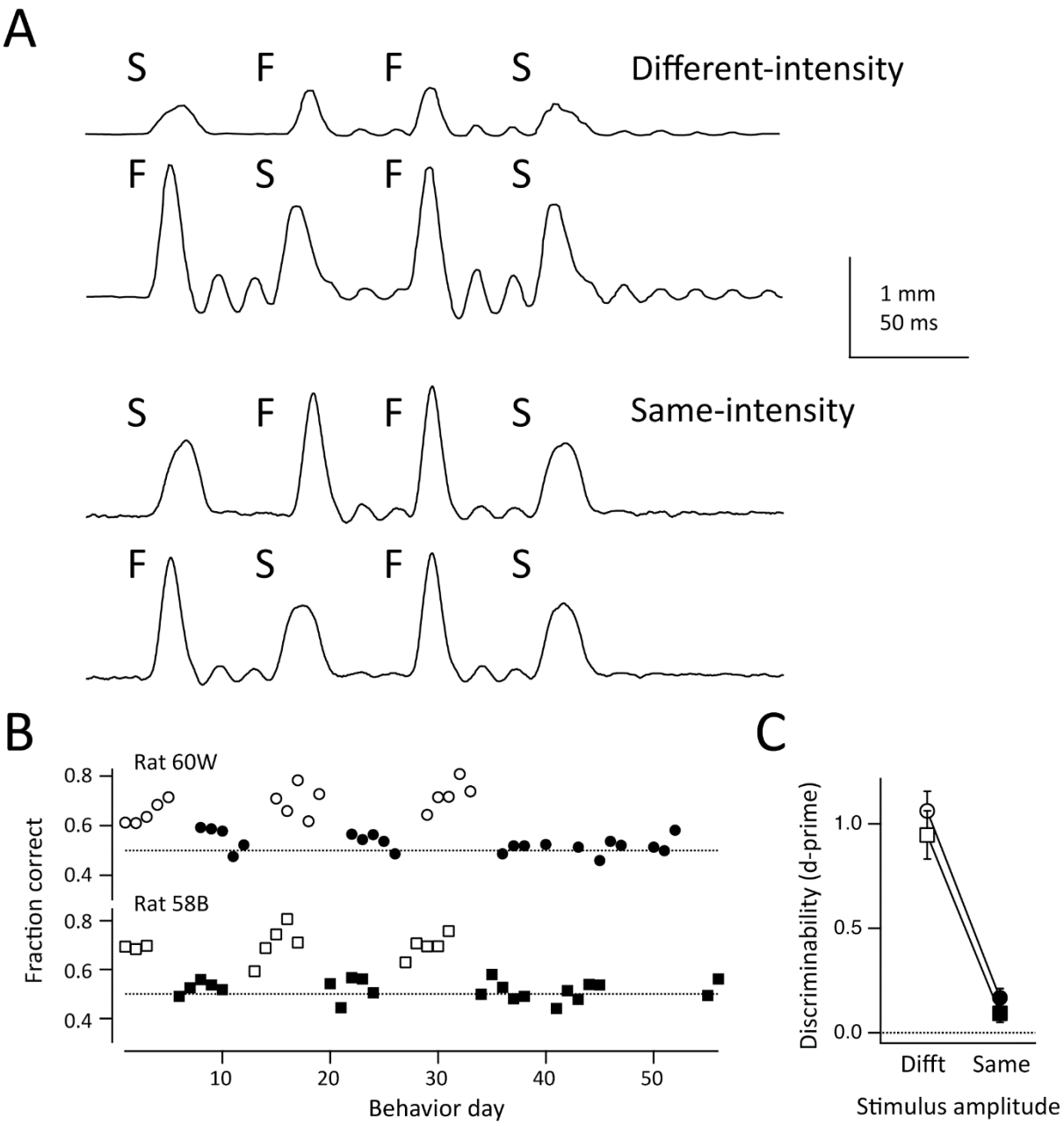

Fig 3. Behavioral performance on FSFS-SFFS discrimination task. (A) Panel kinematics for SFFS and FSFS sequences, showing both different-intensity and same-intensity versions. (B) Behavioral performance across all behavioral sessions, for the two rats trained on this task. Open symbols: sessions using the different-intensity version of the stimuli. Filled symbols: the same-intensity version. Both rats could discriminate the different-intensity version but not the same-intensity version. (C) D-prime analysis of discrimination performance for the same two rats (circles: 60W, squares: 58B), across all behavioral sessions. Symbols are mean ± SEM across sessions. Data for this figure are in S1 Data.

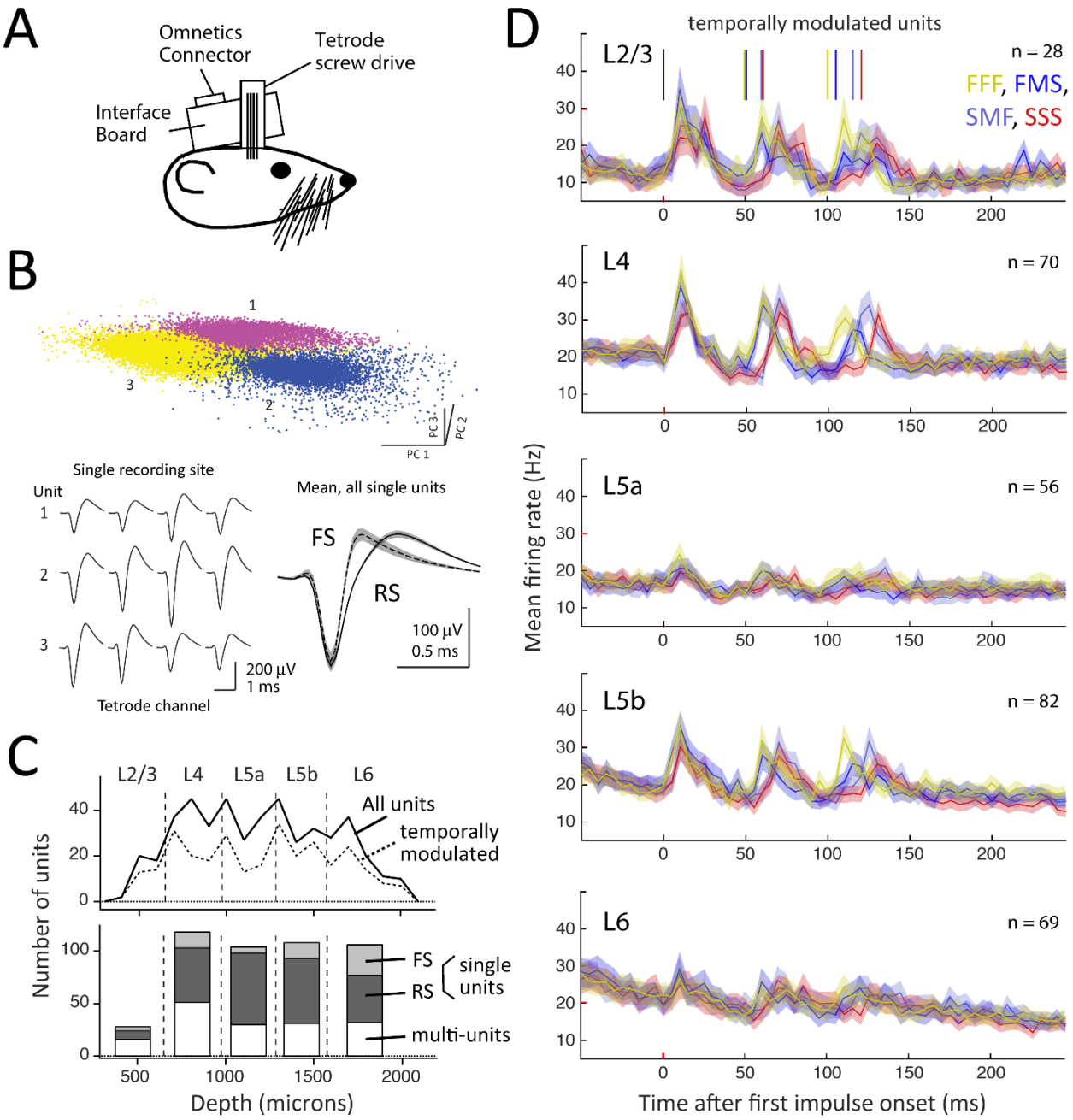

Fig 4. S1 recordings during discrimination behavior. (A) Schematic of multi-tetrode chronic microdrive. (B) Cluster separation for one recording site (top) with mean spike waveforms for three simultaneously recorded single units (bottom left). Bottom right, mean spike waveform for all fast-spike (FS) and regular-spike (RS) single units. (C) Laminar distribution of recorded units. (D) Population peri-stimulus time histogram (PSTH) for all temporally modulated units by layer and stimulus type. Different sequences have different onset times for impulses 2 and 3 (colored ticks). Data for this figure are at crcns.org repository (accession ssc-4).

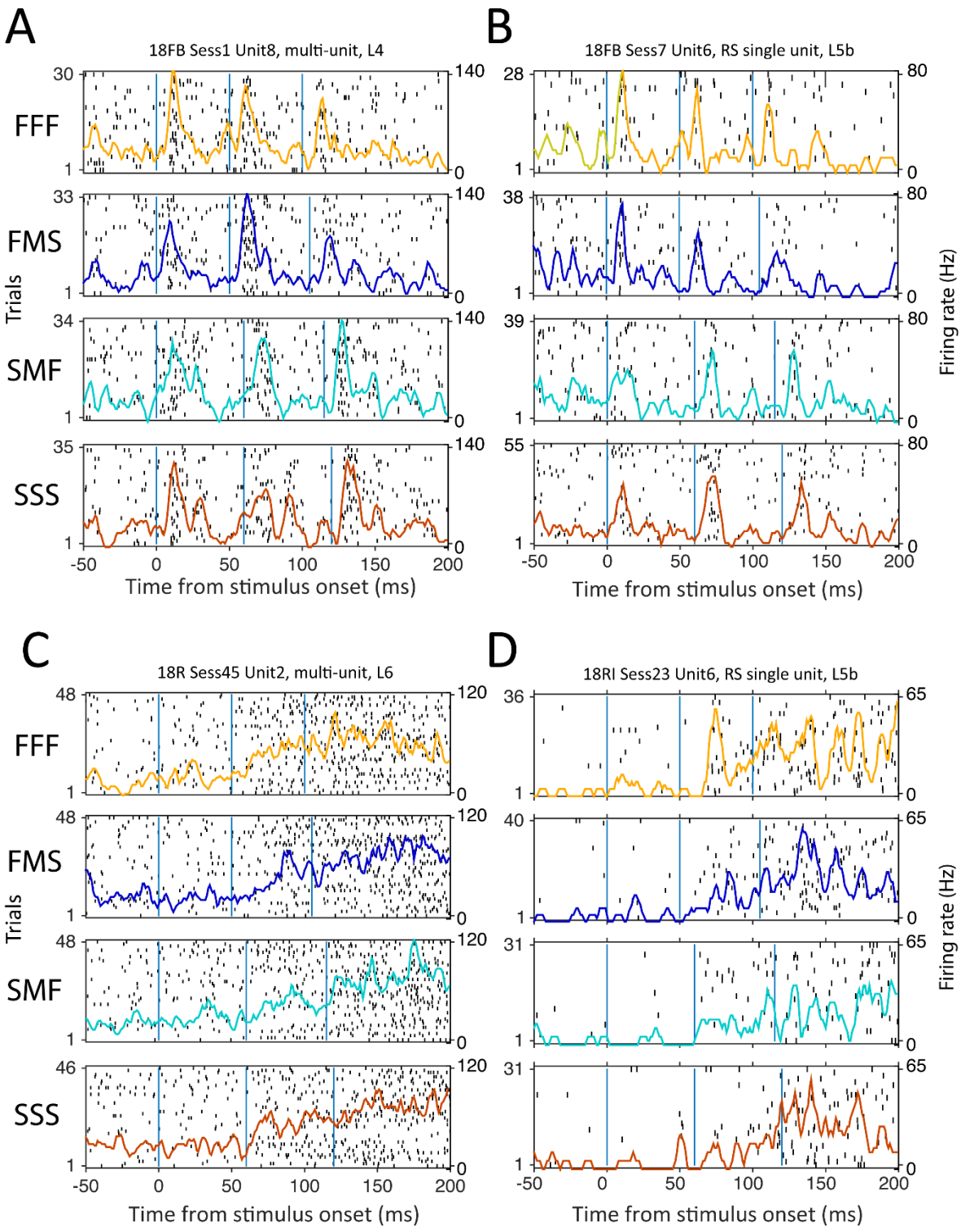

Fig 5. Sequence responses for example units. (A and B) L4 multi-unit and L5b RS single unit with phasic response to each impulse. (C and D) L6 multi-unit and L5b RS single unit with increasing firing rate during the stimulus period. Each panel shows the spike raster and PSTH across trials, for one stimulus sequence. Vertical lines: onset of each impulse. Data for this figure are at crcns.org repository (accession ssc-4).

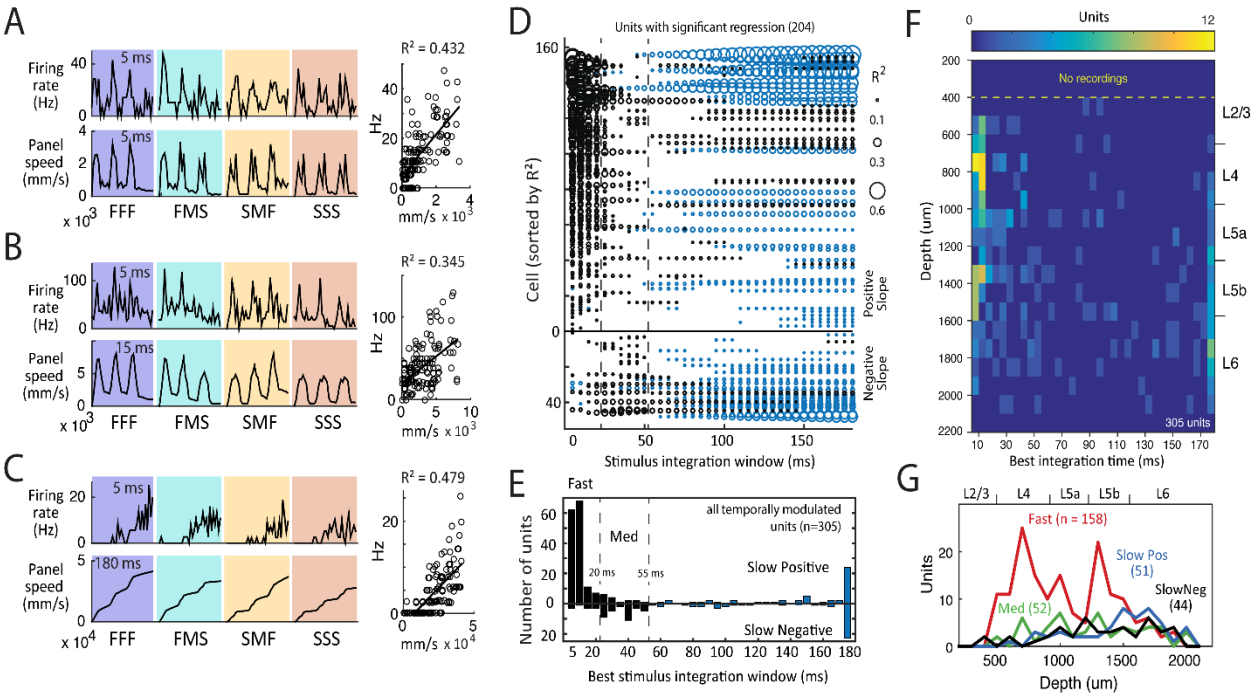

Fig 6. Classification of S1 units by stimulus regression. (A–C) Stimulus regression for three example units. Top, PSTH in 5 ms time bins. Bottom, stimulus panel speed integrated over 5, 15, or 180 ms, which was the best fit stimulus integration window for each unit. Right, regression of firing rate on integrated stimulus speed. (D) Coefficient of determination (R^2) for all stimulus integration windows with a significant regression, for each unit with a significant regression to at least one window. Black: Fast and Medium time scale units (best integration window <55 ms). Blue: Slow units. Cells are sorted by peak R^2 and by sign of the regression slope for the best integration window. (E) Number of units with each best integration window and positive or negative regression slope. (F,G) Laminar distribution of units by best integration window. Data for this figure are in S1 Data.

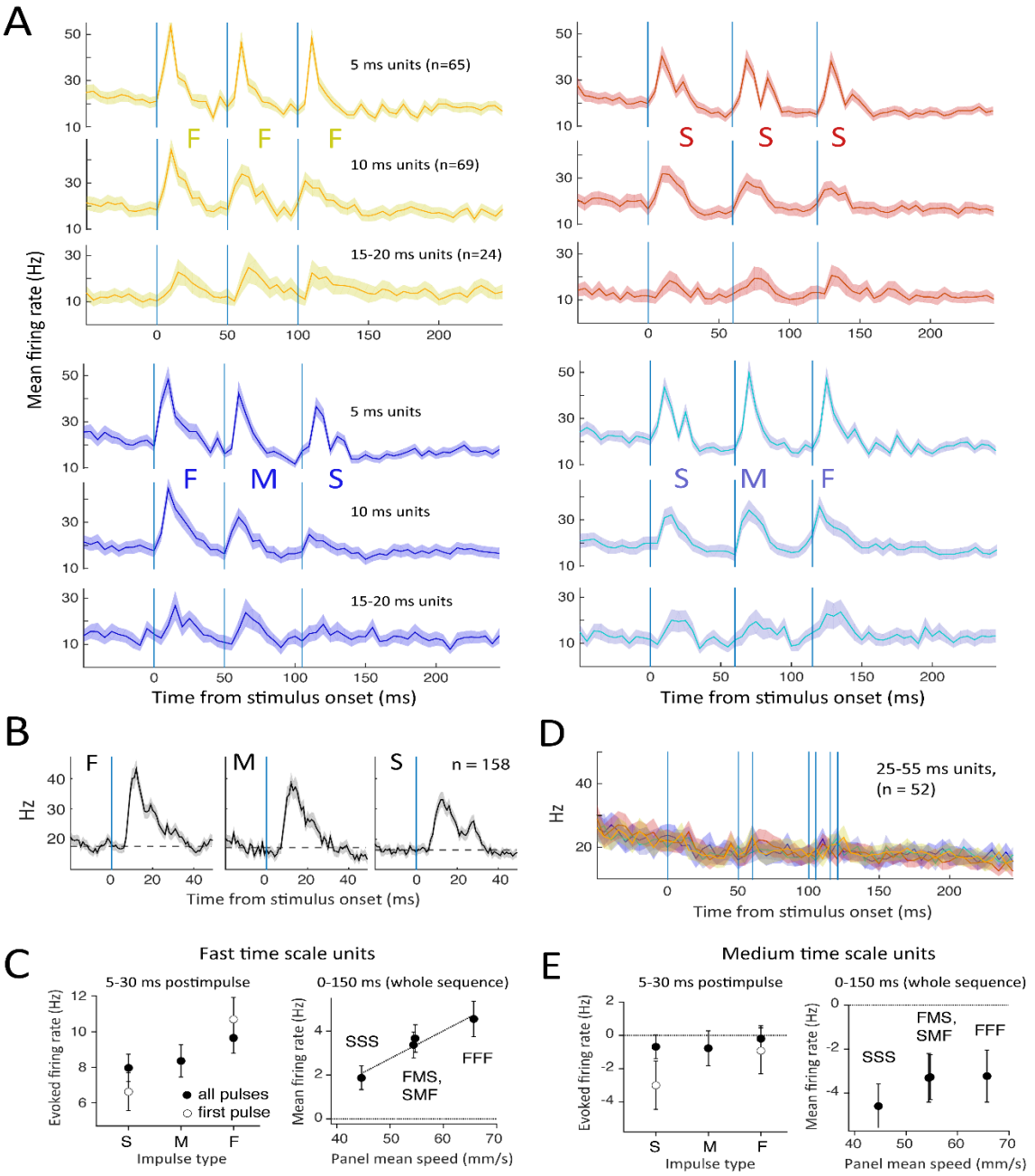

Fig 7. Stimulus coding by fast time scale units. (A) Population PSTH (mean ± SEM) for Fast units with 5, 10, and 15–20 ms best integration windows. (B) Population PSTH for all individual F, M, or S impulses, irrespective of sequence membership, for all Fast units. Dashed line: pre-impulse firing rate. (C) Left: net evoked rate for individual impulses, calculated as post-impulse rate – pre-impulse rate. Right: mean rate across the entire sequence above pre-stimulus baseline, as a function of mean panel speed. Symbols show mean ± SEM across units. Line: regression. (D) Population PSTH for Medium units for FFF, FMS, SMF, and SSS sequences. (E) Net evoked rate for individual impulses and mean rate across the sequence for Medium units. Conventions as in C. Firing rate was suppressed by all impulses and sequences. Data for this figure are at crcns.org repository (accession ssc-4).

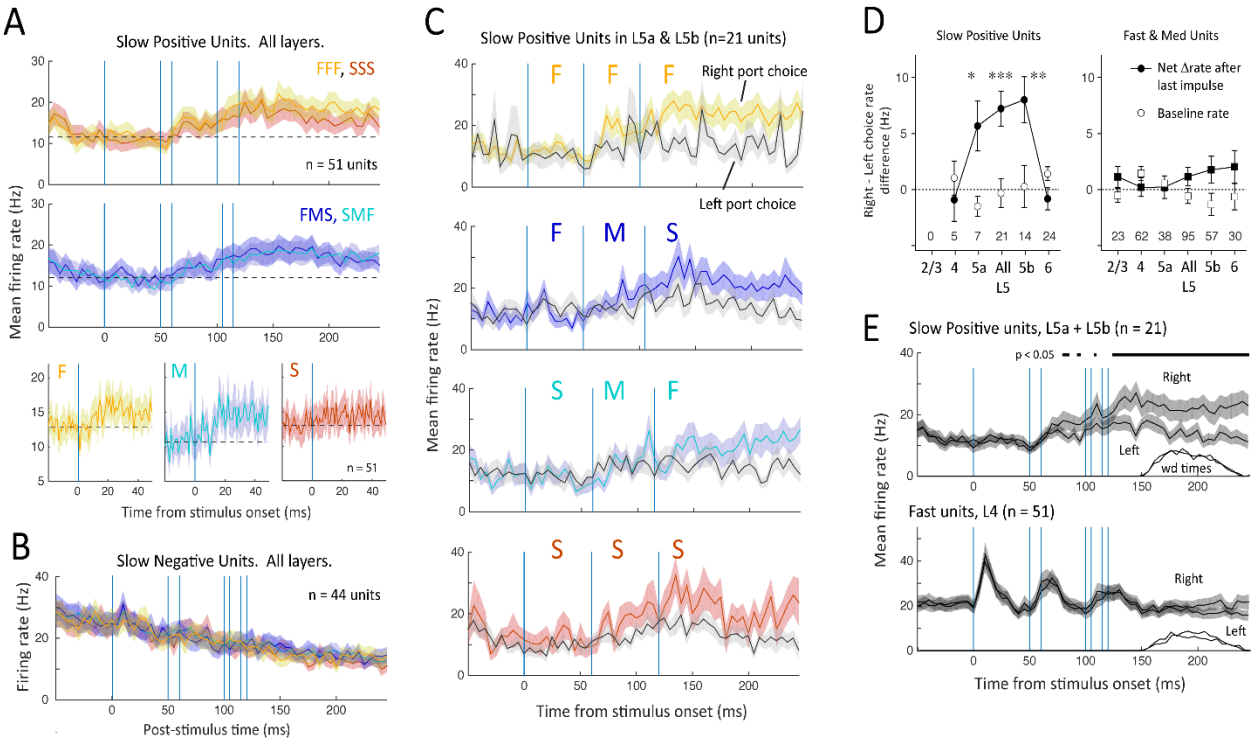

Fig 8. Choice coding by slow time scale units. (A) Top: population PSTH (mean ± SEM) for Slow Positive units across all layers. Responses were indistinguishable between FFF, FMS, SMF and SSS trains. Bottom: population PSTH for individual F, M, and S impulses, irrespective of sequence membership. (B) Population PSTH for slow negative units, showing lack of any impulse-evoked firing rate modulation. (C) Population PSTH for slow positive units in L5a and L5b, separated by stimulus type and drink port choice. Slow Positive units fired more on right-choice trials for all stimuli. (D) Difference in evoked rate between right- and left-choice trials, measured 5–50 ms after start of the final impulse, for all Slow Positive units (left) or Fast and Medium units (right). Number of units in each layer is shown at bottom. Open symbols, baseline rate before sequence onset for the same trials. * $p = 0.022$; ** $p = 9.5^{e-4}$; *** $p = 7.5^{e-5}$, paired t test comparing rate on right versus left choice trials. (E) Population PSTH averaged across all four sequences, for right- versus left-choice trials, for Slow Positive units in L5 (top), and for Fast units in L4 (bottom). Bar shows times when rate is significantly different between right- and left-choice trials by sliding t test ($p < 0.05$). The distribution of nose poke withdrawal times is shown for the same trials. Data for this figure are at crcns.org repository (accession ssc-4).

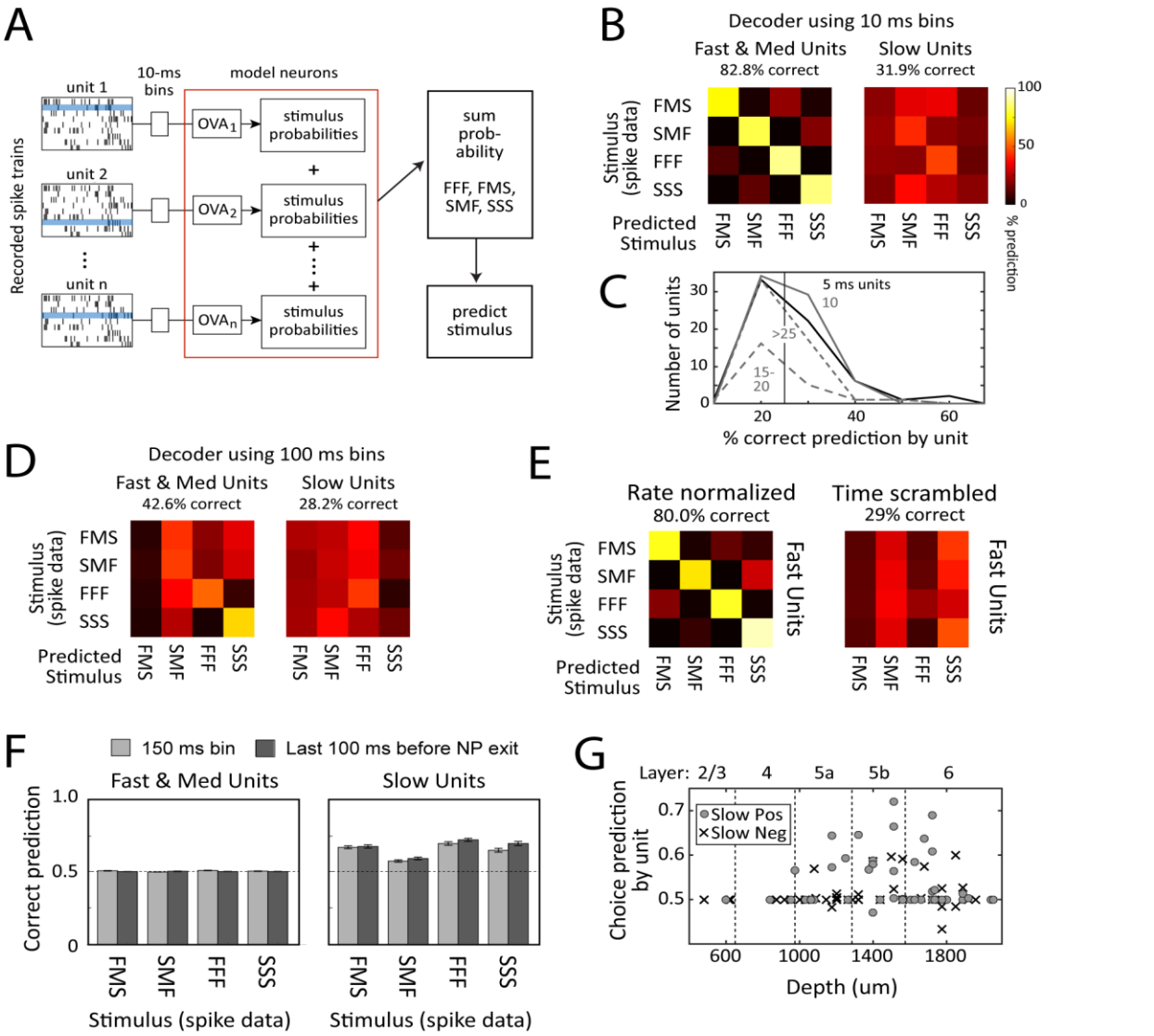

Fig 9. Population decoding of sequence identity and behavioral choice. (A) Decoder architecture for stimulus decoding. Each neuron was represented by a one-versus-all (OVA) classifier, trained by logistic regression to calculate the probability of each stimulus given a single-trial spike train (blue trial). The stimulus with the highest summed probability across neurons was taken as the population prediction. (B) Average performance of stimulus decoder with 10 ms time bins, constructed from all Fast and Medium units or all Slow units. The title reports average percent correct classification across all four stimuli. Entries along the diagonal are percent correct, and rows sum to 1.0. (C) Percent correct performance for each unit in the Fast/Medium model in (B), separated by best integration window. Vertical line, chance prediction of 25%. (D) Average performance of stimulus decoder with a single 150 ms time bin. (E) Average performance of a Fast/Medium stimulus decoder with 10-ms bins, using rate-normalized or time-scrambled spike trains. (F) Performance of behavioral choice decoders, built from Fast and Medium units or Slow units, using two different bin sizes. Chance performance is 50%. (G) Choice prediction for each unit in the Slow model, using a single 100-ms bin prior to nose poke withdrawal. Units are separated by depth and response type. Best choice prediction was by Slow Positive units in L5b. Data for B–E are in S1 Data.

		Baseline Firing Rate (Hz)		Average Firing Rate (Hz)		
Layer	**Type**	**Mean ± SEM**	**Median**	**Mean ± SEM**	**Median**	**N units**
L23	RS	6.0 ± 1.5	4.9	7.6 ± 1.2	8.1	9
L23	FS	7.9 ± 2.4	5.7	9.0 ± 1.6	10.4	5
L23	MU	15.9 ± 3.1	14.5	17.8 ± 3.3	17.3	23
L4	RS	7.8 ± 0.8	5.7	7.4 ± 0.8	5.1	52
L4	FS	9.8 ± 2.7	3.9	10.9 ± 2.8	6.9	15
L4	MU	25.3 ± 2.9	20.9	25.8 ± 2.8	18.8	51
L5a	RS	10.8 ± 0.9	9.6	11.0 ± 1.0	9.0	68
L5a	FS	10.7 ± 4.8	10.9	12.6 ± 5.6	7.6	6
L5a	MU	26.6 ± 3.1	25.8	25.6 ± 2.9	23.9	30
L5b	RS	9.0 ± 1.0	7.0	10.0 ± 1.1	8.4	62
L5b	FS	31.6 ± 9.1	15.2	34.0 ± 8.9	15.8	15
L5b	MU	23.3 ± 2.9	20.7	23.1 ± 2.3	20.2	31
L6	RS	7.7 ± 2.1	2.4	7.2 ± 1.6	3.3	45
L6	FS	21.6 ± 4.1	13.8	22.0 ± 4.3	14.8	29
L6	MU	25.2 ± 4.4	15.5	22.9 ± 3.7	14.9	32

S1 Table. Firing rates by layer and unit type. These data include both temporally modulated and non-modulated units.

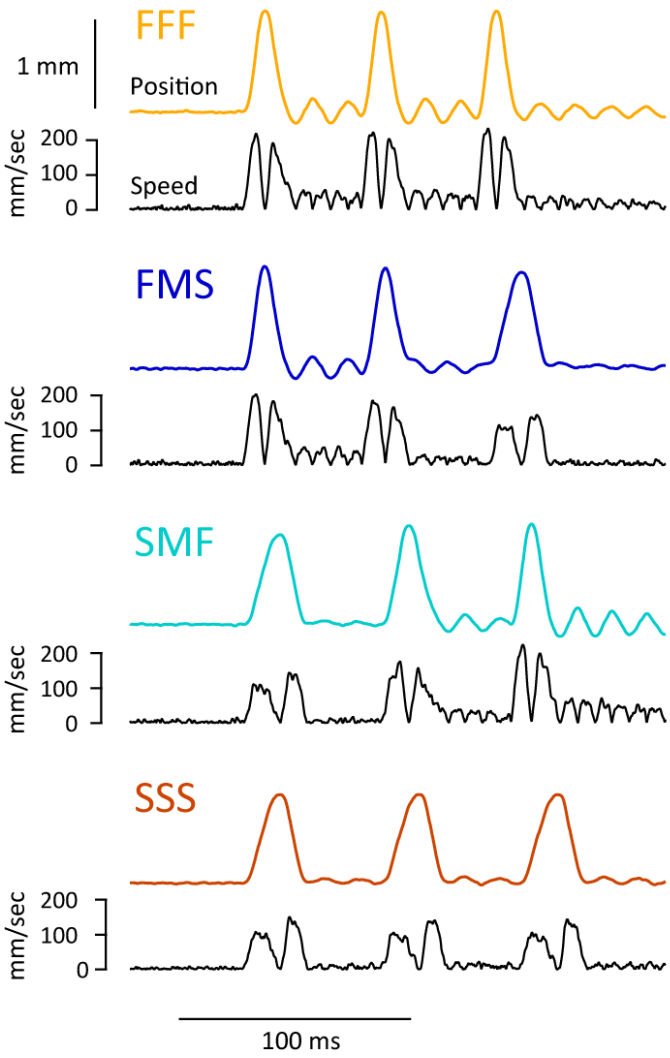

S1 Fig. Speed profile of each stimulus. Position and speed profiles for FFF, FMS, SMF, and SSS stimuli. Data are in S2 Data.

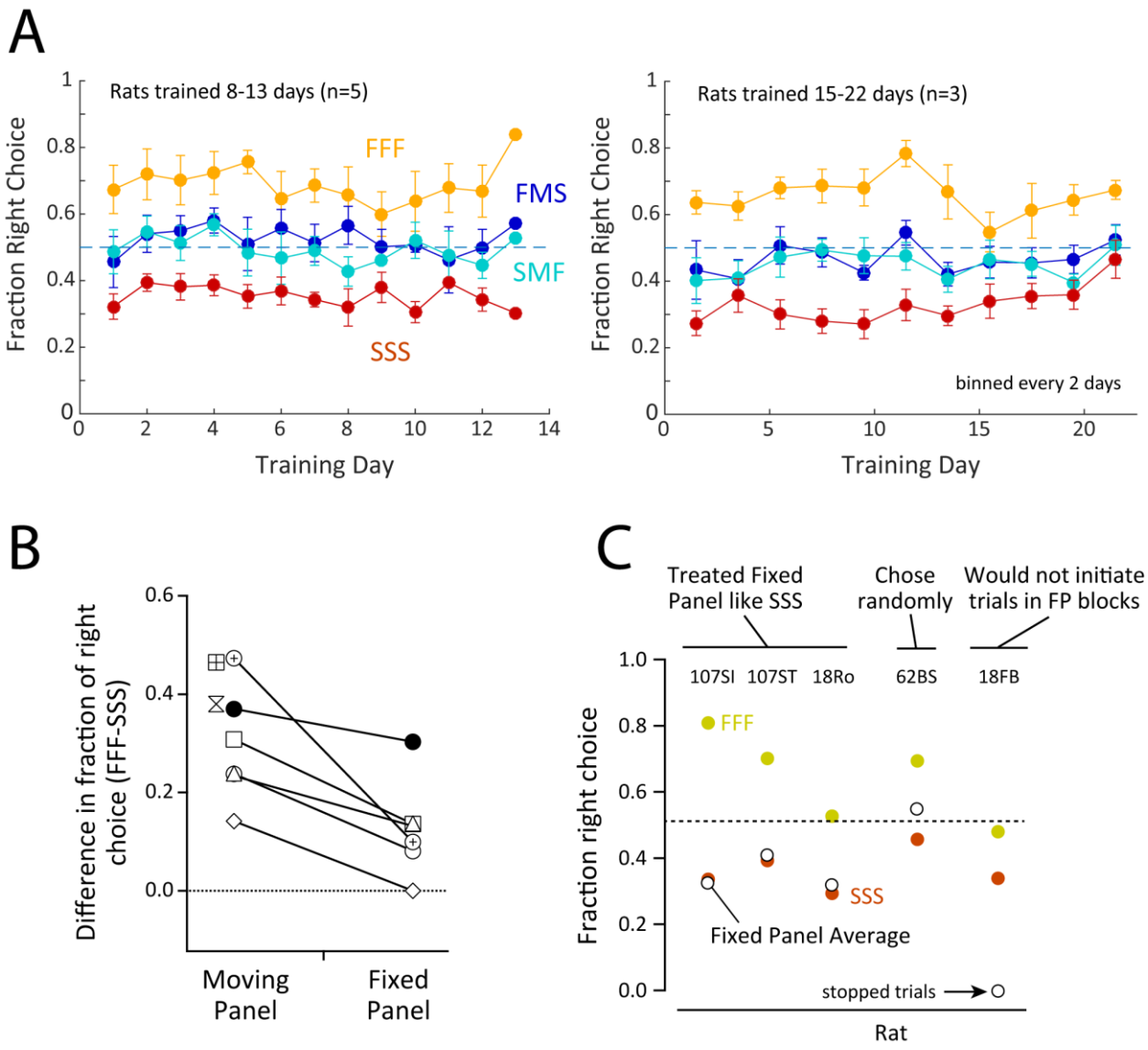

S2 Fig. Additional analysis of FFF-FMS-SMF-SSS behavior. A, Behavior performance was stable over 8–22 d of training. Left, average performance for five rats that had 8–13 d of training. Right, three rats that had 15–22 d of training (2-day bins were used because of low number of animals). Points are mean ± SEM. B, Behavioral effect of fixed panel trials, assessed using a simple alternative to d-prime. FFF versus SSS discrimination was quantified as (fraction of right choices to FFF stimuli – fraction of right choices to SSS stimuli). Discrimination was reduced on fixed panel trials ($p = 0.012$, two-sided paired t test). One rat (filled) was not significantly impaired, suggesting that he based discrimination on inadequately masked auditory cues. C, Varied responses to fixed-panel trials across rats. The plot shows fraction of right-side choice for FFF and SSS moving panel stimuli, and for the average of all fixed-panel stimuli. Only the five rats who showed behavioral impairment in the fixed panel session are included. Three rats treated fixed panel stimuli like SSS; one rat chose right or left nearly at random (50% right-side choice); and one rat did not complete trials during fixed-panel blocks. Data are in S2 Data.

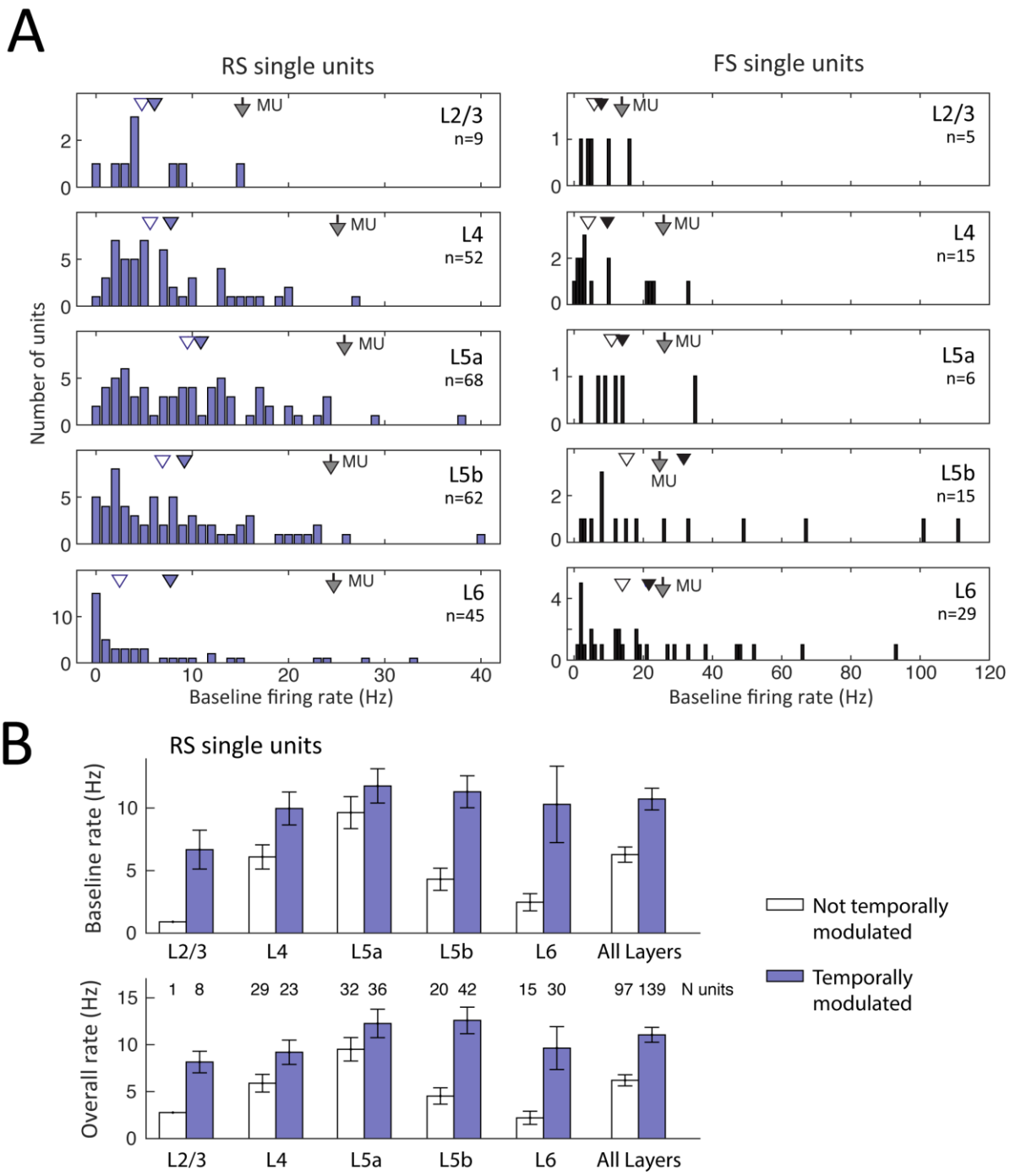

S3 Fig. Firing rate for single units by layer. A, Firing rate distributions for RS single units (left) and FS single units (right). Both temporally modulated and non-modulated units are included. Open triangles, median. Filled triangle, mean. Arrowhead, mean for multi-unit clusters, shown for comparison. Note different firing rate scales for RS and FS units. B, Firing rate (mean ± SEM) for temporally modulated and non-modulated RS single units. Temporally modulated units generally had higher firing rates, even during the baseline period.

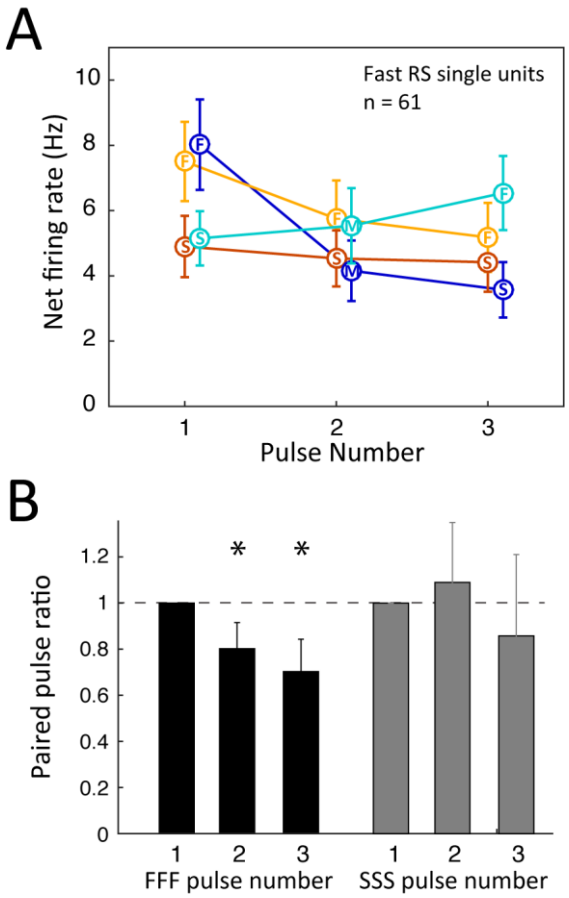

S4 Fig. Adaptation for Fast units. A, Panel-evoked responses to each individual impulse within FFF, FMS, SMF, and SSS trains, measured as firing rate 5–35 ms after impulse onset, above pre-sequence baseline. Points are mean ± SEM across all Fast RS units. Adaptation is evident in FFF but not SSS trains. B, Adaptation quantified by paired pulse ratio during FFF and SSS trains. For the same units as in (A). Paired pulse ratio is defined as panel-evoked firing rate during Pulse N/Pulse 1. Error bars, SEM.

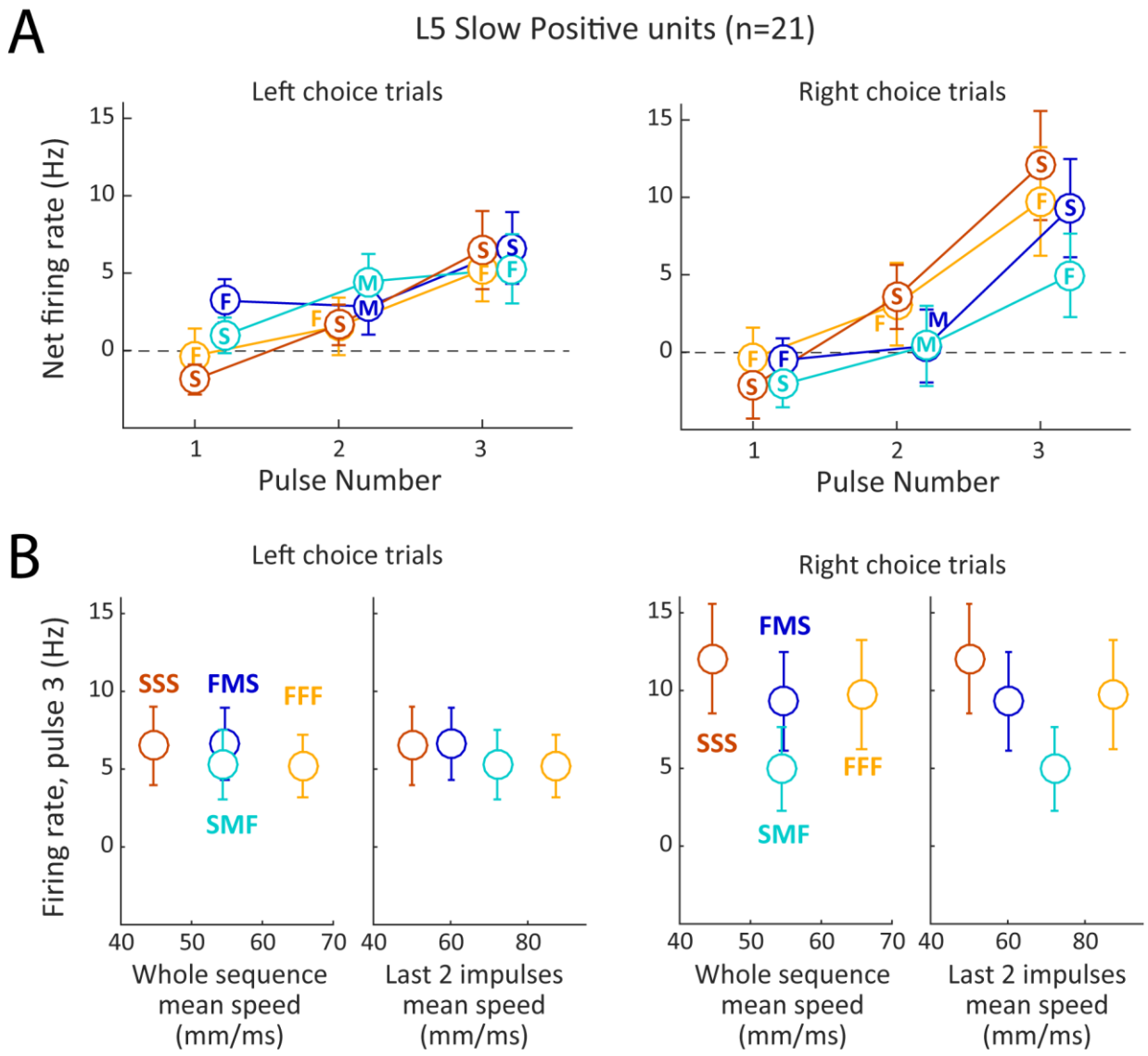

S5 Fig. Responses to panel impulses by L5 Slow Positive units. A, Mean evoked firing during each impulse (defined as in S4 Fig), for all Slow Positive units in L5a and L5b. Left- and right-choice trials were analyzed separately. Error bars are SEM. Right-choice trials had higher firing rate than left-choice trials, consistent with Fig 8. Firing during pulse 3 did not differ between FFF, FMS, SMF, and SSS stimuli, for either left- or right-choice trials. B, Firing during pulse 3 did not correlate with overall mean sequence speed or with mean speed of the preceding two pulses.

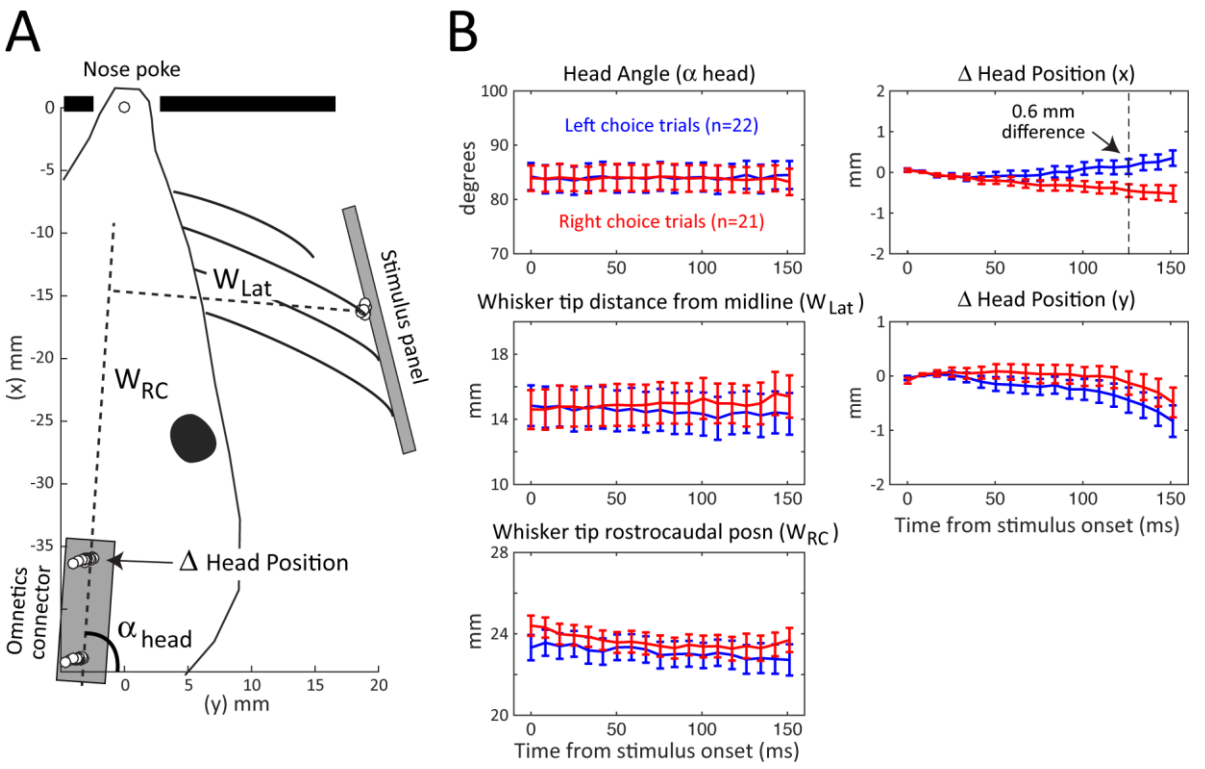

S6 Fig. High-speed video analysis of head and whisker movements during the stimulus presentation period. A, Schematic of a rat in the nose poke with head and whisker position measured during each 8.4-ms frame of a single trial, from 0 to 150 ms after stimulus onset. Nose poke entry occurred 50–75 ms prior to stimulus onset. Circles show measured positions of two points on the head (which were pins on a skull-mounted Omnetics connector) and one whisker tip. Nose poke center position is shown at top. We calculated head angle, head position relative to its starting position, and whisker tip position relative to the head. B, Mean trajectories of each variable across 22 left-choice and 21 right-choice trials (n = 4 rats). Bars are SEM. Significant right-choice versus left-choice differences were found for the x position (right-left position) of the head, but for no other variable. Data are in S2 Data.

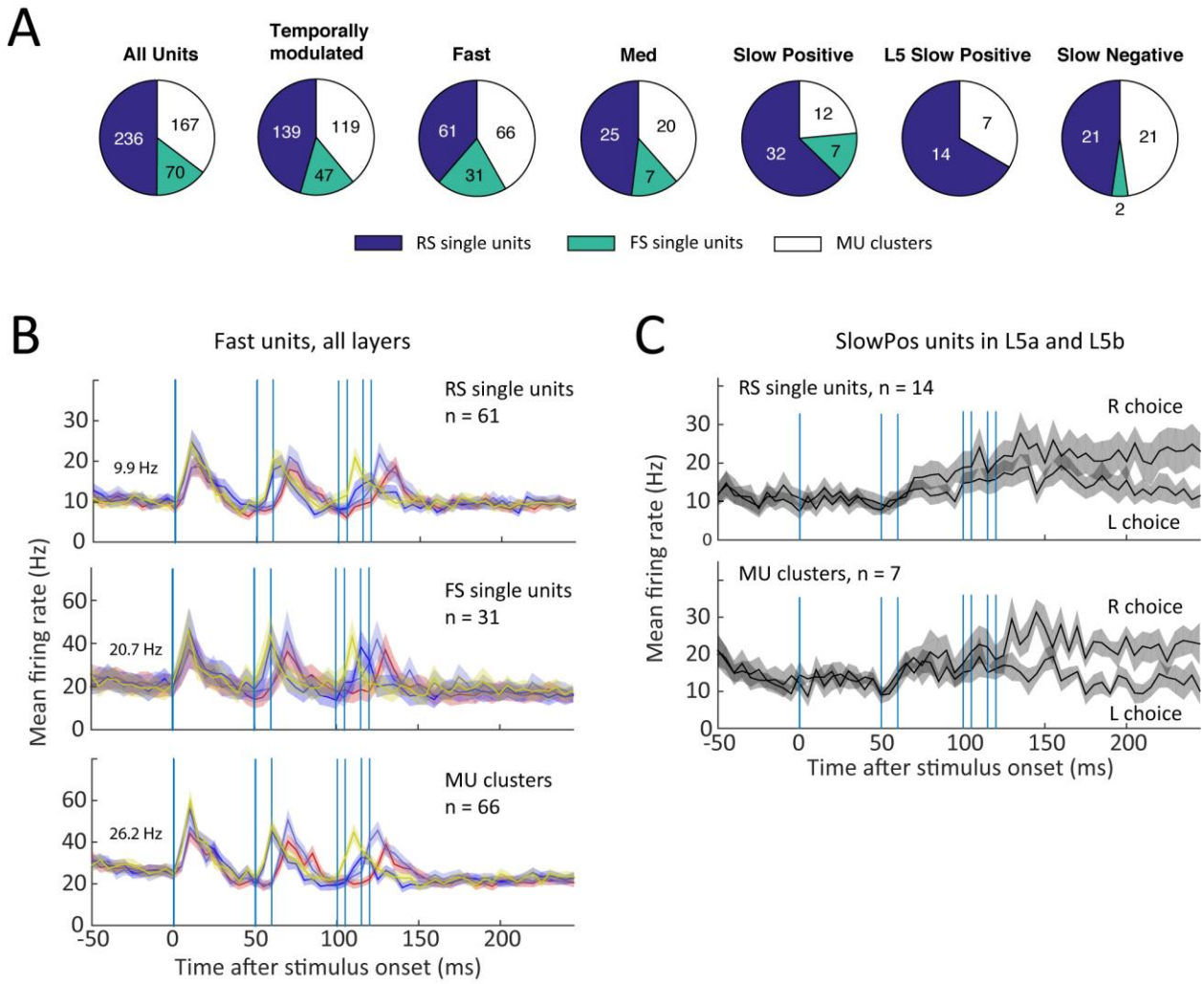

S7 Fig. Contribution of RS and FS units to response classes. A, Prevalence of RS single units, FS single units, and multi-unit clusters within each response class. B, Population PSTHs for Fast units that were RS single units, FS single units, or multi-unit clusters. Each color trace is a different sequence (FFF, FMS, SMF, SSS). Conventions as in Fig 4D. Bars show onset of individual impulses. C, Population PSTH for Slow Positive units in L5 that were RS single units or multi-unit clusters. There were no FS units in this response class. Traces are mean for all four sequences, shown separately for right- and left-choice trials.

Chapter 3

Elementary Motion Sequence Detectors in Whisker Somatosensory Cortex

Keven J. Laboy-Juárez, Daniel E Feldman

3.1 Summary

How somatosensory cortex (S1) encodes complex patterns of touch, as occur during tactile exploration, is unknown. Temporally dense stimulation of local whisker pairs revealed that most S1 neurons are not classical single-whisker feature detectors, but instead are strongly tuned to sequences involving the columnar whisker (CW) and one, specific surround whisker (SW), usually in SW-leading-CW order. This tuning was precise in space and coarser in time, generating a rate code for local motion vectors defined by SW-CW combination identity. Prominent sublinear suppression for suboptimal combinations and near-linearity for preferred combinations sharpened combination tuning relative to linearly predicted tuning. This spatially asymmetric suppression is analogous to computation of elementary motion direction selectivity in vision. SW-tuned neurons, 'misplaced' in the classical whisker map, had the strongest combination tuning. Thus, each S1 column contains a rate code for elementary local motion sequences, providing a basis for higher-order feature extraction.

3.2 Introduction

Tactile exploration generates complex spatiotemporal patterns of touch stimuli, whose representation in somatosensory cortex (S1) is poorly understood. Neurons in primary sensory cortex classically integrate across sensory space and time to generate tuning for local spatiotemporal features[1–3]. But in whisker S1, the canonical touch system of rodents, a 'one-whisker-one-column' model dominates, in which each facial whisker maps to one cortical column and S1 neurons are considered single-whisker feature detectors for velocity, acceleration or bend of the columnar whisker (CW). Natural whisking generates complex, rapid patterns of multi-whisker contact[4–6], suggesting that S1 may compute tuning for ethologically

relevant multi-whisker patterns. How multi-whisker features are represented and organized in S1 remains unclear[7].

Several findings suggest that multi-whisker tuning may be prevalent in S1. S1 neurons spike weakly to optimal single-whisker stimuli[8–10] and have broad subthreshold receptive fields suggesting multi-whisker integration[11,12]. In each column, most neurons are somatotopically tuned to the CW[13,14], but a surprising fraction prefer a surround whisker (SW) over the CW, and are thus 'misplaced' in the classic whisker map [15,16]. These SW-tuned cells may prefer multi-whisker features mapped according to an alternative model of S1 columnar organization. Some neurons are tuned to highly structured multi-whisker features such as global motion wavefronts[17,18] and concentric center-surround motion contrast[19], but these either engage a relatively small fraction of neurons (~25%) or elicit no more spikes than single-whisker stimuli. Tuning for spatiotemporally distributed whisker sequences has been observed, but its organization and effect on coding remain unclear[20]. We hypothesized that S1 neurons may encode a more elementary spatiotemporal feature. If this tuning is a dominant feature of S1 coding, it should be highly prevalent, organized systematically in the S1 map, and constructed through a readily identifiable computation that may involve cross-whisker nonlinearities[21–26].

We tested for tuning within an elementary subspace of multi-whisker stimuli, comprising local pair-wise whisker combinations and sequences, over a physiological range of deflection intervals (Δt). These represent local motion on the whisker pad, have tractable dimensionality, and are the elementary building blocks of all local multi-whisker patterns. We mapped responses densely within this space, and found that most S1 neurons are multi-whisker sequence detectors. Sequence tuning was somatotopically organized, with most neurons being tuned for a specific CW-SW sequence, usually in SW-leading-CW order. Tuning was precise for whisker combination identity (space) and coarse for Δt (time). 'Misplaced' SW-tuned neurons had the strongest sequence tuning. In each neuron, sequence tuning was generated by prominent, spatially asymmetric sublinear suppression for non-preferred sequences, and linearity for preferred sequences. This strongly resembles computation of motion direction selectivity in vision[27–29], suggesting a conserved sensory computation. Diverse sequence tuning created a robust population rate code for local motion in each column. This reveals a novel organization for the S1 map, in which each column encodes a comprehensive set of local motion vectors involving the CW.

3.3 Results

We measured spiking of single units in the D1 or C1 column of S1 in urethane-anesthetized mice (P28-45) using multi-site silicon probes. We independently deflected whiskers in a 3 x 3 array that was centered on the columnar whisker (CW) and included 8 immediate surround whiskers (SWs). Each whisker was deflected with a 40ms triphasic waveform that optimally drives S1 neurons[19]. In *Experiment 1*, we presented single-whisker stimuli and two-whisker

stimuli that included all CW-SW and all SW-SW combinations at 7 different inter-whisker-deflection intervals (Δt = 0, ±10, ±25, ±50 ms) (**Fig. 1a**). Tuning was analyzed in 142 whisker-responsive single units (out of 160 single units) in 8 recording sites in 5 mice. Units were distributed across S1 layers (L2/3 = 36, L4 = 48, L5 = 44, L6 = 14 units).

Single-whisker receptive fields in each S1 column

Classical whisker receptive fields, measured from the single-whisker deflections, showed expected properties. On average across units, the CW evoked the most spikes, followed by within-row SWs, consistent with standard S1 somatotopy[14] (**Fig. 1b, top**). But tuning was diverse at the single unit level, even within the same penetration (**Fig. S1**). 61% of units were driven most strongly by the CW (CW-tuned units, n = 89), and 39% by an SW (SW-tuned units, n = 53). Some SW-tuned units showed nearly equivalent responses to the CW, but others strongly preferred the SW (**Fig. 1b, bottom**). SW tuning was found in all layers, and did not simply reflect broad tuning or weaker responsiveness, because CW- and SW-tuned neurons showed similar tuning sharpness to secondary whiskers in rank-ordered receptive fields (**Fig. S1**). CW- and SW-tuned units also had similar spontaneous activity (0.16±0.03 vs. 0.26±0.05 spikes/sham) and maximal evoked response (0.60±0.06 vs. 0.57±0.08 spikes/stimulus). Thus, a single column contains mostly CW-tuned neurons, but also a substantial fraction of SW-tuned neurons, as in prior reports[15,16,30].

S1 preferentially encodes local motion involving CW-SW sequences

Tuning for whisker combinations was analyzed from the CW-SW and SW-SW stimuli, initially independent of Δt. **Fig. 1c** shows two example single units in the D1 column. Black bars show the response to each whisker deflected singly; colored bars show the response to each whisker combination at whichever Δt (0, 10, 25, 50 ms) drove the strongest response to that combination. Responses are spike counts in a broad, 125-ms window that includes all spikes evoked by both whiskers in the combination. Each unit spiked more to a specific 2-whisker combination than to other stimuli. Note that both units differed in their single-whisker tuning (CW-tuned vs. SW-tuned) but both preferred a combination that contained D1 (the CW). Nearly all units spiked more to the best whisker combination than the best single whisker (slope = 1.26, **Fig. 1d**). For 70% of units, the best combination included the CW (this was 85% for CW-tuned units and 47% for SW-tuned units), which is greater than chance (2/9 = 22%) (**Fig. 1e**). Correspondingly, the best CW-SW sequence evoked more spikes than the best SW-SW sequence (**Fig. 2f**). Thus S1 spiking is focused on CW-SW combinations, rather than SW-SW combinations or single-whisker stimuli.

Whisker combinations are also sequences with a specific Δt. Neurons showed sharper tuning selectivity among CW-SW than SW-SW sequences (**Fig. 1g**). Selectivity was measured as lifetime sparseness[31,32] across sequences varying in both spatial whisker combination and Δt, and thus represents spatiotemporal selectivity. SW-tuned neurons had particularly sharp tuning for CW-SW sequences (**Fig. S2**). Thus, neurons in each S1 column are preferentially tuned for, and discriminate, CW-SW sequences.

Dense spatiotemporal mapping of CW-SW sequence tuning in S1

We studied CW-SW sequence tuning more comprehensively and with greater Δt resolution in *Experiment 2*, which used a reverse correlation method. Stimuli included all CW-SW combinations with Δt uniformly distributed between ±50 ms at 1 ms intervals. Because some S1 neurons are sensitive to CW-SW motion contrast[19], we presented both same- and opposite-direction CW-SW deflections (termed correlated and anti-correlated stimuli). Single whisker stimuli and a subset of SW-SW sequences were also applied (**Fig. 2a**). A total of 247 single-units were isolated in 12 mice, of which 224 (227) were responsive to correlated (anti-correlated) stimuli. These were distributed across layers (L2/3: 54, 54 units [correlated, anti-correlated]; L4: 78, 79 units; L5: 71, 70 units; L6: 21, 24 units). The average whisker deflection rate was 3 Hz.

For each single unit, we applied a model-based smoothing method on evoked spike counts to calculate a Δt tuning function for each whisker combination (see Methods) (**Fig. 2b**). We then plotted a spatiotemporal response function (cwSTRF) that summarizes the mean response to each CW-SW combination at each Δt, after Δt smoothing (**Fig. 2c**). The 'best whisker combination' and 'best Δt' were defined as those that jointly evoked the maximum response. We calculated a combination selectivity index (CSI) at each Δt as lifetime sparseness across the 8 CW-SW combinations at that Δt**.** Correlated and anti-correlated stimuli were analyzed separately for each single-unit, therefore we refer to each cwSTRF as a unit. A unit was considered combination selective if the CSI trace across Δt's was significantly different than for spike count data shuffled across stimuli and trials (see Methods). All p-values are adjusted for multiple comparisons across units.

Combination tuning is strong and prevalent in S1

52% of S1 units (n=129) were significantly combination-selective, based on either correlated or anti-correlated stimuli. Four example units are shown in **Fig. 2d**. The polar plots show the measured spiking response to different CW-SW combinations at the best Δt, relative to CW response alone and to the linear sum of single CW and SW deflections. The latter is used as a null hypothesis for default tuning. All 4 units preferred a specific CW-SW sequence (asterisk) which evoked more spikes than the CW alone. Tuning for CW-SW sequences was consistently sharper than the linear prediction. Many S1 units showed sharp combination tuning (**Fig. S3**).

Across all responsive units, there was a broad range of CSI at the best Δt (**Fig. 2e**). For combination-selective units, the average spatial tuning for CW-SW sequences was very sharp, as shown by aligning combination tuning curves to their peak (by rotating the polar plots). This tuning was not due to stimulus-independent response variability or undersampling, because shuffling spike count data across stimuli and trials abolished tuning structure (**Fig. 2f**). The highest CSI units, which are mostly combination-selective, had very strong mean tuning, while the lowest CSI units, which are mostly non-selective, had nearly uniform responses that resembled shuffled data (**Fig. 2f**). Thus, S1 contains a broad gradient of combination selectivity, including both combination-selective units that represent spatiotemporal sequences, and non-selective units which may primarily encode single-whisker features.

Preferred CW-SW combinations sampled most SWs, but overrepresented SWs that were rostral in the same row as the CW, or ventral to CW (**Fig. 2g**). This bias is evident in mean somatotopically aligned tuning (**Fig. S4**), and may represent ethologically relevant axes of local motion.

Nonlinearities enhance rate coding of whisker combinations

For the great majority of units, CW-SW combination tuning was sharper than predicted from the linear sum of single-whisker responses (p=1e-50, paired t-test) (**Fig. 3a**). This was true for both combination-selective and non-selective units (**Fig. 3b**). This was readily apparent in single example cells (**Fig. 2d, Fig. S3**), and in average aligned combination tuning curves, which showed strong sublinearity for non-optimal combinations, and near-linearity for the optimal combination (**Fig. 3c**). Combination selectivity existed in all layers, but was stronger in L2-4 than L5-6 (1-factor ANOVA, p=.0025) (**Fig. S5**). Thus, tuning for CW-SW combinations is powerfully sculpted from broader tuning predicted by single-whisker input.

The prevalence and diversity of combination tuning suggests a population rate code for whisker combinations in each column. We tested whether a neural population decoder could discriminate CW-SW combination identity using spike count data from single trials. Each neuron in *Experiment 2* was modeled as a one-vs-all classifier, using 10-fold cross-validation and logistic regression, to predict the probability of each CW-SW combination from single-trial spike count data (see Methods). Training and testing data were from combinations with $\Delta t \leq \pm 5$ ms from the unit's best Δt. No Δt smoothing was applied, and neurons were modeled independently. An ensemble of *N* neurons was sampled with replacement from all combination-selective units. The CW-SW combination with the highest summed probability across neurons was taken as the population prediction.

The average single-trial accuracy (computed across all 8 CW-SW combinations) increased with *N*, reaching 42% for $N = 187$. Chance performance is 12.5% (1/8) (**Fig. 3d**). Accuracy was highest for the CW-SW combination involving the rostral within-row SW (82%, computed for $N=187$), and was worst for the 3 dorsal-row SWs (23-28%) (**Fig. 3e**), which matches the somatotopic bias of combination tuning (**Figs. 2g and S4**). In contrast, training and testing the decoder on linearly predicted spike counts resulted in significantly weaker discrimination (**Fig. 3d-e**). Thus, the neural ensemble in a single S1 column accurately encodes CW-SW combinations on single trials and nonlinearities enhance the efficiency and accuracy of this rate code.

SW-tuning enhances rate coding of whisker combinations

We next examined how SW-tuned units, whose single-whisker tuning 'misplaces' them in the classical whisker map, encoded whisker combinations. SW-tuned units showed sharper combination tuning for CW-SW sequences than did CW-tuned units (p=3.4e-4, t-test) (**Fig. 4a**), consistent with *Experiment 1* (**Fig. S2**). This was achieved by sublinear sculpting of linearly predicted tuning, as for other units (**Fig. 4b**). To determine how SW-tuned units contribute to population coding, we constructed 2 separate neural decoders, one based on CW-tuned units,

and the other on SW-tuned units. Decoding of whisker combination identify from CW-tuned units was well above chance, but decoding with SW-tuned units was far more accurate and efficient **(Fig. 4c-d).** Thus, SW-tuned units are sharply tuned for CW-SW combinations (Fig. S2), and enhance population coding of CW-containing sequences.

Spatiotemporally specific linear integration enhances combination tuning in S1

Combination tuning curves show that CW-SW tuning is sculpted from broader, linearly predicted tuning (**Fig. 3c**). These curves also show that the linearly predicted tuning, which reflects asymmetry in the single-whisker receptive field, was biased toward the best CW-SW combination (**Fig. 3c**). Both these processes—non-uniform sublinear sharpening and the bias in predicted linear tuning—appeared weaker, on average, in the least-selective units (**Fig. 3c**). We analyzed how these two processes contribute to combination tuning.

To characterize the sharpening process, we quantified linearity of responses to CW-SW combinations at the best Δt. Across all stimuli and all units, combination responses were strongly predicted by a 64% scaling of the linear sum of single-whisker responses (R^2=0.90). Within this average relationship however, non-optimal combinations evoked strongly sublinear responses, while each unit's best combination evoked a near-linear response (**Fig. 5a**). Best combinations were nearly linear (linearity index of 0.95±0.02, defined as measured response / linear prediction), and non-optimal combinations were sublinear (0.63±0.003, p=1.3e-147, 2 sample t-test) (**Fig. 5b-c**). This difference is not the trivial result of best combinations evoking stronger responses relative to the population linear fit in **Fig. 5a**. This was shown by a shuffling procedure in which pseudo-units were constructed by sampling 8 random points from **Fig. 5a**. The strongest responses of these pseudo-units ('best combinations') and the remaining, weaker responses ('non-optimal combinations') had very similar linearity (0.71 vs. 0.67) (**Fig. 5c**). Sublinearity for non-optimal combinations was not found just at the unit's best Δt, but also at the peak Δt for these whisker combinations (**Fig. 5c**). Thus, near-linear integration is spatiotemporally confined to the best combination and best Δt. This boosts best CW-SW combination responses over a global sublinear scaling, resulting in spatially asymmetric suppression across whisker combinations.

Combination-specific nonlinearities depend on single-whisker tuning

To quantify the contribution of linear and nonlinear components to combination selectivity, we separated them mathematically. We modeled combination-tuning as resulting from two sequential operations: i) a global scaling to 0.64 of linearly predicted responses, analogous to linear summation with divisive normalization; and ii) a combination-specific nonlinear facilitation or suppression process, quantified as the residual between the measured response and the 0.64x scaling. This model (**Fig. 6a**) decouples linear and nonlinear components of combination tuning, independent of how they are implemented physiologically.

To examine model performance, we ranked each CW-SW stimulus by its measured response in each unit, and calculated the mean ranked combination tuning curve across units. Mean tuning was sharper than the 0.64-scaled sublinear predicted tuning predicted from single-whisker

deflections (**Fig. 6b**). The best combination response was greater than the 0.64-scaled sublinear model (p=7e-7, 2-tailed 2-sample t-test, Bonferroni corrected) and the worst combination was weaker (p=6.5e-3). Uniform subtractive inhibition does not account for this sharpening, because it simply shifts the linear prediction along the y-axis (**Fig. 6b**). Hence, sharpening of combination tuning involves combination-specific nonlinearities.

The magnitude of combination-specific nonlinearities was similar between combination-selective and non-selective units: in both cases, there was strong facilitation for the best CW-SW combination, and modest suppression for the 2-3 weakest CW-SW combinations (**Fig. 6c, top**). The magnitude of facilitation did not differ between groups (p=0.24, t-test) and 77% of both selective and non-selective units exhibited maximal facilitation to the best CW-SW combination. There was slightly more suppression for the 2 weakest CW-SW sequences in combination-selective than non-selective units (p=0.001 and p=0.002, 2 sample t-test, 2 tailed Bonferroni correction). Thus, spatially asymmetric suppression is a general computation shared across S1 units, but modestly stronger suppression enhances tuning in combination-selective units.

Combination-selective units differed in the asymmetry of their single-whisker receptive field, and in how linearly predicted responses recruited the nonlinear boosting process. The linearly predicted receptive field was sharper in combination-selective cells than non-selective units (**Fig. 3b; Fig. 6c**). The linear prediction correlated with the relative strength (rank) of combination-evoked responses in combination-selective units (p=1e-4, 1-factor ANOVA), but not in non-selective units (p=0.51) (**Fig. 6c**). As a result, the strongest single SW predicted the best CW-SW combination in 60% of combination-selective units, but only in 31% of non-selective units. Strikingly, combination-selective units nonlinearly facilitated the CW-SW combination that had the greatest linear prediction (p=1.2e-8, 1-factor ANOVA), while non-selective units showed a weaker, opposite trend (p=0.03). The probability distributions of these measurements are shown in **Fig. S6**. Hence, combination-selective units achieve sharp combination tuning by having sharper linearly predicted tuning (i.e., spatially asymmetric single-whisker tuning) (**Fig. 3c**) and boosting responses to combinations involving the strongest SW.

Tuning for Δt reveals space-time inseparability

Finally, we characterized how S1 neurons are tuned for Δt. For best CW-SW combinations, combination-selective units had sharp Δt tuning, with an average half-width of ~10 ms around the best Δt. In contrast, suboptimal combinations evoked weaker responses, on average, with much weaker, broader Δt tuning around the units' best Δt (**Fig. 7a**). Thus, S1 cells are not tuned for a specific Δt independent of combination identity. Next, we examined mean Δt tuning across combination-selective units, calculated after standard Δt smoothing (**Fig. 7b**). On average, the minimum response occurred at -10 ms Δt, consistent with previous studies using arbitrarily chosen 2-whisker sequences. Strong tuning structure was evident by comparing preferred and non-preferred combination stimuli: for best combinations, maximal responses were evoked at -30 to -50 ms Δt (SW leads CW, corresponding to inbound motion toward the

CW). For suboptimal combinations, this time range evoked much weaker responses, and maximal responses were observed at +30 to +50 ms Δt (outbound motion). Thus, combination-selective units have inseparable spatial and temporal tuning and are joint spatiotemporal feature detectors. Non-selective units lacked this structure, and preferred outbound Δt order for both best and suboptimal stimuli (data not shown).

Order selectivity dominates Δt tuning

To understand the diversity of Δt tuning we performed principal components (PC) analysis on all significantly modulated Δt tuning curves (n= 357 tuning curves representing 79% of best combinations, and 1247 tuning curves representing 40% of suboptimal combinations, see Methods). Tuning curves were z-scored before analysis. Three PCs captured 75% of variance in Δt tuning (**Fig. 7c**). PC1 and PC2 resembled filters for tactile sequence order and speed, respectively, while PC3 was a sharper, bimodal filter (**Fig. 7d**). Best- and suboptimal combinations differed strongly in PC1 weighting in combination-selective cells (p=5.7e-16, t-test), but less so in non-selective cells (**Fig. 7e**). This is consistent with inbound order preference for best combinations in selective units. Weighting of PC2 and PC3 did not differ across cell or stimulus types (**Fig. 7e**). Thus, the feature of Δt tuning that is most related to combination-selectivity is the unique inbound order preference for best combination stimuli in selective units.

To test whether CW-SW order was accurately represented by S1 firing rates on single trials, we trained a neural decoder (constructed as in Fig. 4) to report order. After training, the decoder predicted CW-SW deflection order above chance (50%), with performance of ~65% on hold-out trials for *N*=100 units (**Fig. S7**). S1 units tuned to different spatial CW-SW combinations provided equally accurate order decoding (**Fig. S7**).

Order tuning and spatial tuning were related. Combination-selective units that preferred inbound order (best $\Delta t < 0$) were more sharply spatially tuned than those that preferred outbound order (p=0.03, t-test) (**Fig. 7f, left**). Inbound-preferring units also had better alignment between nonlinear and linear components of combination tuning (p=0.01, t-test), which may explain their sharper tuning (**Fig. 7f, right**). When the spatial combination decoder (Fig. 4) was retrained and retested using stimuli within specific Δt ranges, spatial combination decoding was better for inbound order stimuli than outbound order stimuli (**Fig. 7g**). Thus, the inseparability of temporal and spatial tuning yields improved spatial discrimination for inbound stimuli, suggesting that S1 preferentially encodes local spatial features of inbound motion to each column.

3.4 Discussion

Coding for space and time in multi-whisker stimuli

52% of S1 units were significantly tuned for CW-SW combinations, with most units having a single, sharp peak for one specific combination (**Figs. 2 and S3**). Optimal combinations elicited more spikes than the single best whisker. 70% of combination-tuned units preferred a CW-containing sequence, with a strong preference for SW-leading-CW order. Tuning for Δt was coarse (~20ms resolution), with order being represented more strongly than a specific Δt. Spatial and temporal tuning were inseparable for combination-selective neurons. Thus, most S1 neurons act as spatiotemporal feature detectors, which provide a more efficient, compact representation of complex multi-whisker stimuli than do classical single-whisker detectors. S1 neurons exhibited a range of combination selectivity (**Fig. 2**) and thus collectively represent both single-whisker and local spatiotemporal features.

Neurons in each column represented diverse CW-containing sequences, enabling accurate decoding of local motion sequences by firing rate in small neural populations (<50 units). Biases in preferred spatial and temporal features match those expected from natural whisker use: Sharper tuning in space, relative to time, is consistent with head movements during tactile exploration, which make inter-whisker contact intervals highly irregular[6]. Preferences for rostral and ventral SWs match the prevalence of rostrocaudal contact sequences during natural whisking onto frontal objects[6], and the ventral tilt of forward whisking[33]. The strong bias for inbound (SW leading CW) motion sequences is appropriate to reduce redundancy between cortical columns in representing multi-whisker motion stimuli.

Tuning for motion sequences is also highly prevalent in primate S1[34]. In whisker S1, prior studies reported nonlinear responses to 2-whisker stimuli, including prominent cross-whisker suppression and occasional facilitation, and sensitivity to Δt [22,23,35], but did not determine the role of these interactions in generating tuning for specific multi-whisker stimuli. Here, by fully mapping these interactions across all local whiskers, we discovered that they generate sharp tuning for 2-whisker sequences that represent elementary local motion across the whisker pad. 2-whisker interactions are building blocks of more complex multi-whisker features, and are predictive of tuning for global motion across the whisker pad[17]. Pairwise nonlinearities strongly predict higher order interactions for vibrotactile sequences of pairs of whiskers[35], and responses to optimal higher-dimensional (3+ whisker) sequences are no stronger than to 2-whisker sequences[20]. While responses to optimal 2-whisker sequences are stronger than to the single best whisker, those to global motion are not[17]. Together, this strongly suggests that tuning for 2-whisker combinations is a fundamental aspect of S1 sensory coding that may underlie tuning for more complex, higher-order features.

A revised functional role for the S1 column

These findings suggest a novel functional role for the S1 column: rather than representing single-whisker features of the CW, each column also represents the set of all elementary, inbound local motion sequences that involve the CW. This CW-centered, multi-whisker view of the column explains the somatotopic breadth of subthreshold input received by each cell, and is consistent with tuning to concentric motion coherence or motion contrast relative to the CW in S1[19]. It also provides an explanation for the presence of SW-tuned neurons, which do not fit classic somatotopy defined by single-whisker tuning. Half of SW-tuned units preferred a CW-containing sequence, and thus contribute to representation of local motion involving the CW. Both SW-tuned neurons and CW-tuned neurons with strong SW responses and asymmetric single-whisker receptive fields had particularly strong combination tuning, and were essential for accurate population coding of local motion sequences (**Fig. 4**). Since SW responses are strongest at column edges[15], we predict that combination selectivity will be greatest at column edges, where a ring of multi-whisker selectivity has been found to exist[18]. The dominance of SW-leading-CW order selectivity further predicts sharp functional boundaries between neighboring columns based on opposite order tuning.

Sublinear sculpting of local motion tuning

S1 cells used asymmetric, sublinear sculpting to sharpen 2-whisker tuning relative to linearly predicted tuning. Prior studies of 2-whisker integration mostly studied a single arbitrarily chosen CW-SW pair, and reported largely sublinear suppression[21–23,25,35,36]. In some conditions more linear or supralinear integration was observed[24,26], particularly with temporally dense stimulation[20,22]. By mapping all CW-SW combinations we discovered that individual neurons suppress most CW-SW combinations, but fail to suppress (and in ~25% of units, supralinearly facilitate) a single best CW-SW combination. Thus, sublinear suppression and near-linear or supralinear summation work together to construct sharp combination tuning.

Combination tuning was modeled as resulting from a global sublinear integration process, analogous to divisive normalization[37], plus combination-specific nonlinearities, including facilitation for the best combination. Importantly, for combination-selective units the strongest nonlinear facilitation was elicited by the combination with the strongest linearly predicted response (**Fig. 6**). This suggests a simple neuronal implementation for sharpening of combination tuning. Sublinear integration likely reflects a combination of cross-whisker inhibition, dissipation of excitatory driving force, and low-threshold K conductances that all strongly promote sublinear integration of EPSPs in pyramidal cell dendrites[38]. Most cortical neurons strongly express NMDA conductances that boost EPSPs nonlinearly, including generation of “NMDA-spikes” that strongly increase dendritic signal propagation for convergent excitatory inputs[39]. We propose that inputs representing the preferred CW-SW sequence synapse nearby each other on dendrites, and thus preferentially recruit nonlinear boosting by NMDA receptors. This same mechanism generates angular tuning in S1[40] . Combination tuning could be partially synthesized subcortically, but global motion tuning[41] and inter-whisker nonlinearities are generally weaker in thalamus [21,42], and short-latency cortical responses are

mostly linear[17,25], suggesting that cortical circuits are a major site of computation (but see Ref. [43]).

A shared computation for local visual and tactile motion

The sculpting of whisker combination tuning by spatially asymmetric suppression strongly resembles the computation of visual motion direction selectivity (DS) in mammalian retina. Barlow-Levick motion detectors synthesize DS by prominent inhibitory suppression of neural responses to the null direction of visual motion while the preferred direction lacks inhibition[27–29]. DS can also involve selective facilitation for the preferred direction[44] or a combination of suppressive and facilitatory mechanisms[45,46]. We found sublinear integration for non-optimal CW-SW combinations and near-linear integration for the preferred combination, analogous to the Barlow-Levick model. 25% of units did show supralinear facilitation for best sequences (**Fig. 5**). Thus, spatiotemporal tuning in both visual and whisker systems involves suppression of non-preferred motion directions, coupled with linear responses or facilitation to preferred motion directions. Thus, there is a common computational basis for spatiotemporal feature extraction, although the underlying circuit mechanisms are likely to be distinct.

3.5 Conclusion

These findings reveal highly prevalent tuning for elementary local motion sequences in S1, which generates a rate code for local motion in each S1 column. This tuning was highly organized, with each column representing inbound local motion towards the CW. Non-linear integration sculpted linearly predicted tuning through spatially asymmetric suppression. SW-tuned neurons, which appear 'misplaced' in the classical whisker map, have the strongest CW-SW combination tuning, and thus play a key role in columnar representation of local motion.

3.6 Methods

Surgical preparation and *in vivo* electrode placement

All procedures were approved by the UC Berkeley Animal Care and Use Committee and meet NIH guidelines. Male C57BL/6 mice (age: P28-45) used. *Experiments 1* and *2* (**Fig.1**) and *2* (remaining figures) followed the same surgical and data acquisition protocols. Mice were anaesthetized with urethane and chlorproxithene (1.3 g/kg and 0.02 mg in 10 mL saline). Body temperature was maintained at 36.5C using a feedback-controlled heating pad (FHC, 40-90-8D). Anesthetic depth was assessed via toe pinch and supplemental urethane (10% of initial dose) was provided as needed. The skull was exposed, cleaned and a stainless steel head-post was implanted. A 2 mm craniotomy was made over S1 (coordinates: 1.5 mm rostral, 3.3 mm lateral of bregma). The target column (C1 or D1) was localized using receptive field mapping of multi-unit activity in L4, recorded with a tungsten microelectrode.

A silicon laminar probe (NeuroNexus, 32 channel, 1 shank, poly2 or poly3 channel geometries (A1x32-Poly2-5mm-50s-177-A16 and A1x32-Poly3-6mm-50-177-A32) was then inserted radially into the target column via a small durotomy. The probe was slowly advanced until the deepest recording pad was in L4. Simultaneous L2/3 and L4 recordings were made at this depth. Subsequently, in a subset of animals, the probe tip was further advanced to L6, and simultaneous L6 and L5a/b recordings were made at this position. L2/3, L4, L5 and L6 were defined by microdrive depths as 100-417, 418-587, 588-889 and 890-1154 μm below the pia[47].

For all recording penetrations, we confirmed post-hoc that silicon probe multi-unit activity in L4 was tuned to C1 or D1, based on single-whisker deflections. In a subset of cases, recording location was confirmed by coating the recording electrode with DiI, perfusing the mouse, and recovering DiI staining in cytochrome oxidase stained flattened tangential sections, which show the L4 barrels.

Whisker stimulation

Calibrated deflections were applied independently to a 3 x 3 grid of whiskers, centered on the columnar whisker for the recorded column (either C1 or D1). Stimuli were controlled using custom software in Igor Pro (Wavemetrics). Each whisker was trimmed to 8 mm length, and inserted into a glass tube carried on a piezoelectric bender actuator. The piezo was positioned to deflect the whisker at 5 mm distance from the face. Each whisker was deflected rostrocaudally with triphasic waveform that was shown previously to optimally drive S1 neurons and captured most of the evoked response variance in S1 (first common filter)[19] (Fig. 1a). The waveform was 40 ms duration, 300 μm peak amplitude, and had a mean frequency content of 53Hz. The waveform resembles a linear combination of position and velocity filters, which are two kinematic features that are strongly represented across the whisker-to-barrel system[19,48,49].

Experiments 1 and *2* differed in the stimulus set that was applied. *Experiment 1* had a total of 261 unique stimuli; 9 single-whisker deflections and 252 2-whisker sequences (that is, 9 choose 2 spatial combinations, each of which was delivered at 7 Δt's: 0, ±10, ±25 and ± 50ms) (Fig. 1a). Each single-whisker stimulus was delivered 125-175 times (136.67 ± 14) and each 2-whisker sequence 40-150 times (82.76 ± 35). Thus, *Experiment 1* sampled all possible 2-whisker combinations within the 3x3 grid at a subset of Δt's. All stimuli were randomly interleaved at 0.6 s inter-stimulus interval, yielding an overall average deflection rate for any whisker of 3 Hz. Each recording was 3.5-4.5 hours.

Experiment 2 had a total of 3000 unique stimuli; 18 single-whisker deflections (9 whiskers with peak deflection amplitude in either the rostral or caudal direction), 1600 CW-SW sequences (8 correlated and 8 anti-correlated CW-SW combinations at 100 Δt's within ± 50 ms range) and 1400 SW-SW sequences (7 correlated and 7 anti-correlated SW-SW combinations at 100 Δt's within ± 50 ms range). Only SW-SW combinations that involved the SW located rostral and within the same row as the CW were presented. Thus, for D1 column recordings, all SW-SW combinations involving D2 were presented, but no other SW-SW combinations were presented.

This was necessary to achieve a tractable number of unique stimuli for this experiment. Each single-whisker stimulus was delivered 140-300 times (222.52 ± 44.72) and each unique 2-whisker sequence 0-50 times (8.42 ± 4.2). Thus, *Experiment 2* sampled all possible CW-SW combinations, plus a subset of SW-SW combinations focused on one chosen SW, with denser and uniform sampling compared to *Experiment 1.* All stimuli were randomly interleaved at 0.6 s inter-stimulus interval, yielding an overall average deflection rate for any whisker of 3 Hz. Each recording was 4.5-6 hours in duration. In both experiments, Sham stimuli (blank trials in which no whisker was deflected) were also interleaved to quantify spontaneous spiking.

Data acquisition, preprocessing and spike sorting

Recordings were amplified and bandpass filtered (Plexon Instruments PBX2/16sp-G50, × 1,000 amplification, 0.3-8 kHz bandpass) and digitized at 31.25 kHz**.** Noise was reduced by common average referencing[50]. Poly 2 electrode sites were divided into groups of 4 spatially adjacent channels (tetrodes; adjacent sites were 50µm apart). Poly 3 electrode sites were divided into groups of 4 channels, selecting channels the maximal signal-to-noise ratios located within a 50µm depth range. Negative-going spikes were detected using an amplitude threshold (2.8-3.2s.d. of noise floor), with a shadow period of 0.66ms after each threshold-crossing. Detected spikes were clipped (1.5-ms waveforms) for spike sorting.

Spike sorting used UltraMegaSort2000[51], implemented in Matlab. Clusters were excluded if they had < 1000 spikes, >0.8% refractory period violations (defined as inter-spike interval < 1.5ms), or > 30% estimated missed spikes (based on Gaussian fit of detected spike amplitudes relative to the detection threshold). For each recording site, this initial spike sorting process was used to identify the mean spike waveforms of all detectable, sortable units. Then, to improve efficiency of detecting spikes, we re-performed the spike detection process using a template-matching based spike detection method, in which the mean waveforms of the previously identified clusters were used to identify spikes from the raw voltage recordings, rather than a defined amplitude threshold. This method successfully re-detected the great majority of the spikes that were detected via the initial threshold-based method, but also detected a significant number of spikes that had been suppressed by the shadow period. All spikes detected by the template method were then clipped and spike-sorted using the same process as described above.

Analysis of neuronal data

Spiking responses for single-whisker stimuli were quantified as the average number of spikes that occurred within 125ms following whisker deflection onset. Responses to 2-whisker sequences used the same window, following deflection of the first whisker in the sequence. This broad window captures essentially all spikes evoked by both whiskers. Units that showed statistically significant responses relative to baseline to any of the 9 stimulated whiskers were classified as whisker responsive. Statistical significance was assessed via likelihood ratio test that assumed Poisson statistics across the 9 whisker and sham stimulation. This test is analogous to performing a one-way analysis of variance (ANOVA) across the 10 stimulus classes

but assumes that spiking responses follow a Poisson rather than Gaussian-distribution. Thus, the test outputs the probability that spiking is equal across the 10 classes assuming Poisson statistics. Neurons were classified as responsive if the p-value < .05.

Δt smoothing: 2-whisker sequence responses were quantified as the number of spikes that occurred within a 125ms time window after the deflection of the first whisker involved in the sequence. The large number of stimulus repetitions in *Experiment 1* allowed us to compute mean sequence responses by simply averaging across stimulus repetitions (mean: 82 per Δt). *Experiment* 2 had a significantly lower number of stimulus repetitions (mean: 8.4 per Δt) preventing a simple averaging procedure to accurately capture neural responses. To address this we adapted a model based smoothing method originally used to smooth post-stimulus-time-histograms (PSTHs)[52]. This method assumes that 2-whisker combination responses follow an inhomogeneous Poisson process whose firing rate varied as a function of Δt.

Tuning curves were first calculated at a 1ms resolution by averaging single-trial spiking responses at each Δt. This was done in 90% of the total observations (training set) and the log Poisson likelihood of the rest of the data (test set) was calculated based on this initial, un-smoothed tuning curve. Afterwards the tuning curve was smoothed by convolving it with a Gaussian kernel with a standard deviation that ranged from 0.5 to 30ms at 0.2ms resolution. The training and test sets were selected via 10-fold cross-validation, repeated 50 times. Finally, the Gaussian kernel with a standard deviation that maximized the cross-validated log-likelihood was used to smooth the 1ms resolution tuning curve calculated on all the data. This process effectively low-pass filters the Δt tuning curve with a cutoff frequency chosen via maximum likelihood and cross-validation.

Tuning curves whose likelihood monotonically increased across all smoothing (likelihood function had no maximum) were classified as not significantly Δt modulated, and the Δt tuning curve was assumed to be constant and equal to the mean response across all Δt's. 33% of Δt tuning curves had monotonically increasing likelihoods. Tuning curves whose non-smoothed likelihood exceeded the likelihood of all smoothed tuning curves were classified non-modulated as well. These tuning curves would imply that S1 units are sensitive to Δt at a 1ms resolution, which is not physiologically likely in S1, and a likelihood ratio test revealed that none of these tuning curves had a statistically significant fit to the data. This happened in 23% of tuning curves, hence 56% (a total of 2004 out of 3608 tuning curves) were assumed to be constant across Δt.

Combination-selectivity: For each single-unit, the 8 CW-SW smoothed Δt tuning curves in either correlated or anti-correlated directions were grouped to build two separate columnar whisker spatiotemporal receptive field (cwSTRF) that described spiking responses as a function of Δt and CW-SW combination identity. The cwSTRF's in correlated and anti-correlated directions were analyzed separately and labeled as a unit. A combination selectivity index (CSI) for each Δt was calculated via the lifetime sparseness equation[31,32]:

$$\text{Sparseness} = \frac{1-\frac{E(r)^2}{E(r^2)}}{1-\left(\frac{1}{n}\right)}$$

where r is the spiking response to each combination, E denotes the mean across combinations and n the number of combinations which was 8 CW-SW combinations for all units. To establish statistically significant selectivity we shuffled single-trial spiking data across combinations 5000 times for each Δt, computed a non-smoothed Δt tuning curve at a 1 ms resolution and then convolved each Δt tuning curve with its corresponding Gaussian kernel for smoothing (the standard deviations were derived from non-shuffled, measured data as described in the previous section). We then built a cwSTRF from the smoothed shuffled data and computed the CSI across combination responses for each Δt. We then computed a distribution of expected CSI traces expected from shuffled data by computing the Mahalanobis distance of the 5000 CSI traces to the mean CSI trace of the shuffled data. With this distribution we computed the p-value for the Mahalanobis distance of the measured CSI trace (example shown in fig. 2c) from the shuffled data. The threshold for statistical significance was 0.05 and controlling for multiple comparisons across units via false discovery rate control[53].

Neural decoders: A neural decoder was constructed to predict CW-SW combination identity, or order (-Δt vs. +Δt) from single-trial spike counts. Each unit was represented by a one-versus-all (ova) classifier that was trained by logistic regression to report the probability of each combination based on the number of spikes counted within the evoked time window on one trial (0–125 ms after the deflection onset of the first whisker in the sequence), selected randomly from recorded spike counts for that unit. Linearly predicted spike counts for each CW-SW combination were generated by sampling individual spike counts evoked by single-whisker deflections of the corresponding CW and SW and then adding them together. Each classifier comprised eight logistic functions (or just one in order decoding), one for each combination. Logistic functions were fit using logistic regression and 10-fold cross-validation. Model fitting was performed using a randomly chosen subset of the recorded trials (90%), and decoder performance was assessed on the remaining trials. The population stimulus prediction was calculated by summing the probabilities of each stimulus over all units and selecting the stimulus with the maximal summed probability. Model fitting was repeated 1000 times and population decoding 2500 times across different ensemble sizes that were built by randomly sampling the population of model units (or ova classifiers) with replacement. This framework models the population as if all single units are independent.

3.7 References

1. Priebe, N. J. & Ferster, D. Mechanisms of Neuronal Computation in Mammalian Visual Cortex. *Neuron* (2012). doi:10.1016/j.neuron.2012.06.011

2. Sadagopan, S. & Wang, X. Nonlinear Spectrotemporal Interactions Underlying Selectivity

for Complex Sounds in Auditory Cortex. *J. Neurosci.* (2009). doi:10.1523/JNEUROSCI.1286-09.2009

3. Stettler, D. D. & Axel, R. Representations of Odor in the Piriform Cortex. *Neuron* (2009). doi:10.1016/j.neuron.2009.09.005

4. Sachdev, R. N. S., Sellien, H. & Ebner, F. Temporal organization of multi-whisker contact in rats. *Somatosens. Mot. Res.* (2001). doi:10.1080/135578501012006192

5. Grant, R. A., Mitchinson, B., Fox, C. W. & Prescott, T. J. Active Touch Sensing in the Rat: Anticipatory and Regulatory Control of Whisker Movements During Surface Exploration. *J. Neurophysiol.* (2008). doi:10.1152/jn.90783.2008

6. Hobbs, J. A., Towal, R. B. & Hartmann, M. J. Z. Spatiotemporal Patterns of Contact Across the Rat Vibrissal Array During Exploratory Behavior. *Front. Behav. Neurosci.* (2016). doi:10.3389/fnbeh.2015.00356

7. Estebanez, L., Férézou, I., Ego-Stengel, V. & Shulz, D. E. Representation of tactile scenes in the rodent barrel cortex. *Neuroscience* (2018). doi:10.1016/j.neuroscience.2017.08.039

8. Barth, A. L. & Poulet, J. F. A. Experimental evidence for sparse firing in the neocortex. *Trends in Neurosciences* (2012). doi:10.1016/j.tins.2012.03.008

9. Jadhav, S. P., Wolfe, J. & Feldman, D. E. Sparse temporal coding of elementary tactile features during active whisker sensation. *Nat. Neurosci.* (2009). doi:10.1038/nn.2328

10. Crochet, S., Poulet, J. F. A., Kremer, Y. & Petersen, C. C. H. Synaptic mechanisms underlying sparse coding of active touch. *Neuron* (2011). doi:10.1016/j.neuron.2011.02.022

11. Moore, C. I. & Nelson, S. B. Spatio-Temporal Subthreshold Receptive Fields in the Vibrissa Representation of Rat Primary Somatosensory Cortex. *J. Neurophysiol. Chapin Chapin Lin Simons Carvell* (1992). doi:8930286

12. Zhu, J. J. & Connors, B. W. Intrinsic firing patterns and whisker-evoked synaptic responses of neurons in the rat barrel cortex. *J. Neurophysiol.* (1999). doi:10.1111/j.1469-7793.1999.00123.x

13. Welker, C. Receptive fields of barrels in the somatosensory neocortex of the rat. *J. Comp. Neurol.* (1976). doi:10.1002/cne.901660205

14. Simons, D. J. Response properties of vibrissa units in rat SI somatosensory neocortex. *J. Neurophysiol.* (1978). doi:10.1152/jn.1978.41.3.798

15. Sato, T. R., Gray, N. W., Mainen, Z. F. & Svoboda, K. The functional microarchitecture of the mouse barrel cortex. *PLoS Biol.* (2007). doi:10.1371/journal.pbio.0050189

16. Clancy, K. B., Schnepel, P., Rao, A. T. & Feldman, D. E. Structure of a Single Whisker Representation in Layer 2 of Mouse Somatosensory Cortex. *J. Neurosci.* (2015). doi:10.1523/JNEUROSCI.3887-14.2015

17. Jacob, V., Le Cam, J., Ego-Stengel, V. & Shulz, D. E. Emergent Properties of Tactile Scenes Selectively Activate Barrel Cortex Neurons. *Neuron* (2008). doi:10.1016/j.neuron.2008.10.017

18. Vilarchao, M. E., Estebanez, L., Shulz, D. E. & Férézou, I. Supra-barrel Distribution of Directional Tuning for Global Motion in the Mouse Somatosensory Cortex. *Cell Rep.* (2018). doi:10.1016/j.celrep.2018.03.006

19. Estebanez, L., Boustani, S. El, Destexhe, A. & Shulz, D. E. Correlated input reveals coexisting coding schemes in a sensory cortex. *Nat. Neurosci.* (2012). doi:10.1038/nn.3258

20. Ramirez, A. *et al.* Spatiotemporal receptive fields of barrel cortex revealed by reverse correlation of synaptic input. *Nat. Neurosci.* (2014). doi:10.1038/nn.3720

21. Brumberg, J. C., Pinto, D. J. & Simons, D. J. Spatial gradients and inhibitory summation in the rat whisker barrel system. *J. Neurophysiol.* (1996). doi:10.1152/jn.1996.76.1.130

22. Ego-Stengel, V., Mello e Souza, T., Jacob, V. & Shulz, D. E. Spatiotemporal characteristics of neuronal sensory integration in the barrel cortex of the rat. *J. Neurophysiol.* (2005). doi:10.1152/jn.00912.2004

23. Shimegi, S., Ichikawa, T., Akasaki, T. & Sato, H. Temporal characteristics of response integration evoked by multiple whisker stimulations in the barrel cortex of rats. *J. Neurosci.* (1999).

24. Shimegi, S., Akasaki, T., Ichikawa, T. & Sato, H. Physiological and anatomical organization of multiwhisker response interactions in the barrel cortex of rats. *J. Neurosci.* (2000). doi:10.1523/JNEUROSCI.20-16-06241.2000

25. Mirabella, G., Battiston, S. & Diamond, M. E. Integration of multiple-whisker inputs in rat somatosensory cortex. *Cereb. Cortex* (2001). doi:10.1093/cercor/11.2.164

26. Ghazanfar, a a & Nicolelis, M. a. Nonlinear processing of tactile information in the thalamocortical loop. *J. Neurophysiol.* (1997). doi:10.1152/jn.1997.78.1.506

27. Barlow, H. B. & Levick, W. R. The mechanism of directionally selective units in rabbit's retina. *J. Physiol.* (1965). doi:10.1113/jphysiol.1965.sp007638

28. Mauss, A. S., Vlasits, A., Borst, A. & Feller, M. Visual Circuits for Direction Selectivity. *Annu. Rev. Neurosci.* (2017). doi:10.1146/annurev-neuro-072116-031335

29. Gruntman, E., Romani, S. & Reiser, M. B. Simple integration of fast excitation and offset, delayed inhibition computes directional selectivity in Drosophila. *Nat. Neurosci.* (2018).

doi:10.1038/s41593-017-0046-4

30. Le Cam, J., Estebanez, L., Jacob, V. & Shulz, D. E. Spatial structure of multiwhisker receptive fields in the barrel cortex is stimulus dependent. *J. Neurophysiol.* (2011). doi:10.1152/jn.00044.2011

31. Rolls, E. T. & Tovee, M. J. The responses of single neurons in the temporal visual cortical areas of the macaque when more than one stimulus is present in the receptive field. *Exp. Brain Res.* (1995). doi:10.1007/BF00241500

32. Vinje, W. E. & Gallant, J. L. Sparse coding and decorrelation in primary visual cortex during natural vision. *Science (80-.).* (2000). doi:10.1126/science.287.5456.1273

33. Hill, D. N., Bermejo, R., Zeigler, H. P. & Kleinfeld, D. Biomechanics of the Vibrissa Motor Plant in Rat: Rhythmic Whisking Consists of Triphasic Neuromuscular Activity. *J. Neurosci.* (2008). doi:10.1523/JNEUROSCI.5008-07.2008

34. Pei, Y.-C. & Bensmaia, S. J. The neural basis of tactile motion perception. *J. Neurophysiol.* (2014). doi:10.1152/jn.00391.2014

35. Boloori, A.-R. The Dynamics of Spatiotemporal Response Integration in the Somatosensory Cortex of the Vibrissa System. *J. Neurosci.* (2006). doi:10.1523/JNEUROSCI.4056-05.2006

36. Simons, D. J. Temporal and spatial integration in the rat SI vibrissa cortex. *J Neurophysiol* (1985). doi:10.1152/jn.1985.54.3.615

37. Carandini, M. & Heeger, D. J. Normalization as a canonical neural computation. *Nature Reviews Neuroscience* (2012). doi:10.1038/nrn3136

38. Silver, R. A. Neuronal arithmetic. *Nature Reviews Neuroscience* (2010). doi:10.1038/nrn2864

39. Schiller, J., Major, G., Koester, H. J. & Schiller, Y. NMDA spikes in basal dendrites of cortical pyramidal neurons. *Nature* (2000). doi:10.1038/35005094

40. Lavzin, M., Rapoport, S., Polsky, A., Garion, L. & Schiller, J. Nonlinear dendritic processing determines angular tuning of barrel cortex neurons in vivo. *Nature* (2012). doi:10.1038/nature11451

41. Ego-Stengel, V., Le Cam, J. & Shulz, D. E. Coding of Apparent Motion in the Thalamic Nucleus of the Rat Vibrissal Somatosensory System. *J. Neurosci.* (2012). doi:10.1523/JNEUROSCI.3890-11.2012

42. Simons, D. J. & Carvell, G. E. Thalamocortical response transformation in the rat vibrissa/barrel system. *J. Neurophysiol.* (1989). doi:10.1152/jn.1989.61.2.311

43. Higley, M. J. & Contreras, D. Cellular Mechanisms of Suppressive Interactions Between

Somatosensory Responses In Vivo. *J. Neurophysiol.* (2007). doi:10.1152/jn.00777.2006

44. Hassenstein, B. & Reichardt, W. Systemtheoretische analyse der zeit, reihenfolgen, und vorzeichenauswertung bei der bewegungsperzepion des Rüsselkäfers Chlorophanus. *Naturforsch* (1956).

45. Livingstone, M. S. Mechanisms of direction selectivity in macaque V1. *Neuron* (1998). doi:10.1016/S0896-6273(00)80991-5

46. Mikami, a, Newsome, W. T. & Wurtz, R. H. Motion selectivity in macaque visual cortex. I. Mechanisms of direction and speed selectivity in extrastriate area MT. *J. Neurophysiol.* (1986). doi:10.1152/jn.1986.55.6.1308

47. Lefort, S., Tomm, C., Floyd Sarria, J. C. & Petersen, C. C. H. The Excitatory Neuronal Network of the C2 Barrel Column in Mouse Primary Somatosensory Cortex. *Neuron* (2009). doi:10.1016/j.neuron.2008.12.020

48. Petersen, R. S. *et al.* Diverse and Temporally Precise Kinetic Feature Selectivity in the VPm Thalamic Nucleus. *Neuron* (2008). doi:10.1016/j.neuron.2008.09.041

49. Bale, M. R., Davies, K., Freeman, O. J., Ince, R. A. A. & Petersen, R. S. Low-Dimensional Sensory Feature Representation by Trigeminal Primary Afferents. *J. Neurosci.* (2013). doi:10.1523/JNEUROSCI.0925-13.2013

50. Ludwig, K. A. *et al.* Using a Common Average Reference to Improve Cortical Neuron Recordings From Microelectrode Arrays. *J. Neurophysiol.* (2009). doi:10.1152/jn.90989.2008

51. Fee, M. S., Mitra, P. P. & Kleinfeld, D. Automatic sorting of multiple unit neuronal signals in the presence of anisotropic and non-Gaussian variability. *J. Neurosci. Methods* (1996). doi:10.1016/S0165-0270(96)00050-7

52. Shinomoto, S. Estimating the Firing Rate. in *Analysis of Parallel Spike Trains* (2010). doi:10.1007/978-1-4419-5675-0

53. Benjamini, Y. & Hochberg, Y. Controlling the false discovery rate: a practical and powerful approach to multiple testing. *J. R. Stat. Soc. Ser. B* (1995). doi:10.2307/2346101

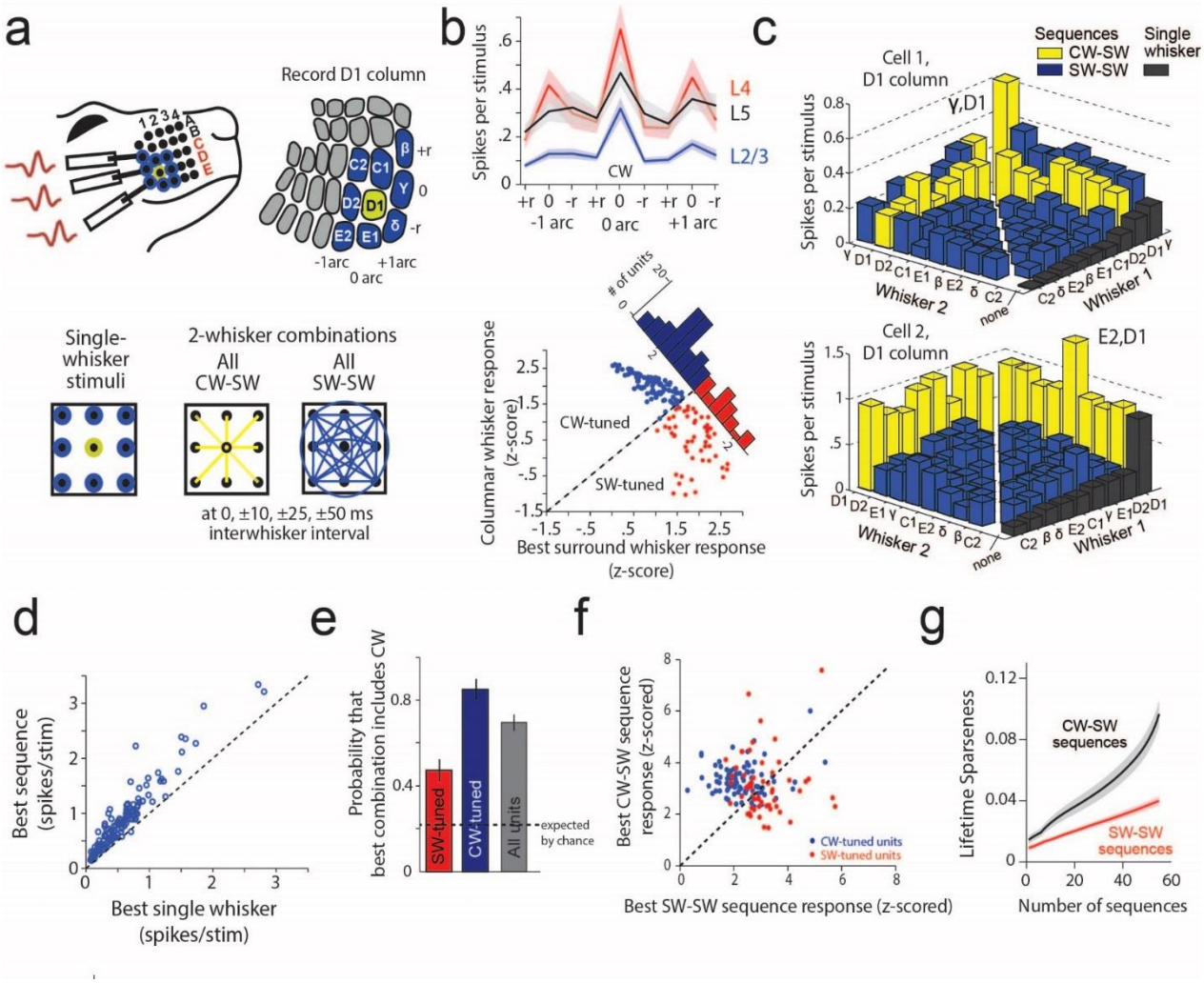

Figure 1. S1 neurons preferentially encode CW-SW sequences **(a)** Whisker deflections applied within a 3x3 array of whiskers, while recording from the S1 column corresponding to the central whisker (here, D1). Bottom: Single-whisker and pairwise whisker stimuli that were interleaved in *Experiment 1*. **(b)** Top, Mean single-whisker tuning across all units in L2/3, L4 and L5. Bottom, Spiking response (z-scored within each unit) to individual deflection of the CW vs. the best SW for each unit. Histogram shows distribution of CW-tuned and SW-tuned units. **(c)** Tuning curves for single and pairwise sequences of 2 example units. Blue and yellow bars are arranged in a 9x9 grid and denote the unit's response to CW-SW or SW-SW combinations respectively; bars in the upper and lower triangular regions show the unit's peak response at negative ($\Delta t<0$) or positive Δt's respectively. Black bars show mean single-whisker responses. **(d)** Response of each unit to its best pairwise whisker sequence vs. best single whisker. Linear regression slope was 1.26. **(e)** Fraction of units whose best sequence contained the CW. **(f)** Spiking response (z-scored within each unit) to best CW-SW sequence vs. best SW-SW sequence for each unit. **(g)** Tuning sharpness, quantified as lifetime sparseness, among different sets of pairwise whisker sequences. Within each set, sequences were ranked from strongest to weakest spiking response, and lifetime sparseness was calculated for increasing number of sequences ranked. Thus, tuning sharpness can be compared between the N best CW-SW sequences and the N best SW-SW sequences (at X=N on the x-axis).

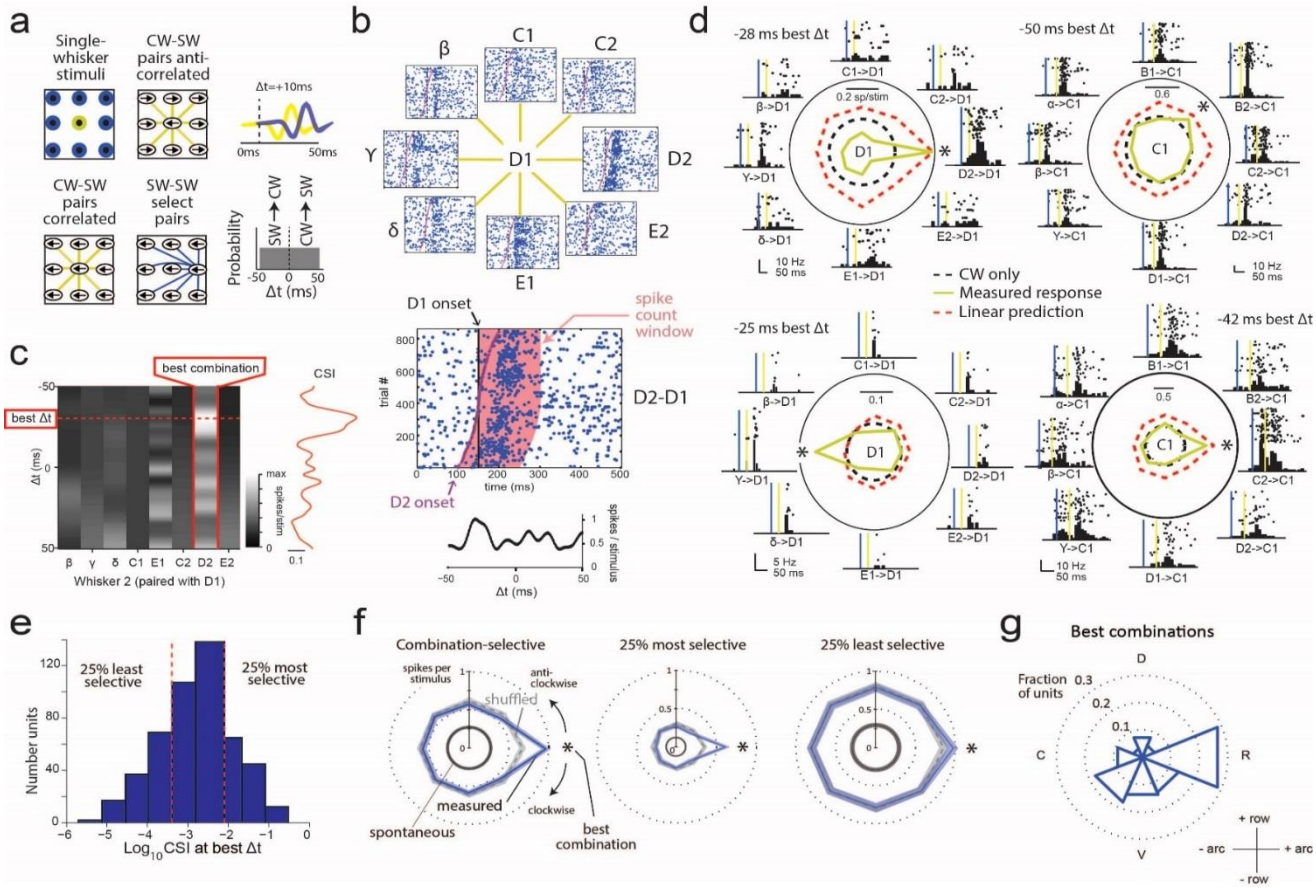

Figure 2. Dense spatiotemporal mapping of CW-SW sequences reveals combination tuning in S1 **(a)** Multi-whisker stimulus protocol: all possible pairwise whisker combinations involving the CW (yellow) or an SW (blue lines) were delivered at a Δt range of ±50ms at a 1ms resolution. All sequences were delivered in a correlated and anti-correlated fashion. Top right plot shows the stimulus waveforms for a CW-SW combination at +10ms Δt **(b)** Example unit for which we quantified spiking responses for each correlated CW-SW combination as a function of Δt (Δt tuning curve). Each raster plot shows spiking across all Δt's for each combination. Δt tuning curves were calculated by averaging spikes in the spike count window for each Δt and smoothing via a model-based method (see Methods). **(c)** Columnar-whisker spatiotemporal receptive field (cwSTRF) of the example unit shown in b. Spiking responses were normalized by the unit's maximum response and combination selectivity was quantified by the lifetime sparseness across combinations for each Δt. **(d)** Combination tuning curves for correlated CW-SW combinations of 4 combination-selective example single-units in polar coordinates. Spiking responses were averaged across ± 5ms relative to each unit's best Δt. PSTH's and rasters are built from trials that lie within that Δt range. The single-unit in the top left is the same as (b) and (c). **(e)** Distributions of the $\log_{10}$combination selectivity index for significantly combination selective and non-selective units. Left and right dashed lines show the first and last quartiles of the distribution. **(f)** Average polar tuning curves for all combination selective units and the 25% most and least selective units as determined by ranking the CSI values. All tuning curves were aligned by rotating their peak response to 0 degrees. Dashed gray lines show tuning after spike counts were shuffled across combinations. **(g)** Angle histogram of best CW- SW combination identities across units. Best combination identity was not uniformly distributed (Rayleigh test, p=4e-19). The angular axis denotes the identity of the CW-SW combination.

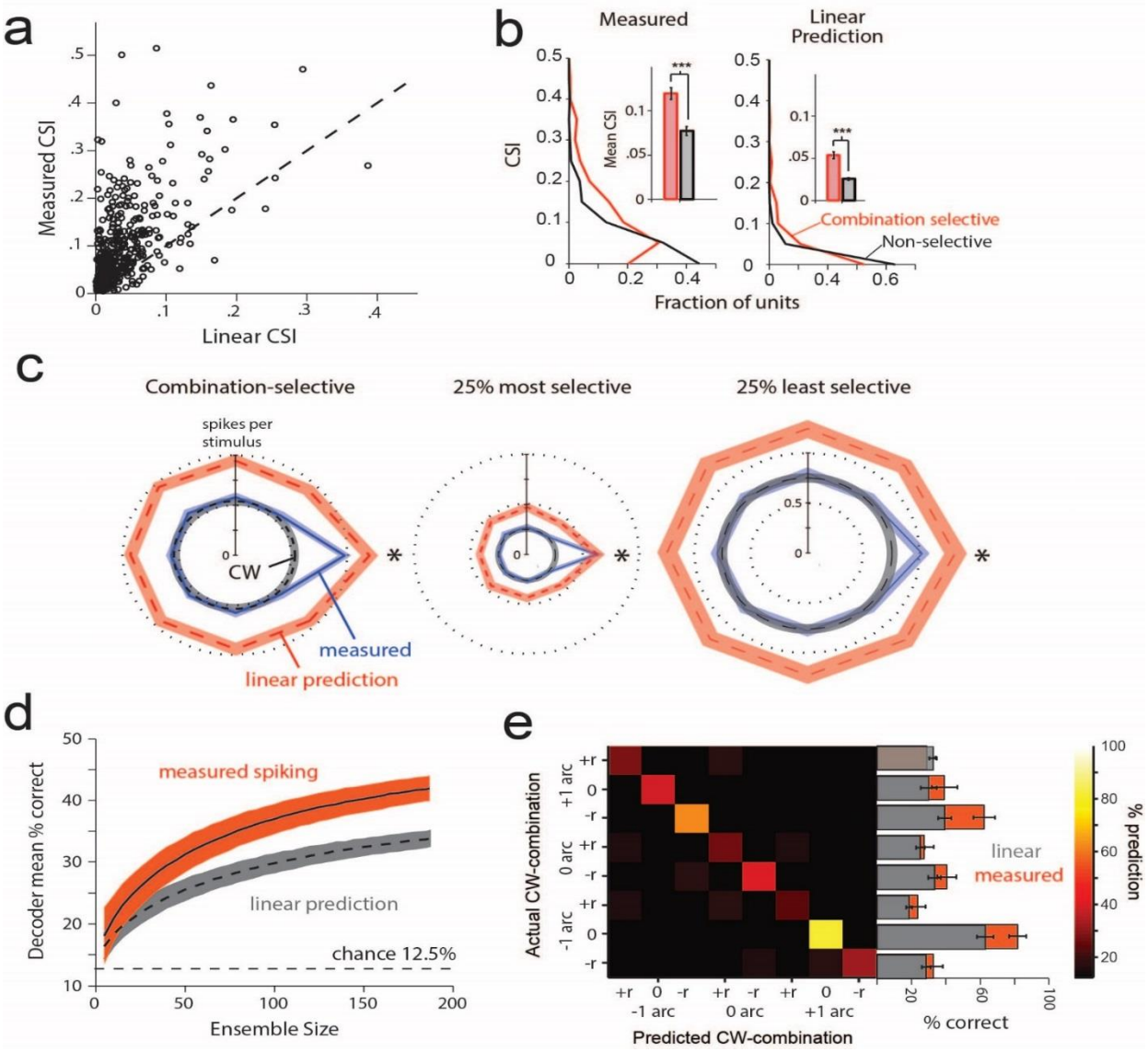

Figure 3. Nonlinear sharpening of combination tuning enhances rate coding for whisker combinations in S1. **(a)** Comparison of measured and linearly predicted CSI at best Δt. **(b)** Probability distributions of measured and linearly predicted CSI between combination-selective and non-selective units. Inset show mean CSI **(c)** Average polar tuning curves for all combination selective units and the 25% most and least selective units as determined by ranking the CSI values. As in fig. 2f all tuning curves were aligned to their peak response. Includes the linearly predicted responses (aligned to each unit's best combination) and single-whisker response to the CW. **(d)** Average performance of a neural population decoder that predicts CW-SW combination identity based on single-trial spiking activity of combination selective units. Spiking responses were drawn from ± 5ms relative to each unit's best Δt or from single-whisker responses to generate a linear prediction. Units were randomly sampled (with replacement) 1000 times for each ensemble size; shaded regions are the standard deviations across same-size ensembles. **(e)** Mean confusion matrix of neural decoder with 187 combination-selective units. Entries along the diagonal are percent correct classifications for each CW-SW combination and rows sum to 1. Orange and gray bars are % correct classification for measured and linear responses respectively.

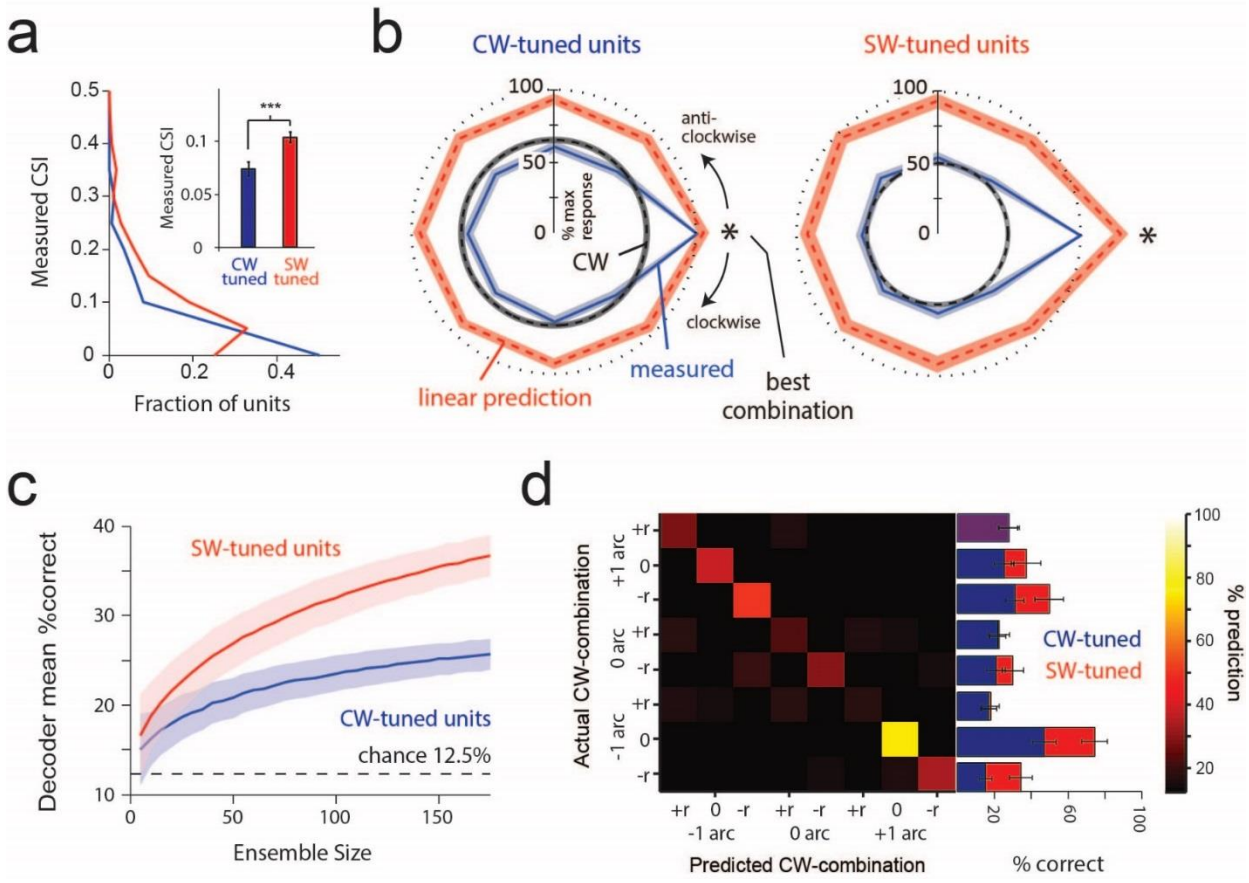

Figure 4. Strong SW responses enhance rate coding for whisker combinations in S1. **(a)** Probability distributions of combination-selectivity indices for CW and SW-tuned units. Insets show mean CSI **(b)** Mean, normalized CW-SW combination tuning for CW and SW-tuned units. Tuning curves were aligned at the best combination. **(c)** As fig. 3d decoders predicted CW-SW combination identity but were separately trained on spike counts from either CW or SW-tuned units only. **(d)** Same as fig. 3e but the confusion matrix is for the decoder trained on SW-tuned units only. Red and blue bars denote SW and CW-tuned units respectively.

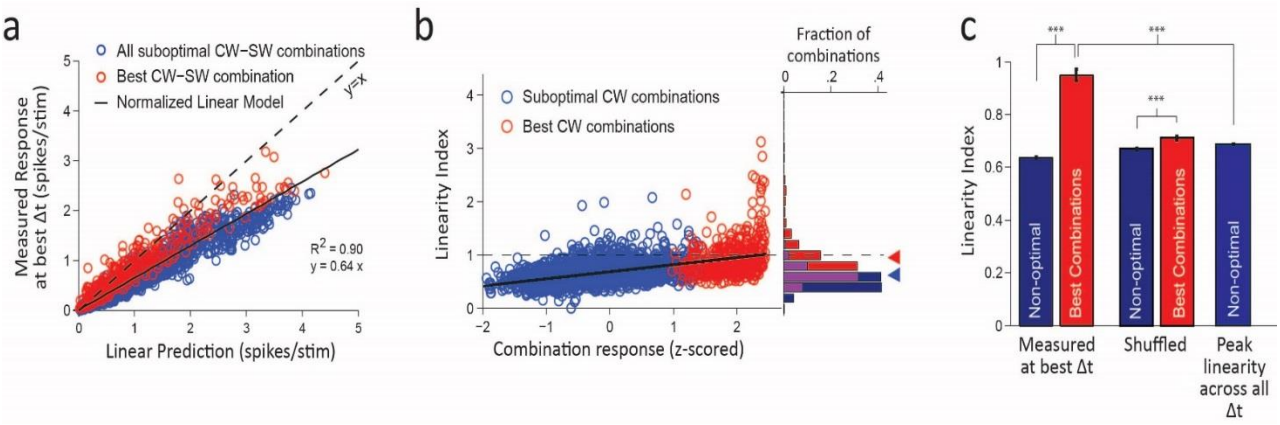

Figure 5. Best combination responses at best Δt are boosted relative to a global sublinear scaling **(a)** Comparison of measured and linearly predicted combination responses at each unit's best Δt. Black line is the line of best fit with the y-intercept set to 0. **(b)** Left, comparison between linearity (measured response divided by the linear prediction) and z-scored CW-SW combination response. Right, distribution of linearity indices for best and suboptimal combinations. Dashed lines are the mean linearity indices. **(c)** Average linearity indices (measured response divided by the linear prediction) for best and suboptimal combinations at best Δt for measured and shuffled data. The peak linearity index across all Δt's is also shown for suboptimal stimuli.

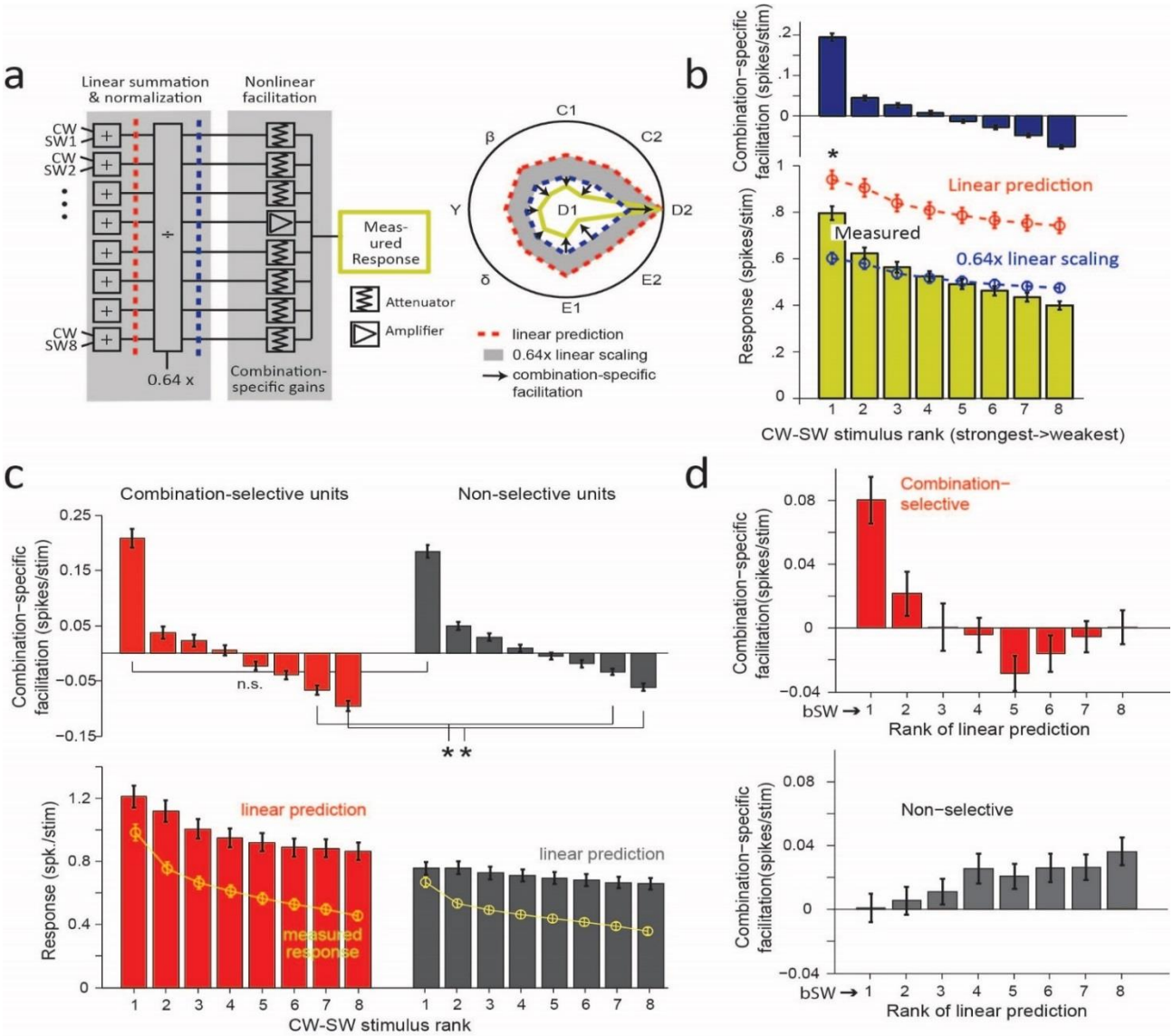

Figure 6. Organization of linear and nonlinear computations for combination tuning **(a)** Schematic of model that describes how combination responses are constructed from single-whisker responses. The model has 2 stages after linear summation: a multiplicative scaling that conserves combination tuning from linear summation (normalization) and a combination-specific facilitation process that can change combination tuning relative to the linear expectation. Amplifiers and attenuators represent facilitation and suppression relative to the linear response. The polar tuning curve of an example combination-selective unit provides a graphical representation of these steps (linear summation->scaling->combination-specific facilitation ->measured response). **(b)** Comparison of the average linear, normalized and measured spiking responses across CW-SW combinations ranked by response magnitude (color legend is the same as (a)). Top, combination-specific facilitation across ranks **(c)** Comparison of the average nonlinear, linear, and measured responses across CW-SW combination rank for combination-selective and non-selective units. **(d)** Comparison of combination-specific facilitation across CW-combinations ranked by their linear prediction. Upper and lower plots are for combination-selective and non-selective units respectively.

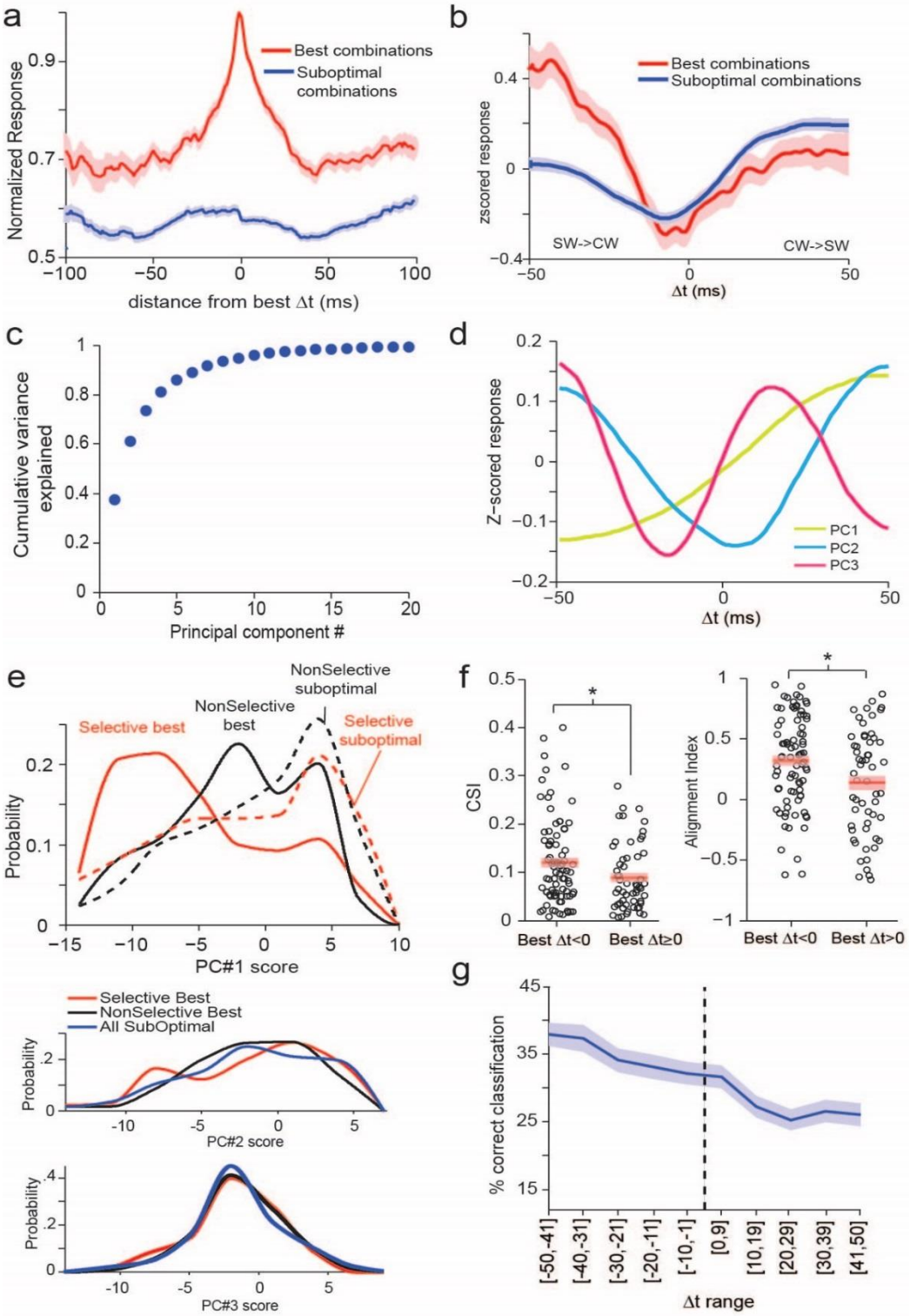
a
Normalized Response
Best combinations
Suboptimal combinations
distance from best Δt (ms)
b
zscored response
Best combinations
Suboptimal combinations
SW->CW
CW->SW
Δt (ms)
c
Cumulative variance explained
Principal component #
d
Z-scored response
PC1
PC2
PC3
Δt (ms)
e
Selective best
NonSelective best
NonSelective suboptimal
Selective suboptimal
Probability
PC#1 score
Selective Best
NonSelective Best
All SubOptimal
PC#2 score
PC#3 score
f
CSI
Best Δt<0
Best Δt≥0
Alignment Index
Best Δt<0
Best Δt>0
g
% correct classification
[-50,-41]
[-40,-31]
[-30,-21]
[-20,-11]
[-10,-1]
[0,9]
[10,19]
[20,29]
[30,39]
[41,50]
Δt range

Figure 7. S1 preferentially encodes tactile sequences inbound to the CW. **(a)** Mean Δt tuning curves aligned at best Δt. All Δt tuning curves were normalized by each unit's peak response. **(b)** Mean z-scored Δt tuning curves. Z-scoring was done separately for each unit. **(c)** Cumulative fractional variance explained by the principal components (PCs) of z-scored Δt tuning curves. **(d)** First three PCs. **(e)** Distribution of weights (or score) for PC 1 across different combination types: best and suboptimal combinations for combination-selective and non-selective units. Bottom 2 plots are the same for PC 2 and 3 but suboptimal stimuli were not separated by unit type. **(f)** CSI and alignment indices for combination-selective units that had a negative or positive best Δt. Open circles are individual units, red line is mean and shaded region is its standard error. The alignment index was the Pearson correlation coefficient between linearly predicted combination responses and combination-specific facilitation (measured – 64% of the linearly predicted response); see Fig. 6. **(g)** Decoding of combination identity (as in Fig. 4) across different ranges of Δt.

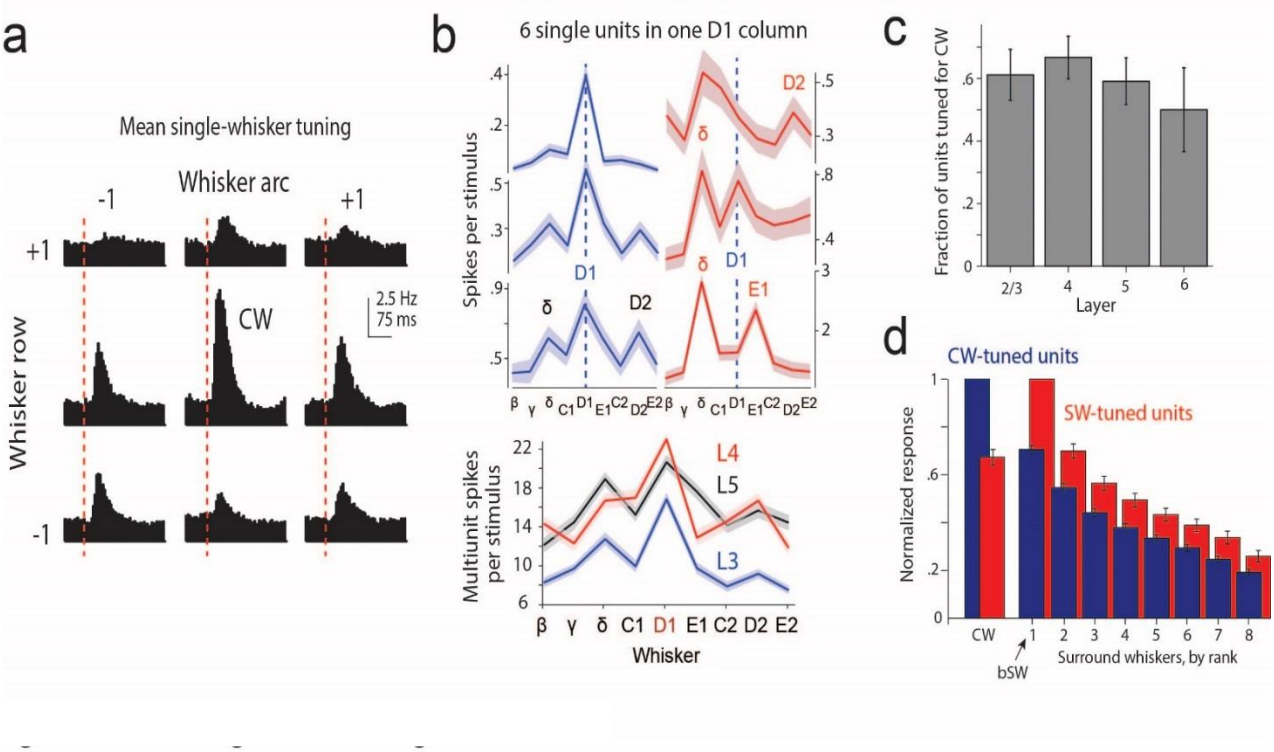

Figure S1 Diverse single-whisker tuning in within the S1 column. **(a)** Average PSTH response to single whisker deflections across all units. **(b)** Top, single-whisker tuning curves of 6 example units that were recorded in the same penetration of the D1 column. Bottom, multiunit activity across layers, multiunit activity was the number of voltage transients that exceeded 3 standard deviations of baseline. **(c)** Fraction of units that had their peak single-whisker response to CW deflections (CW-tuned units) across layers. **(d)** Average single-whisker receptive fields of CW and SW-tuned units. Responses were normalized to each unit's maximum spiking response and surround whiskers were ranked by response strength.

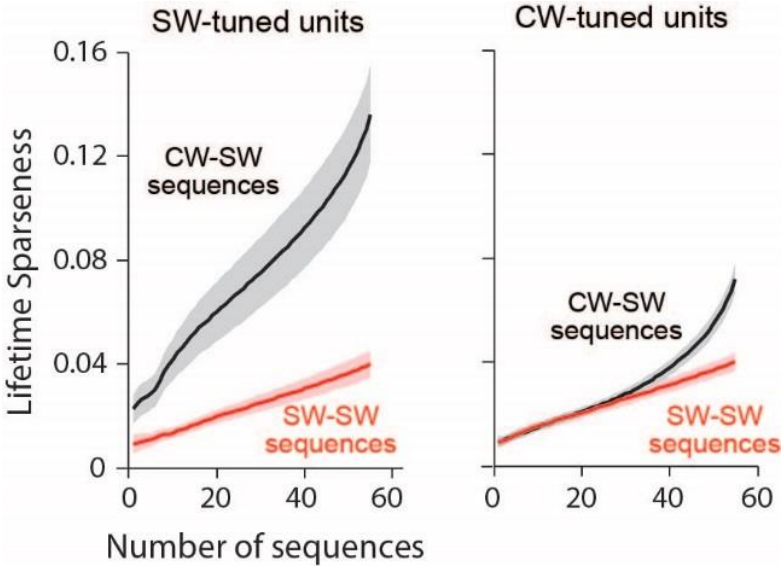

Figure S2. SW-tuned units have the sharpest CW-SW sequence tuning. Tuning sharpness, quantified as lifetime sparseness, among different sets of pairwise whisker sequences. Within each set, sequences were ranked from strongest to weakest spiking response, and lifetime sparseness was calculated for increasing number of sequences ranked. Thus, tuning sharpness can be compared between the N best CW-SW sequences and the N best SW-SW sequences (at X=N on the x-axis).

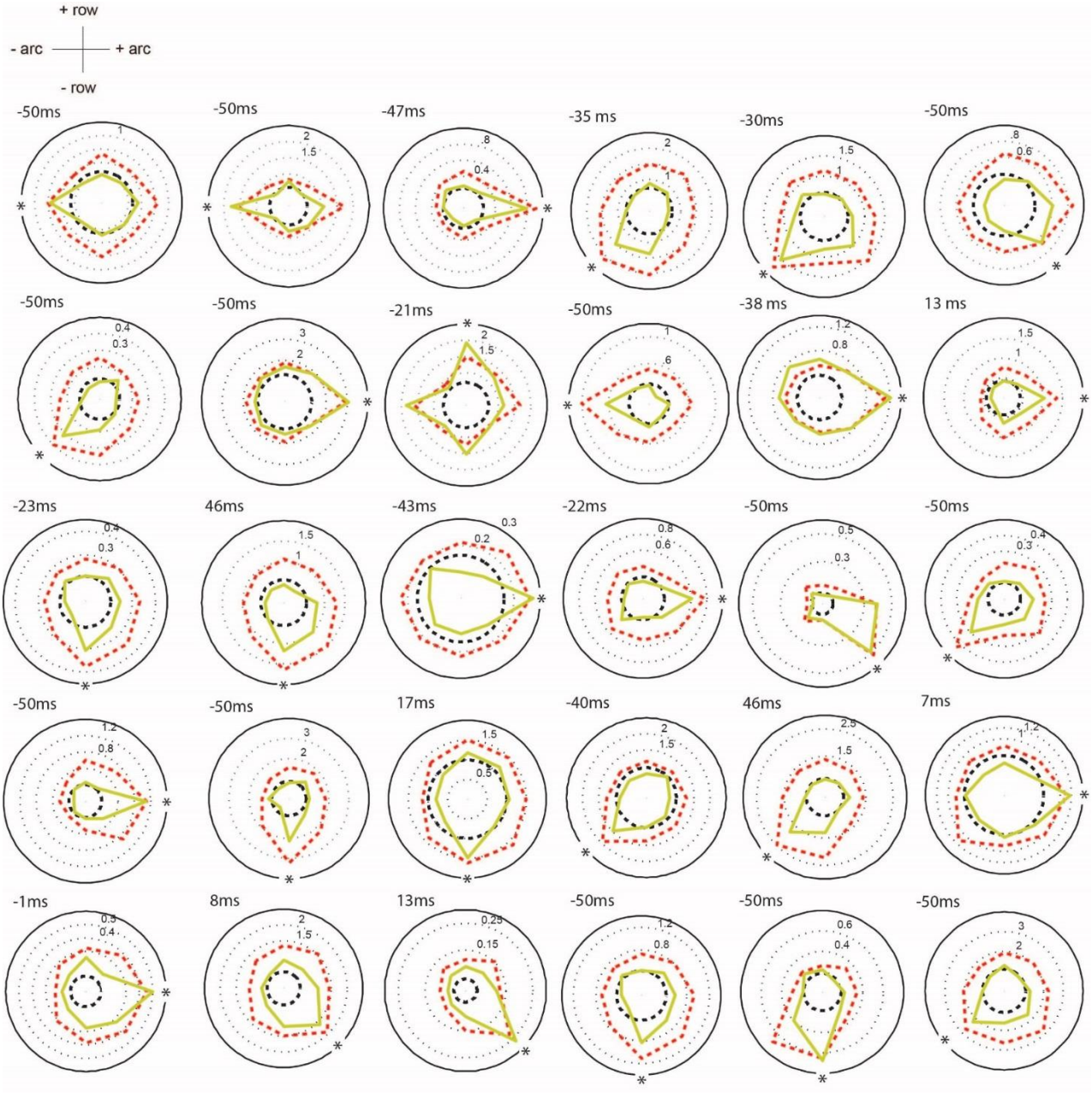

Figure S3. Diversity of combination tuning in S1. Combination tuning curves of 30 combination-selective units, chosen to be representative of the population. Asterisks denote peak responses. Best Δt's are shown in the top left of each unit.

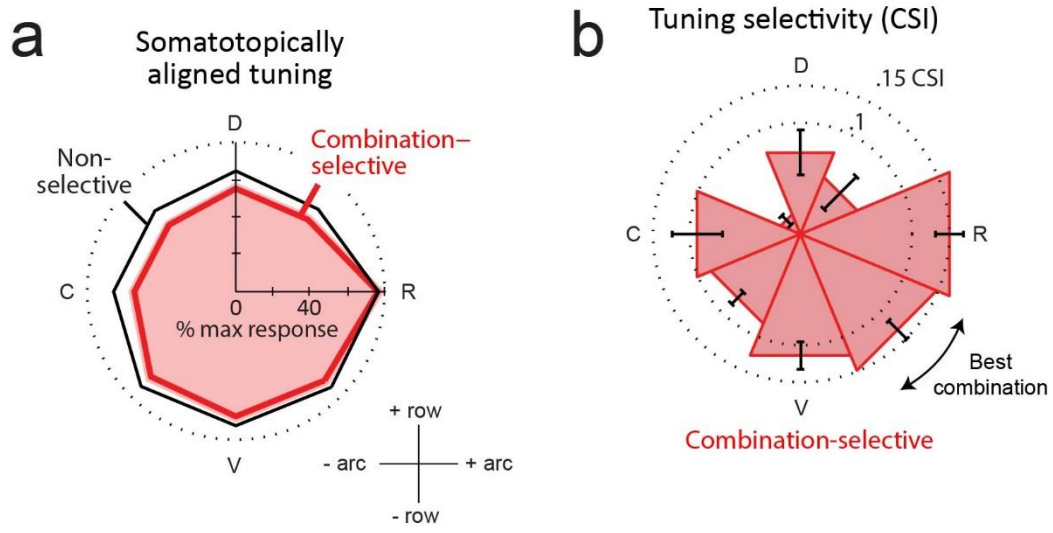

Figure S4. Somatotopic bias of combination tuning in S1. **(a)** Average, rate normalized, combination tuning curves for combination-selective and non-selective units. **(b)** Average combination selectivity across combination-selective units that prefer a specific CW-SW combination. Each point at each angle is the average CSI of units that prefer the corresponding CW-SW combination.

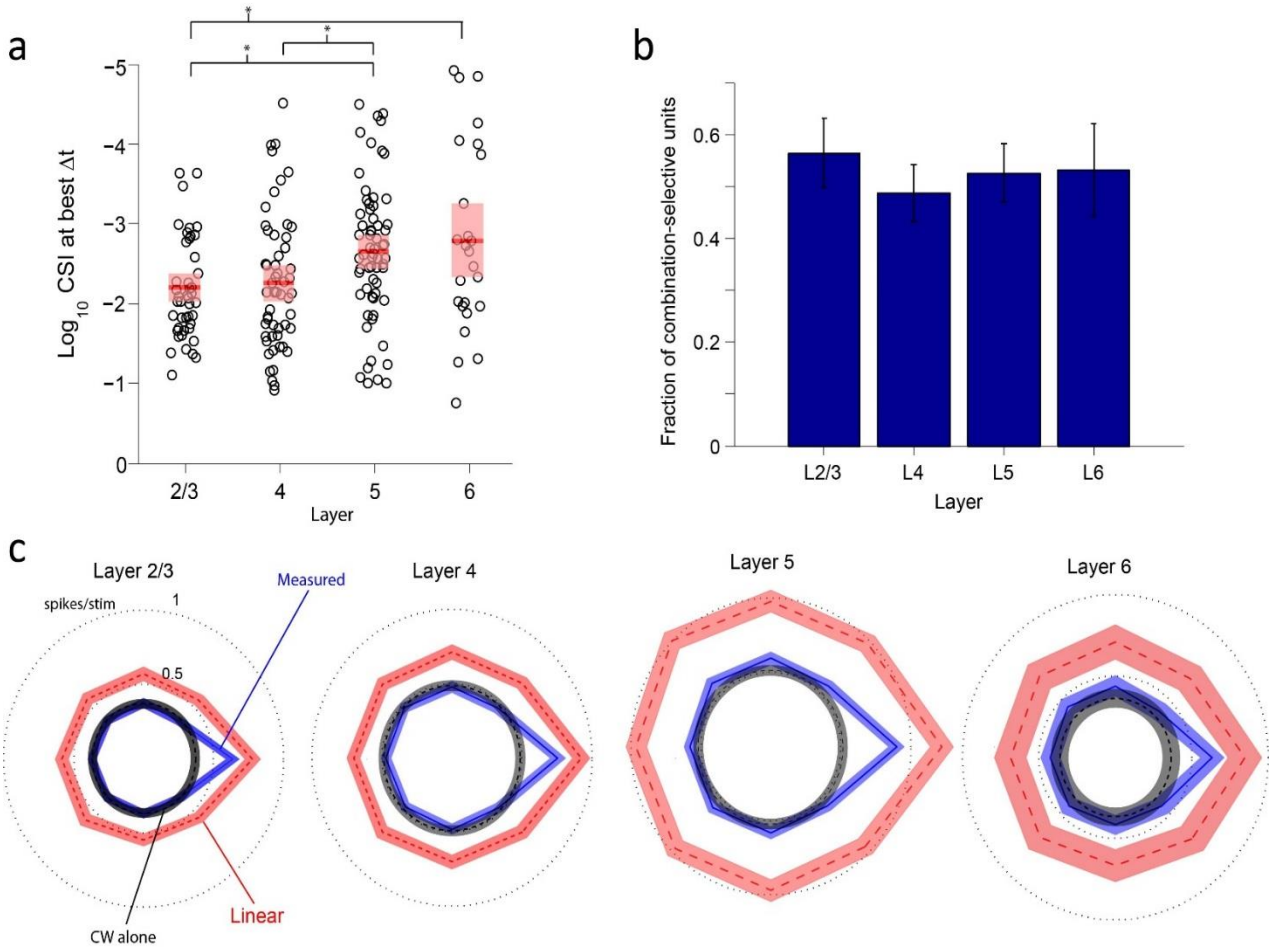

Figure S5 Properties of combination tuning across layers. **(a)** Log_{10} CSI across layers for combination-selective units. Open circles are individual units, red line is the mean and shaded region is the 95% confidence interval. Asterisks denote statistically significant differences. **(b)** Fraction of combination-selective units across layers. **(c)** Average polar tuning curves aligned to the best stimulus for each layer. Axes are in spikes per stimulus and are the same across all plots.

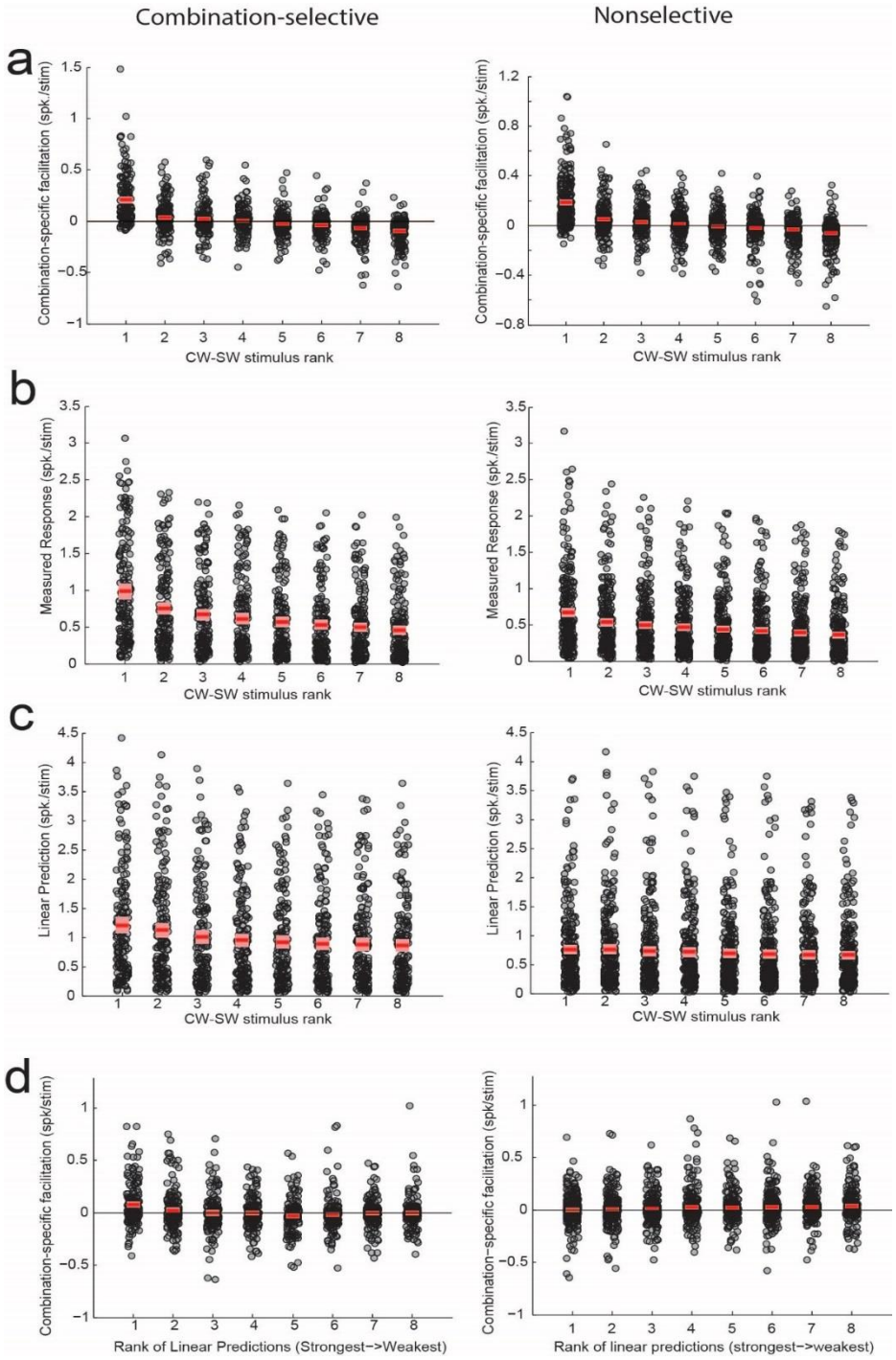

Figure S6.
Distributions of linear and nonlinear components of combination tuning. Combination-specific facilitation, measured and linear response are defined as in Fig. 6. For all panels left and right plots are for combination-selective and non-selective units respectively. **(a)** Combination-specific facilitation as a function of CW-SW combination rank. Open circles are individual units, red line is mean and shaded region is 95% confidence intervals. **(b)** and **(c)** Same as (a) but for measured response and linear prediction respectively. **(d)** Combination-specific facilitation as a function of the linear prediction rank.

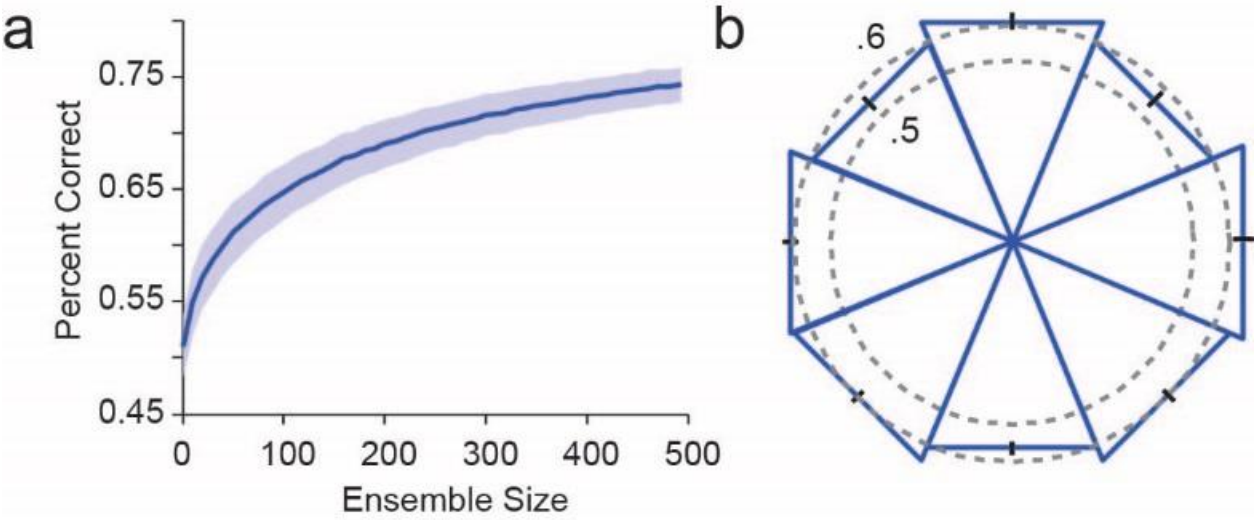

Figure S7. Rate coding for CW-SW sequence order in S1 **(a)** Average performance of a neural population decoder that predicts sequence order (inbound -Δt vs. outbound + Δt) based on, single-trial spiking activity. –Δt and + Δt responses were defined as spike counts evoked by a combination with a Δt within [-50ms,-10ms] and [10ms, 50ms] range. Only combination responses for best combinations were used in this analysis. **(b)** Decoding performance across different combination identities. The order of each CW-SW combination was decoded from units that had that combination as their best combination.

Chapter 4

Conclusion

Chapter 2 showed that S1 neurons in layers 2/3 and 4 code for whisker kinematic features at a very fast timescale, while neurons in layer 5 coded for non-sensory features (i.e. behavioral choice). This was consistent with the results of Chapter 3, where the sharpest 2-whisker combination tuning was found in layers 2/3 and 4 with significantly weaker sensory tuning in layers 5 and 6 (Fig. S5 of Chapter 3; page 76). These results show that S1 can have remarkably precise tuning to different tactile features and reveal novel functional differences across cortical layers.

A canonical computation for spatiotemporal feature extraction in whisker sensation and vision?

Chapter 3 describes a novel and prevalent nonlinear computation that enhances sensory tuning in whisker S1. This computation consisted of near-linear integration to best whisker combinations and prominent sublinear suppression to suboptimal whisker combinations; largely consistent with the spatially asymmetric suppression that yields motion direction selectivity in many areas of the visual system. In the Barlow-Levick motion detection model, a classical model of motion direction selectivity in vision, direction selectivity is constructed via suppression of neural responses to motion along null or non-preferred axes of motion and a lack of suppression to preferred directions[1,2]. This is seen in direction selective retinal ganglion cells of the mammalian retina[3] and a similar phenomenon was recently described in the fly T4 cells where sublinear summation of sequential photoreceptor activation along the null but not in the preferred direction, enhanced direction selectivity beyond that expected from linear integration alone[4].

Motion direction selectivity is also common in primary sensory cortex. Our results show that most S1 neurons prefer multi- over single-whisker stimuli (Fig. 1d of Chapter 3; page 64), are tuned to specific 2-whisker combinations (Fig. 2 and S3 of Chapter 3; pages 65 and 74) and sharpen 2-whisker tuning with a stereotyped nonlinearity (Fig. 5 of Chapter 3; page 68). This implies that local motion in the whisker pad (consisting of sequential deflections of individual whiskers) is a fundamental aspect of sensory coding in S1. Most V1 neurons respond more strongly to moving over static stimuli (e.g. drifting gratings over oriented edges)[5]. Both simple and complex cells exhibit strong motion direction selectivity[6]. Simple cells, although linear in how they compute orientation tuning, sharpen motion direction selectivity nonlinearly. Studies comparing neural responses to stimuli consisting of individual spots of light vs. sequences showed that responses of V1 simple cells to the preferred direction of motion often match the

linear prediction but responses to non-preferred directions are suppressed relative to the linear prediction[7]; sharpening motion direction selectivity in a way that is analogous to what we described in Chapter 3 (Fig. 5 and 6; page 68 and 69). Moreover, this direction selectivity is critically dependent on spatiotemporally inseparable receptive fields with cells having spatiotemporally separable receptive fields exhibiting no motion direction selectivity[8]. Complex cells also exhibit this tuning and modeling complex cell spiking as arising from a weighted sum of spatiotemporally inseparable subunits accurately predict motion direction preference[8]. This need for spatiotemporally inseparable receptive fields in the visual system is analogous to how S1 neurons sharpen whisker combination tuning with space-time inseparable multi-whisker receptive fields (Fig. 7b of Chapter 3; page 70). Thus, S1 cells with 2-whisker sequence tuning show important analogies with both simple and complex cells in V1. This suggests that classical models for visual direction selectivity provide a powerful and intuitive tool to understand multi-whisker tuning and suggests generalized and evolutionary conserved nonlinear operations for spatiotemporal feature extraction.

References

1. Barlow, H. B. & Levick, W. R. The mechanism of directionally selective units in rabbit's retina. *J. Physiol.* (1965). doi:10.1113/jphysiol.1965.sp007638

2. Borst, A. & Euler, T. Seeing Things in Motion: Models, Circuits, and Mechanisms. *Neuron* (2011). doi:10.1016/j.neuron.2011.08.031

3. Mauss, A. S., Vlasits, A., Borst, A. & Feller, M. Visual Circuits for Direction Selectivity. *Annu. Rev. Neurosci.* (2017). doi:10.1146/annurev-neuro-072116-031335

4. Gruntman, E., Romani, S. & Reiser, M. B. Simple integration of fast excitation and offset, delayed inhibition computes directional selectivity in Drosophila. *Nat. Neurosci.* (2018). doi:10.1038/s41593-017-0046-4

5. Emerson, R. C. & Gerstein, G. L. Simple striate neurons in the cat. I. Comparison of responses to moving and stationary stimuli. *J Neurophysiol* (1977). doi:10.1152/jn.1977.40.1.119

6. Hubel, D. H. & Wiesel, T. N. Receptive fields of single neurones in the cat's striate cortex. *J. Physiol.* (1959). doi:10.1113/jphysiol.1959.sp006308

7. Reid, R. C., Soodak, R. E. & Shapley, R. M. Directional selectivity and spatiotemporal structure of receptive fields of simple cells in cat striate cortex. *J. Neurophysiol.* (1991). doi:10.1152/jn.1991.66.2.505

8. DeAngelis, G. C., Ohzawa, I. & Freeman, R. D. Receptive-field dynamics in the central visual pathways. *Trends in Neurosciences* (1995). doi:10.1016/0166-2236(95)94496-R